PROTON SPIN-LATTICE RELAXATION IN H_2-Ar, H_2-N_2, H_2-N_2O AND CH_3Cl

By

LAKSHMAN PANDEY

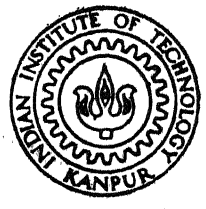

DEPARTMENT OF PHYSICS

INDIAN INSTITUTE OF TECHNOLOGY KANPUR

JULY, 1979

PROTON SPIN-LATTICE RELAXATION IN H_2-Ar, H_2-N_2, H_2-N_2O AND CH_3Cl

A Thesis Submitted
In Partial Fulfilment of the Requirements
for the Degree of

DOCTOR OF PHILOSOPHY

By

LAKSHMAN PANDEY

to the

DEPARTMENT OF PHYSICS

INDIAN INSTITUTE OF TECHNOLOGY KANPUR

JULY, 1979

PHY-1979-D-PAN-PRO

CERTIFICATE

Certified that the work described in this thesis is the original work of Mr. Lakshman Pandey performed under my supervision, and has not been submitted elsewhere for a degree.

Lalita Sarkar

K. Lalita Sarkar
Assistant Professor of Physics
Indian Institute of Technology
Kanpur 208016 (U.P.) India

July 3, 1979.

ACKNOWLEDGEMENTS

I express my sincere gratitude to Dr. K. Lalita Sarkar for her inspiring guidance throughout the course of this research work. I always found it pleasant to work with her. I feel that the type of experience I have gained while working with her will be of great help to me in pursuit of my scientific career.

I am deeply indebted to Professor V. Subba Rao of Chemical Engineering for his constant help and encouragement.

I am greatly obliged to Shri K.M.S. Prasad for his continuous help during the experimental part of the work.

Thanks are due to Professor S.V. Babu and Dr. S. Rajan for many fruitful discussions.

I am thankful to the members of the Low Temperature Laboratory for their cooperation.

I thank all the technical personnel who helped me in many ways. Thanks are due to Shri R.P. Yadav, H.K. Panda and L. Singh for their day to day help, and to Bajpai for neat tracings.

I place on record my deep sense of gratitude to all my friends and colleagues who helped me directly or indirectly in the successful completion of this work. In particular, I am grateful to C.P.K. Reddy for his help during the experiments, to Devendra Kumar who gave his valuable time for proof readings and to A.N. Singh, B.N. Singh, K.S. Singh, M. Prasad, Om Prakash, Jain V.K., Mishraji and A.K. Singh for their help and jovous company.

I am grateful to Shri Nihal Ahmad who took great pains in typing the manuscript.

Financial assistance from C.S.I.R. and IIT Kanpur is gratefully acknowledged.

I am indebted to my parents and family members for their moral support and tremendous patience all these years which helped me in pursuing my higher studies.

Lakshman Pandey

CONTENTS

LIST OF FIGURES

LIST OF TABLES

SYNOPSIS

Title of Thesis	PROTON SPIN-LATTICE RELAXATION IN H_2-Ar, H_2-N_2, H_2-N_2O AND CH_3Cl
Programme	Ph.D.
Name of Student	Lakshman Pandey
Thesis Supervisor	Dr. K. Lalita Sarkar
Department	Physics Indian Institute of Technology Kanpur

The thesis presents a study of proton spin-lattice relaxation in gas mixtures H_2-Ar, H_2-N_2 and H_2-N_2O, T_1 minimum study in pure CH_3Cl and an analysis of the existing data in BF_3, NH_3, F_2 and HCl.

Proton spin-lattice relaxation times T_1 were measured as a function of density and temperature in hydrogen mixtures. This data together with the measurements done by Foster et al. in H_2-Ar mixtures and by Williams in H_2-N_2 mixtures were analysed using Bloom-Oppenheim theory to extract information on the anisotropic intermolecular interaction between these molecules. In CH_3Cl, T_1 were measured as a function of density in the low density region at room temperature and T_1 minimum was obtained. From the experimental value of T_1 minimum the effective spin-rotation coupling constant for

protons in CH_3Cl was evaluated. The data obtained by Courtney and Armstrong in F_2, by Tward and Armstrong in HCl and by Armstrong and Hanrahan in NH_3 and BF_3 were analysed using Bloom-Oppenheim theory and a model first proposed by Rajan et al. for finding out the correlation time for spin-rotation interaction was tested.

All the measurements were done with a spin-echo spectrometer having an operating frequency of 30 MHz using phase coherent detection. The subject matter is divided into six chapters as described below:

The Chapter I contains an introduction to the basic principles of Nuclear Magnetic Resonance and the phenomenon of spin-lattice relaxation.

In Chapter II the method of spin-echoes to measure the relaxation times and the spin-echo spectrometer used for this purpose are described together with the details of the sample-holder and sample preparation.

The experimental data and its analysis in the mixtures of H_2 with Ar, N_2 and N_2O and a review of the Bloom-Oppenheim theory are presented in Chapter III. T_1 was measured as a function of density ($10 < \rho < 70$ amagats) and composition in the temperature range of 300-600K for H_2-Ar and H_2-N_2 and 200-400K for H_2-N_2O mixtures. Bloom-Oppenheim two level theory for proton spin-lattice relaxation in H_2 predicts a

non-linear behaviour of T_1/ρ as a function of composition of the mixture H_2-X where X may be Ar, N_2 or N_2O. Since the fractional population of the rotational states higher than J=3 for ortho- and J=4 for para-H_2 are not negligible at temperatures above 450K, this theory can not be applied at higher temperatures. In the absence of an exact theory which is applicable to higher temperatures, the T_1/ρ data was fitted to the following empirical relation using the method of least squares as was done by some previous workers for H_2-He mixtures

$$T_1/\rho = A_o + A_1 X_x + A_2 X_x^2$$

where A_o, A_1 and A_2 are constants and X_x is the fractional concentration of X in the mixture. (T_1/ρ) for X_x=1 gives the value of T_1/ρ due to H_2-X collisions alone and is denoted by $(T_1/\rho)^{O-X}$. Since the deviation from linear dependence is not very prominent up to 63% of the solvent gas, the data was also fitted with a linear fit to obtain the value of $(T_1/\rho)^{O-X}$. The $(T_1/\rho)^{O-X}$ values obtained by the empirical fit and a linear fit differ by 8% at 300K and by 2% around 600K. Model potentials for the intermolecular interactions were proposed in all the three cases and the strengths of the attractive and repulsive terms were obtained using the experimental value of $(T_1/\rho)^{O-X}$. It was found that the values of the relative anisotropy in the attractive

term of the intermolecular potentials for H_2-Ar and H_2-N_2 are 0.137 and 0.131 respectively whereas the polarizability data gives a value of 0.128. Agreement between the values obtained from this analysis and from polarizability data justifies the use of the proposed model potential to explain the NMR data in these systems. For H_2-N_2O the quadrupole moment of N_2O, calculated from the strength of the attractive term was found to be 4.65×10^{-26} esu cm^2 while the recommended value is 3.0×10^{-26} esu cm^2. The potential proposed for this system may be taken as a tentative potential.

In Chapter IV the T_1 measurements in CH_3Cl have been reported. T_1 were measured in CH_3Cl gas in low density region ($0.2 < \rho < 6.5$ amagats) at room temperature. Since T_1/ρ is very long (370 msec/amagat) a pulse train consisting of $\pi/2$-burst followed by $\pi/2$-π pulses was used to save the experimentation time. The spectrometer was modified for this purpose. From the T_1 minimum the value of the effective spin-rotation coupling constant, C_{eff}, for proton in CH_3Cl was obtained which is 0.32 KHz.

Chapter V contains an application of the model first proposed and used by Rajan et al. to evaluate the correlation time of spin-rotation interaction in some gases. In this model, it is assumed that the correlation time of the spin-rotation interaction can be approximated by the life time of the molecule in a J state if spin-rotation interaction is the dominant mechanism of relaxation in the gas. Using this model T_1 results (available in literature) for NH_3, BF_3, F_2

and HCl have been analysed using Bloom-Oppenheim theory to find the dominant multipole moments of these molecules. It was found that the quadrupole moment Q of F_2 and dipole moment μ of HCl are comparable to the results obtained from other experiments while Q for BF_3 and μ for NH_3 are quite different from the reported values. Thus it is concluded that this model works well in some cases, especially for spherical top molecules such as CH_4 as discussed by Rajan et al. and also for linear molecules as is found in the present work. Perhaps the model does not work well in symmetric top molecules. Keeping in view the remarks made by Armstrong and Courtney about the possible inadequacy of the existing theory for spin-relaxation in symmetric top molecules it can be said that the discrepancy observed in the values of multipole moments in the present analysis may be either due to the inadequacy of the model proposed by Rajan et al or due to the inadequacy of the spin-relaxation theory for symmetric top molecules itself.

Conclusions of the work presented are given in Chapter VI. The circuit diagrams of the different parts of the spectrometer are given in Appendix.

CHAPTER I

INTRODUCTION

I.1 Outline of the Principle of NMR

Magnetic resonance is a phenomenon found in systems that possess magnetic moment as well as angular momentum and occurs in the presence of external static and oscillating magnetic fields applied perpendicular to each other. The principles of magnetic resonance are given in detail elsewhere[1,2] and are presented here in brief.

A static magnetic field $\vec{H}_o$ applied along, say, Z direction produces an interaction Hamiltonian, which for a nucleus with spin angular momentum $\vec{I}$ and magnetic moment $\vec{\mu} = \gamma\hbar\vec{I}$ where γ is the gyromagnetic ratio, is given by

$$\mathcal{H} = -\vec{\mu}\cdot\vec{H}_o = -\gamma H_o \hbar I_z \qquad (1.1)$$

The allowed energy levels are

$$E_m = -\gamma\hbar H_o m \qquad (1.2)$$

where $m = -I, -I+1, \ldots, +I$.

The fractional populations of these energy levels at equilibrium are given by

$$P_m = \frac{\exp(-E_m/kT)}{\sum_m \exp(-E_m/kT)} \tag{1.3}$$

where k is the Boltzmann constant and T is the absolute temperature of the system. For N weakly interacting spins, the equilibrium magnetization is given by

$$M_o = N \sum_m P_m \gamma \hbar m \tag{1.4}$$

$$= N \gamma^2 \hbar^2 I(I+1)/3kT \tag{1.5}$$

where the high temperature approximation $\gamma\hbar H_o/kT \ll 1$ is used.

The approach to equilibrium of a spin system disturbed from its thermal equilibrium is often describable by the phenomenological Bloch equations

$$\frac{d\vec{M}}{dt} = \gamma \vec{M} \times \vec{H} - \frac{M_x \hat{i} + M_y \hat{j}}{T_2} + \frac{M_o - M_z}{T_1} \hat{k} \tag{1.6}$$

where T_1 and T_2 are called the longitudinal and transverse relaxation times respectively and $\vec{H}$ is the magnetic field. If the relaxation effects are neglected, the equation of motion for $\vec{M}$ in a reference frame rotating about Z axis with angular frequency ω may be written as

$$\frac{\partial \vec{M}}{\partial t} = \gamma \vec{M} \times (\vec{H} + \frac{\vec{\omega}}{\gamma}) \tag{1.7}$$

From this it is seen that $\vec{M}$ is stationary in the rotating frame for $\vec{H} = H_o \hat{k}$ if $\vec{\omega} = -\gamma H_o \hat{k}$, which implies that, in the

laboratory frame the magnetic moment $\vec{M}$ precesses about the field $H_o\hat{k}$ with an angular frequency $\vec{\omega}_o = -\gamma H_o \hat{k}$. This frequency is called Larmor frequency.

The energy levels (eq.(1.2)) of a magnetic system, say nucleus, in an external static magnetic field $H_o\hat{k}$ are discrete and can be detected by some form of spectral absorption if the system is subjected to an interaction that can cause transitions between them. In order to cause transitions between two levels having energy E_1 and E_2 ($E_1 < E_2$), the interaction must have a nonvanishing matrix element joining them and should satisfy the conservation of energy, i.e. the interaction must be time dependent and of an angular frequency ω such that

$$\hbar\omega = E_2 - E_1 \tag{1.8}$$

These requirements are very well satisfied by an alternating magnetic field of frequency ω applied perpendicular to the static field. If the alternating field is written as

$$\vec{H}_1(t) = H_1 (\hat{i} \cos \omega t + \hat{j} \sin \omega t) \tag{1.9}$$

then

$$\vec{H} = \vec{H}_1(t) + H_o\hat{k} \tag{1.10}$$

and a perturbation term $\mathcal{H}'$ is introduced in the total Hamiltonian

$$\mathcal{H}' = -\gamma\hbar H_1 (I_x \cos \omega t + I_y \sin \omega t) \qquad (1.11)$$

The matrix elements of $\mathcal{H}'$ between the states m and m' vanish unless $m' = m \pm 1$. Therefore, the transitions occur between levels adjacent in energy and

$$\hbar\omega = E_2 - E_1 = \gamma\hbar H_o \qquad (1.12)$$

or $$\omega = \gamma H_o \qquad (1.13)$$

Therefore, in order to produce transitions, the alternating field must have a frequency equal to the precession frequency of the magnetic system in the static field.

With both the fields applied together, the equation of motion of $\vec{M}$ in the rotating frame is given by

$$\frac{\partial \vec{M}}{\partial t} = \gamma \vec{M} \times [(H_o + \frac{\omega}{\gamma})\, \hat{k} + H_1\, \hat{i}] \qquad (1.14)$$

$$= \gamma \vec{M} \times \vec{H}_{eff} \qquad (1.15)$$

where $$\vec{H}_{eff} = (H_o + \frac{\omega}{\gamma})\, \hat{k} + H_1\, \hat{i} \qquad (1.16)$$

The eq. (1.15) tells that $\vec{M}$ precesses about $\vec{H}_{eff}$ with an angular frequency $-\gamma\vec{H}_{eff}$. When $\omega = \omega_o$, $\vec{H}_{eff} = H_1\, \hat{i}$ and the magnetization, therefore, precesses about $\vec{H}_1$. A magnetic moment that is parallel to the static field initially will then precess in the YZ plane always remaining perpendicular to $\vec{H}_1$ and, thus, periodically line up opposite to $\vec{H}_o$. All the energy it takes to tilt $\vec{M}$ away from $\vec{H}_o$ is returned in a

complete cycle. There is no net absorption of energy from the alternating field but rather alternately receiving and returning of energy. This phenomenon is known as Nuclear Magnetic Resonance.

At resonance the precession frequency is γH_1 and therefore if $\vec{H}_1$ is switched on for a time t_ω, $\vec{M}$ will precess about H_1 through an angle $\theta = \gamma H_1 t_\omega$. θ can be made $180^\circ(\pi)$ or $90^\circ(\pi/2)$ by choosing H_1 and t_ω appropriately. After application of a $\pi/2$ pulse $\vec{M}$ precesses in the XY plane about $\vec{H}_o$ and induces an emf in the sample coil kept perpendicular to $\vec{H}_o$. This induced signal is known as Free Induction Decay (F.I.D.). If a π pulse is applied at a time $t = \tau$ after the $\pi/2$ pulse, the spins tend to rephase in the XY plane at a time 2τ resulting in a free induction signal known as a spin-echo.

If the total magnetic field is written as

$$\vec{H} = H_o \hat{k} + (2H_1 \cos \omega t)\, \hat{i}\,, \quad H_1 \ll H_o \tag{1.17}$$

then the solution of the Bloch equations (eq. 1.6), in the absence of H_1, are obtained as

$$M_x(t) = M_{xy}(0)\,[\cos(\omega t + \phi)] \exp(-t/T_2) \tag{1.18}$$

$$M_y(t) = M_{xy}(0)\,[\sin(\omega t + \phi)] \exp(-t/T_2) \tag{1.19}$$

$$M_z(t) = M_o + [M_z(0) - M_o] \exp(-t/T_1) \tag{1.20}$$

where $M_{xy} = \sqrt{M_x^2 + M_y^2}$ and the relaxation effects have also been considered.

By observing $M_x(t)$ (or $M_y(t)$) and $M_z(t)$ as a function of time, the values of T_2 and T_1 respectively can be determined experimentally. The measurements and interpretation of only T_1 are presented in this thesis.

I.2 A Note on Relaxation Mechanisms

After the spin-system has been disturbed from equilibrium by an external agency, it tends to approach the thermal equilibrium again by transferring its excess energy to the other degrees of freedom (called 'lattice'). The process of this transfer of energy is called spin-lattice relaxation and occurs through different types of interactions within the molecule and outside. The interactions usually assumed to be responsible for thermal relaxation are:

(a) The Intramolecular dipolar and quadrupolar (for $I > \frac{1}{2}$ only) interactions between neighbouring nuclei of the same molecule. These interactions transform as $Y_{2m}(\Omega)$ under rotations of the molecule where Ω denotes the orientation of a vector fixed to the molecule with respect to the space fixed frame.

(b) The Intermolecular dipolar interactions between nuclei on two different molecules.

(c) The intramolecular spin-rotational interactions between nuclear spin and the rotational angular momentum of the molecules. The dominant terms of this interaction transform as $\vec{J}$, the rotational angular momentum of the molecule.

It is usually assumed in the conventional theories for relaxation that all the three mechanisms mentioned above contribute independently to the relaxation process, so that one can write

$$\frac{1}{T_1} = R_A + R_B + R_C \qquad (1.21)$$

where R_A, R_B and R_C are the contributions to the relaxation rate due to the mechanisms a, b and c respectively. In molecular gases which are not too dense, R_B is negligible, so that the relaxation rate $\frac{1}{T_1}$ can be written as

$$\frac{1}{T_1} = R_A + R_C \qquad (1.22)$$

Expressions for relaxation rates for H_2 were obtained by Schwinger[3], Needler and Opechowski[4] and Johnson and Waugh[5] in terms of the correlation times of the intramolecular interactions assuming that only J=1 state is populated. Bloom and Oppenheim[6-10] have developed a theory in which this restriction is removed and transitions between different J states are allowed. They have also obtained expressions for the correlation times of the intramolecular interactions

in terms of the intermolecular interaction by treating the dynamics of the system with 'Constant Acceleration Approximation' (CAA). Kinsey et al. [11], Foster and Rugheimer[12] and Shafer and Gordon[13] have done Quantum Scattering Calculations. Gordon[14-16] has developed a theory based on kinetic theory of gases and obtained expressions for spin-relaxation rates in terms of the intermolecular potentials for molecules in gas phase. For heavier molecules, where large number of rotational states are populated, Rajan et al.[17] have obtained expressions for T_1 in terms of the intermolecular potentials assuming that the correlation time of the dominant intramolecular interactions is equal to the life time of the molecule in a J state.

I.3 Information from T_1 Measurements

(a) Intermolecular Potentials

In a gas, the molecules are always colliding with each other in a random way. During the collisions the intermolecular forces cause reorientation of the molecules (i.e. change the rotational states) resulting in a change of the local fields set at the sites of the nuclei. Due to these randomly fluctuating local fields the nuclei approach thermal equilibrium. The rate, $1/T_1$, at which the nuclear spins approach the state of equilibrium can

be measured experimentally. Therefore, measurement of spin-lattice relaxation time T_1 provides detailed information on the process of molecular reorientation which in turn gives information about the anisotropic interaction between the molecules. The distance of closest approach for the molecules decreases as the temperature increases and, thus, it is possible to probe more into the short range part of the intermolecular potential by measuring T_1 at higher temperatures.

There have been several previous experimental investigations of T_1 in H_2[10,18-20] and in the mixtures of H_2 with other gases[5,12,21-24] where information on the anisotropic part of the intermolecular potential has been obtained from the analysis of the proton T_1 measurements of the ortho-H_2 molecules as a function of density, temperature and concentration of H_2 in the binary gas mixtures. However, not much work has been done at higher temperatures ($T > 300K$).

A part of the work presented in this thesis covers a study of proton spin-lattice relaxation in the mixtures of H_2 with mono-, di- and tri-atomic gases, namely, Ar, N_2 and N_2O as a function of density, composition and temperature. T_1 were measured in H_2-Ar and H_2-N_2 mixtures in the temperature range of 300-600K whereas in H_2-N_2O in the range of 200-400K. These data together with T_1 values

available for H_2-Ar[12] and H_2-N_2[24] mixtures below room temperature were analysed using Bloom-Oppenheim theory to extract information about the intermolecular anisotropic potentials.

(b) Intramolecular Interactions

The rate of spin-lattice relaxation is determined essentially by the component, at the Larmor frequency, of the fluctuating fields at the site of nuclei and depends upon the duration as well as on the strength of the interaction responsible for relaxation. If the average time between collisions that change the state of the molecule be τ_c, it is expected that $\frac{1}{T_1} \propto \tau_c$ if the fluctuations are very fast ($\frac{1}{\tau_c} >> \omega_o$); i.e. shorter the τ_c is, the smaller is the component of the field at Larmor frequency. As τ_c increases, the fluctuating fields will have maximum effect when $\frac{1}{\tau_c}$ is of the order of ω_o. T_1 thus goes through a minimum at $\frac{1}{\tau_c} \simeq \omega_o$. For a dilute gas it can be shown that at constant temperature $\tau_c \propto \rho^{-1}$ where ρ is the density of the gas. Therefore, T_1 as a function of density shows a minimum which is different for different temperatures. Since stronger the strength of the interaction between the nuclear spins and the fluctuating field, faster the rate of relaxation, the value of T_1 minimum yields information on the strength of the intramolecular interactions.

One of the contributions of this thesis is the T_1 minimum study in CH_3Cl gas.

I.4 Scope of the Present Work

The apparatus and experimental techniques that were used to obtain the T_1 data are presented in Chapter II. In Chapter III the theory used to interpret the T_1 data in H_2-Ar, H_2-N_2 and H_2-N_2O mixtures along with the analysis of the data to obtain information about the intermolecular potential is given. T_1 minimum studies and the analysis of the data to obtain the value of the effective spin-rotation coupling constant for protons in CH_3Cl are described in Chapter IV. Chapter V contains an application of a model first proposed and used by Rajan et al.[17] to evaluate the correlation time of the dominant intramolecular interaction in molecules having large moment of inertia. Using their model T_1 results (available in literature) for NH_3[25], BF_3[25], F_2[26] and HCl[27] have been analysed to find the strengths of the dominant multipole moments of these molecules. Chapter VI presents the conclusions. The circuit diagrams of various parts of the spectrometer are given in Appendix.

CHAPTER II

EXPERIMENTAL TECHNIQUES AND APPARATUS

II.1 The Method of Spin-Echoes

The nuclear spin relaxation times can be directly measured using the method of spin-echoes[28] which is described below:

Let us consider a bulk sample containing large number of nuclear spin moments placed between the pole pieces of a strong magnet. When the field $\vec{H}_o$, say in the Z-direction, is switched on, the tiny nuclear moments tend to align themselves along $\vec{H}_o$ giving rise to a state of thermodynamic equilibrium for the sample with a net macroscopic magnetization $\vec{M}_o$ along the Z axis. As described in chapter I, if a radio frequency field $\vec{H}_1$ at Larmor frequency γH_o, where γ is the gyromagnetic ratio of the spins, is applied to the sample for a time t_ω, and in a direction perpendicular to $\vec{H}_o$, the magnetization $\vec{M}_o$ is tilted away from the Z direction by an angle θ given by

$$\theta = \gamma H_1 t_\omega \qquad (2.1)$$

Intense rf pulses are used to tip the magnetization $\vec{M}_o$ through an angle θ in a time much shorter than T_1 or T_2 so that the relaxation effects while $\vec{H}_1$ is on can be neglected. In the absence of $\vec{H}_1$, $\vec{M}_o$ precesses about $\vec{H}_o$. A $\pi/2$ rf pulse applied to the sample coil whose axis is along the X direction rotates the magnetization $\vec{M}_o$ to the XY plane. Let us visualize this situation in a frame X'Y'Z' rotating with rf and where Z' and Z coincide. Following the $\pi/2$ pulse applied along positive X' direction, the magnetization $\vec{M}_o$ lies entirely along the Y' axis (Fig. 1a)[29] and sees the field $\vec{H}_o$. Thus, when looked at from the laboratory frame XYZ, it precesses about $\vec{H}_o$ but lying in the XY plane. It induces an emf in the sample coil which can be detected and observed. This signal is known as 'Free Induction Decay' (FID). Due to transverse relaxation this signal decays. The time constant of the decay in the X-Y plane would be T_2 if the field $\vec{H}_o$ is perfectly homogeneous. However, for all the practical sample sizes, which cannot be too small due to signal amplification limitations, there exists an inhomogeneity, say ΔH_o, over the sample dimensions. So the nuclear moments, in the different parts of the sample experience different fields and hence precess with different Larmor frequencies. Thus, there is a spread of precession frequencies centered at ω_o. If this situation is visualized from a reference frame rotating with frequency ω_o about Z axis,

the spins will appear to fan out since some nuclei precess faster and some slower than the frame (Fig. 1b). Thus the magnetization in X-Y plane decays in time of the order of $(1/\gamma \Delta H_o)$ due to field inhomogeneity. Application of a π pulse at time t much smaller than T_1 or T_2 after the $\pi/2$ pulse rotates the fanning out moments through 180^o about the X axis (Fig. 1c). So the phase differences produced following the $\pi/2$ pulse, due to field inhomogeneity, are reversed (Fig. 1d). The spins continue to precess in the same direction as they were before the application of the π pulse. This leads to reclustering of the tiny spin moments (Fig. 1e) at a time $t = 2\tau$ after the $\pi/2$ pulse and a maximum signal is built up in the coil which decays again due to same reasons given above. This second signal is known as 'spin-Echo'.

Though the free induction decay can also be used to measure T_1, the spin-echo has got, from experimental point of view, several advantages few of which are: (i) the π and $\pi/2$ pulses are off during the time the echo is observed. The observed signal is, therefore, free from the interference due to the pulses, (ii) when the echo appears the receiving system has already recovered from saturation and other effects produced by intense rf excitation pulses and stands ready to normally receive the signal.

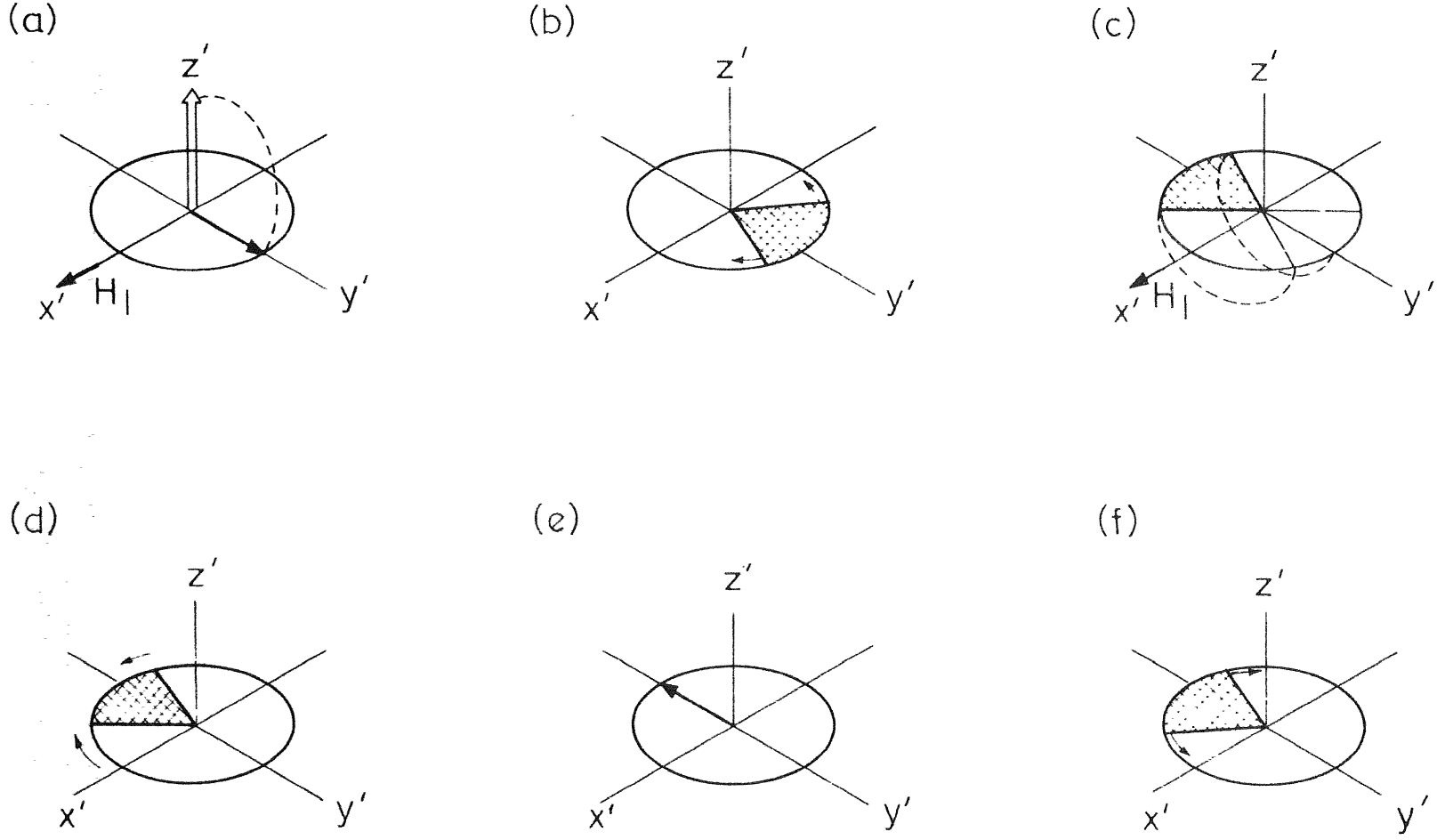

Fig. 1 Echo formation following a $\pi/2$-τ-π sequence.

II.2 Measurement of Spin-Lattice Relaxation Time T_1

Measurement of T_1 by the pulse technique[1,28] is described here briefly.

Bloch's[30] equation predicts that the growth of magnetization along the Z-axis would be given by (see eq.(1.20)

$$M_z(t) = M_o + [M_z(0) - M_o] \exp(-t/T_1) \qquad (2.2)$$

where M_o is the equilibrium magnetization. From this equation it is seen that a plot of $\log [M_o - M_z(t)]$ versus t gives a straight line with a negative slope equal to $1/T_1$. Therefore, experimentally, T_1 can be measured by first disturbing the system from equilibrium and then monitoring the growth of the Z-component of the magnetization as a function of time. $[M_o - M_z(t)]$ can be measured by applying a proper combination of π and $\pi/2$ pulses. Two different pulse sequences were used, for convenience, in the present work to measure short and long T_1. The procedure is described below:

(i) Measurement of Short T_1 ($T_1 < 0.1$ sec, as for H_2-Ar, H_2-N_2 and H_2-N_2O mixtures)

In this case a π-t-$\pi/2$-t'-π pulse sequence was used. The first π pulse tipped the magnetization M_z to the negative Z direction and its growth from $-M_o$ to $+M_o$ along the Z axis was monitored by the $\pi/2$-t'-π pulse sequence

applied at a time t after the first π pulse. t' was kept constant ($\sim$0.5 msec) throughout the experiment so that the amplitude of the echo is proportional to the value of M_z preceding the $\pi/2$ pulse whereas t was varied continuously. M_z for $t \geq 10\ T_1$ was taken to be the value of M_o. The π-t-$\pi/2$-t'-π pulse sequence was repeated after every time interval T_{rept} which was taken to be about $10T_1$ ($T_{rept} \geq 10T_1$) to ensure that the spins relax and attain equilibrium in between the successive repetitions and after every repetion, i.e. for a new value of t, $M_z(t)$ starts growing from $-M_o$. The time t between the first π pulse and $\pi/2$ pulse was measured with a Beckmann Model 7370 counter. In order to improve the signal to noise ratio a Boxcar integrator Model No. CW1 of Princeton Applied Research was used to sample the detected output from the receiver. The Boxcar was triggered by the $\pi/2$ pulse and the sampling gate width of the Boxcar was adjusted to sample the echo height. To avoid any possible integration distortion effects of the Boxcar integrator, the time t between the first π pulse and $\pi/2$ pulse was swept very slowly and the integration time constant RC of the Boxcar integrator was chosen to satisfy the following relation[31] between the repetition rate, T, of the pulse sequence and the sampling gate width, t_s, of the Boxcar

$$\frac{T}{t_s}\ RC << \propto T_1 \qquad (2.3)$$

where α is the inverse of the rate at which the separation t between the first π pulse and $\pi/2$ pulse was varied and T_1 is the spin-lattice relaxation time of the sample used. The output of the Boxcar, which gives the magnitude of the echo and hence the recovery of M_z, was plotted on a Bausch and Lomb strip chart recorder Model VOM6. The M_z values at different times were identified by using an event marker on the recorder. T_1 was obtained by plotting $\log[M_o - M_z(t)]$ versus t.

Here it should be noted that if the interval t between the first π pulse and $\pi/2$ pulse is varied not continuously but in steps manually, the relation given by eq. (2.3) need not be satisfied. But in that case one has to wait for a long time before changing over to a new t till a large number of repetitions with the same interval between the first π and $\pi/2$ pulses enter the Boxcar and the Boxcar shows a steady output.

(ii) Measurement of long relaxation times T_1 ($T_1 > 0.1$ sec as for CH_3Cl)

If T_1 is measured according to the scheme written in (i) above, one has to wait for a long time of the order of $10T_1$ between any two successive π-t-$\pi/2$-t'-π pulse sequences. For long T_1 it is a time consuming process and, to save experimentation time, the following technique[32] was used to measure T_1:

Here the pulse sequence [$\pi/2$ burst]-t-$\pi/2$-t'-π was used. The $\pi/2$ pulses in the burst brought the magnetization M_z to 0 and the growth of M_z from 0 to $+M_o$ was monitored by the $\pi/2$-t'-π pulse sequence. The height of the echo following the π pulse was measured and it gave the value of $M_z(t)$ just before the $\pi/2$ pulse. To ensure that M_z really started growing from zero a large number ($\sim$100) of $\pi/2$ pulses (a $\pi/2$ burst) were applied in a time (duration of the burst) much smaller than T_1 or T_2. t' was kept constant and t was varied from 0 to about $10T_1$. The value of $M_z(t)$ for $t \geq 10T_1$ was taken to be the value of M_o. It should be noted that the spin system need not go to equilibrium before each pulse sequence. Since the $\pi/2$-burst serves to ensure that no Z component of magnetization remains, it can be applied immediately after the echo and thus the [$\pi/2$ burst]-$\pi/2$-π sequence is repeated after a time interval much smaller than $10T_1$.

The measurement of time t and recording of the signal was done exactly in the same way as described in (i) for the measurement of short T_1. The plot of log $[M_o-M_z(t)]$ versus t is again a straight line with a negative slope equal to $1/T_1$.

II.3 The Spin-Echo Apparatus

(i) General remarks

The spin-echo spectrometer built by Rajan et al.[17,34] based on the standard techniques as described by Hahn[28] and

Clark[33] was used in the present work. It has an operating frequency of 30 MHz and makes use of phase sensitive detection. The timing circuit of the spectrometer which usually gave $\pi-\pi/2-\pi$ pulse sequence was, however, modified to give the pulse sequence [$\pi/2$ burst]$-\pi/2-\pi$ also. Thus, the spectrometer could be used to measure short as well as long relaxation times. Circuit details are given in Appendix. A block diagram of the spectrometer is shown in Fig. 2. The major items are described below briefly.

(ii) Timing Circuit and the pulse sequencer

(a) $\pi-\pi/2-\pi$ Pulse sequence

This pulse sequence was generated by using a combination of the following three units: (i) a waveform generator Tek 162 (shown as unit 1 in the Fig. 3), (ii) a pulse generator Tek 163 (unit 2), and (iii) another waveform generator Tek 162 (called as slow-sawtooth generator and shown as unit 3 in the Fig. 3) which is similar to the waveform generator stated above in item (i) but modified to give a slow running sawtooth. A block diagram of the pulse programmer is shown in Fig. 3.

The waveform generator (unit 1) operated in recurrent mode produced (i) a triggering pulse, at a changeable repetition rate, which was used to produce the first π pulse and (ii) a sawtooth. The sawtooth started running down at the

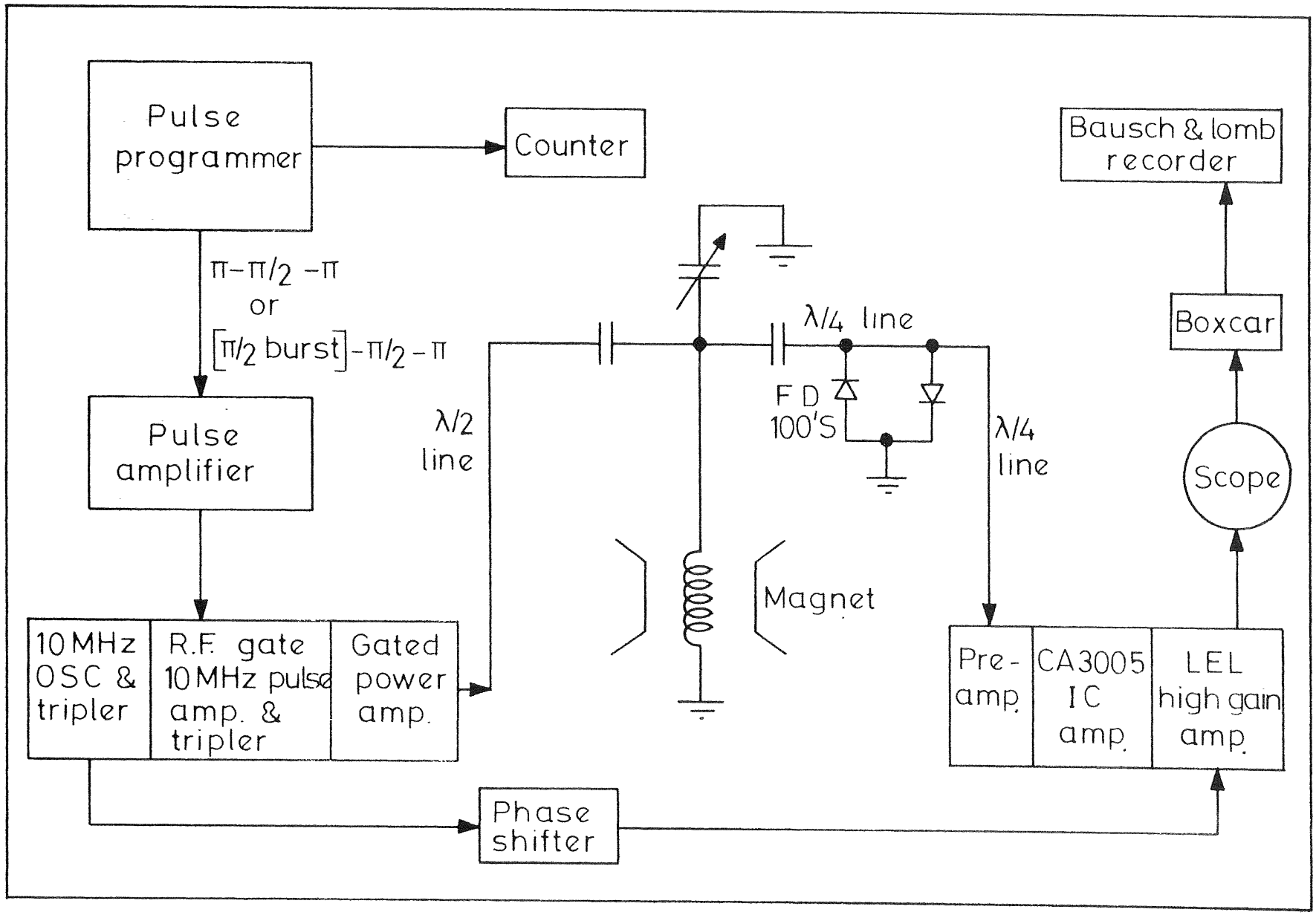

Fig. 2 Block diagram: spin-echo spectrometer.

same time when the pulse began and had a width equal to the interval between the triggering pulses. This sawtooth was used to trigger the pulse generator (unit 2) which, within the duration of the sawtooth, gave a pulse of adjustable width and height at a time depending upon its triggering level which can be adjusted manually as well as by the help of an external sawtooth. The slow-running sawtooth from the slow-sawtooth generator (unit 3) was used to serve this purpose. By using the slow-sawtooth it was possible to change the triggering level and hence the time between the first π pulse and the pulse from the pulse generator (unit 2) continuously. A reset mechanism was incorporated in the slow-sawtooth generator to enable one to stop and start the rundown at any time instead of waiting for the rundown to be completed of its own.

The pulse from the pulse generator (unit 2) was taken to a pulse sequencer (Fig. A1) to produce two pulses whose separation was controlled by the pulse width of the input pulse. The pulse from the waveform generator (unit 1) and the second pulse from the pulse sequencer were added together in a mixer circuit. These two pulses were, then, taken to the 180° channel of the pulse width generator whereas the first pulse from the pulse sequencer went to the 90° channel of the pulse width generator.

(b) [π/2 burst]-π/2-π Pulse sequence

In this case a collection of Tektronix waveform generators Tek 162 and pulse generators Tek 161 and Tek 163 were used. A block diagram of the pulse programmer is shown in Fig. 4. Positive pulses from the waveform generator Tek 162 (unit 1 in Fig. 4) operated in recurrent mode trigger the pulse generator Tek 163 (unit 2) which gives pulses of adjustable height and width. These in turn trigger another waveform generator Tek 162 (unit 3) to give sawtooths of changeable duration that are fed to a pulse width generator (unit 4). Its delayed pulse output was used to gate another waveform generator (unit 5) which gave a burst of very short pulses during the gating period. The number of pulses in the burst can be adjusted by changing the duration of the gate as well as the repetition rate of this unit. The pulse from the pulse generator (unit 2) was taken to pulse sequencer (Fig. A1) to produce two pulses whose separation was controlled by the pulse width of the input pulse. The burst of short pulses from the last waveform generator (unit 5) and the first pulse from the pulse sequencer were added together in a mixer circuit (Fig. 4) and then given to the 90° channel of the pulse width generator while the second pulse from the pulse sequencer was given to the 180° channel. The time t between the π/2-burst and the π/2 pulse was changed by changing the repetition rate of the unit 1.

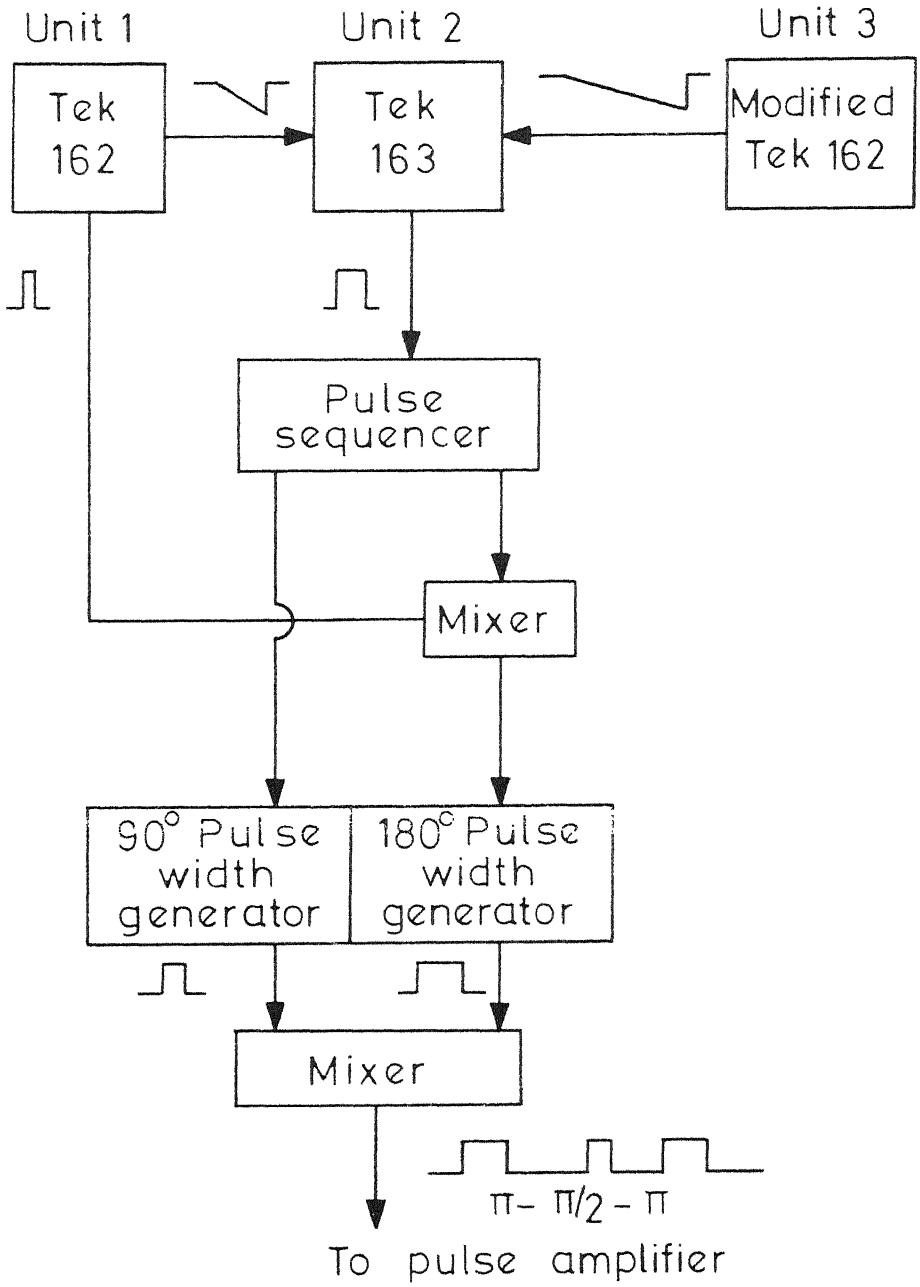

Fig. 3 Block diagram: pulse programmer for producing $\pi - \pi/2 - \pi$ pulse sequence.

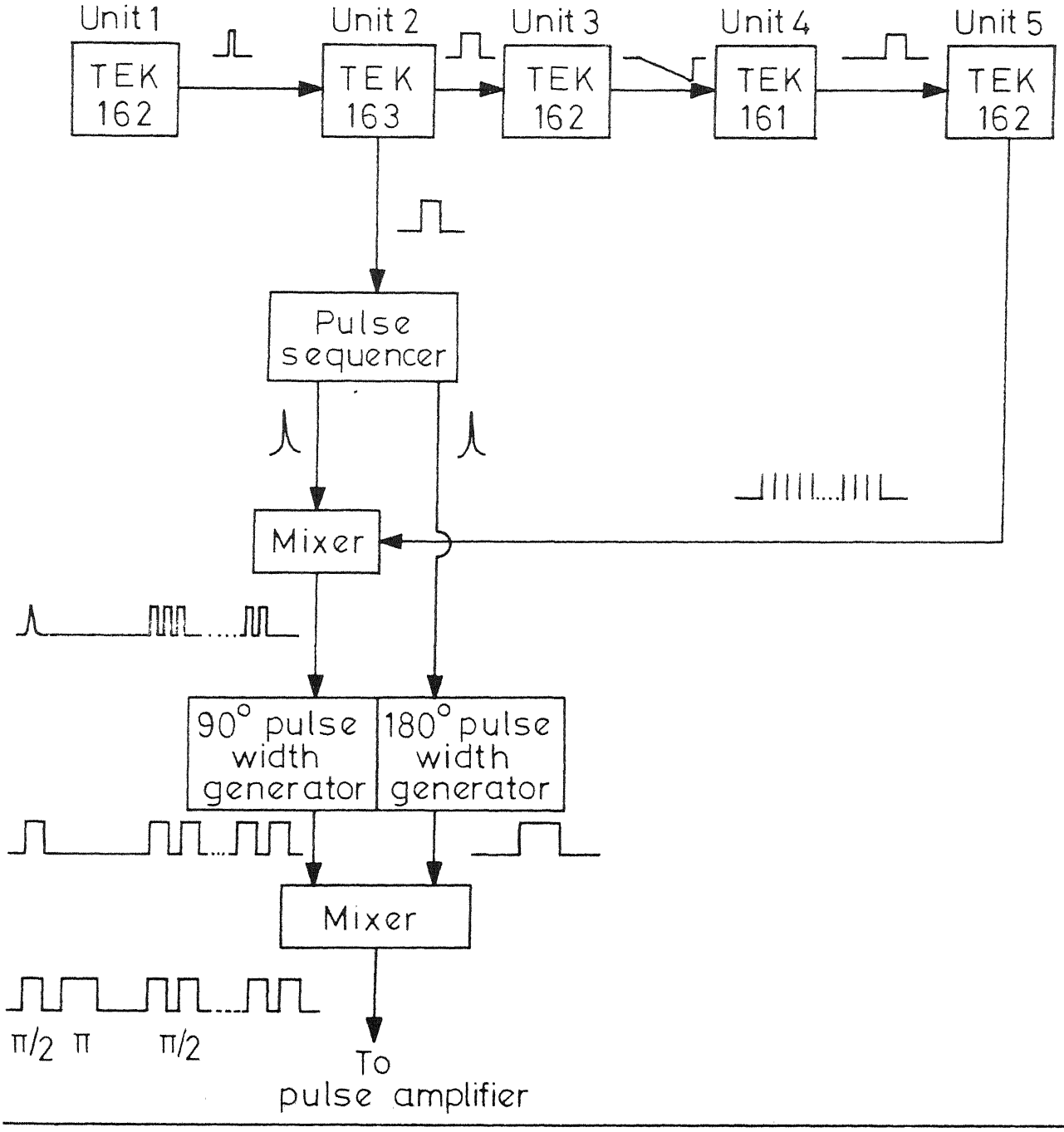

Fig. 4 Block diagram: pulse programmer for producing [π/2 burst] - π/2 - π pulse sequence.

The two 90° and 180° channels of the pulse width generator (Fig. A2) were identical and were designed using phantastron circuits. The range of the pulse width could be varied from 0-70 μsecs continuously (which can be further increased by changing RC appropriately). These pulses were amplified in a pulse amplifier (Fig. A3) and then sent to the transmitter to gate it.

(iii) Transmitter

The transmitter was designed to deliver high pulsed power output at 30 MHz with short rf rise and fall times. Class C operation was preferred in certain stages to meet the power requirements. A crystal controlled oscillator (Fig. A4) at 10 MHz, housed in a rf leak tight copper can, was used as a source generator. The 10 MHz source signal was gated by the pulses from the pulse amplifier using a triode 7077 and then amplified (Fig. A5). The amplified output was trippled (Fig. A6) and then further amplified by a push-pull stage. The output from the push-pull stage was fed to the final power stage at 30 MHz (Fig. A7). The power amplifier produced reasonably rectangular rf pulses of 1200 volts peak-to-peak amplitude.

To make use of the phase sensitive detection the following arrangement was done. The output from the master oscillator was passed through a phase-shifter Ad-Yu

type 559 m which was a commercial delay line and produced a delay of 0.4 μsecs. The delayed output was passed through a trippler (Fig. A8) and then coupled to the last stage of the high gain L.E.L. amplifier in the receiver part of the spectrometer for phase sensitive detection.

(iv) Receiver

The voltage level of the signal induced in the sample coil was first raised by using a preamplifier (Fig. A9) which was similar to the design by Clark[33] and makes use of tube 7722. The voltage gain of the preamplifier was about 10 and the output impedance about 80 ohms. The signal was further amplified by an RCA 3005 integrated rf amplifier having a power gain of 25 db and output and input impedances of 50 ohm. The circuit of the integrated amplifier is shown in Fig. A10. The design was taken from the RCA application note ICAN-5022. The amplified NMR signal was, then, fed to the receiver which was a L.E.L. amplifier of the Varian Associates, model No. 1MN2-30-15-50, having a centre frequency of 30 MHz, 3 db bandwidth of 10 MHz and input impedance of 50 ohms. One of the two output terminals provided in the L.E.L. amplifier lies just after the detection and has a gain of 90 db maximum while the other one is after a video stage and has a gain of 115 db minimum at 0 volt bias.

The L.E.L. amplifier used a 1N295A diode detector. Ordinary diode detection is not linear over the entire region and the non-linearity becomes important while dealing with small signals. However, a diode detector can be made to operate in the linear region by using phase sensitive detection. In phase sensitive detection the diode detects the sum of reference voltage that biases it and the signal. So using the phase sensitive detection the diode detector of the L.E.L. amplifier was made to operate in the linear region by choosing the reference voltage properly so that the operating point fell in the linear region. To find the proper biasing (reference) voltage for the diode an experiment was performed. For a given setting of the spectrometer, the reference voltage was varied and the output signal level was recorded each time. The output signal strength was plotted as a function of reference voltage (Fig. 5). From the Fig. 5 it is seen that the reference voltage biasing the diode detector must be kept between -1.5 and -2.5 volts for linear detection. To avoide distortion the signal input to the diode detector was kept below 1/10 of the reference voltage.

(v) Sample coil, sample holder and the gas handling system

The spectrometer makes use of a single coil which optimizes the transmitting and receiving modes. The schematic

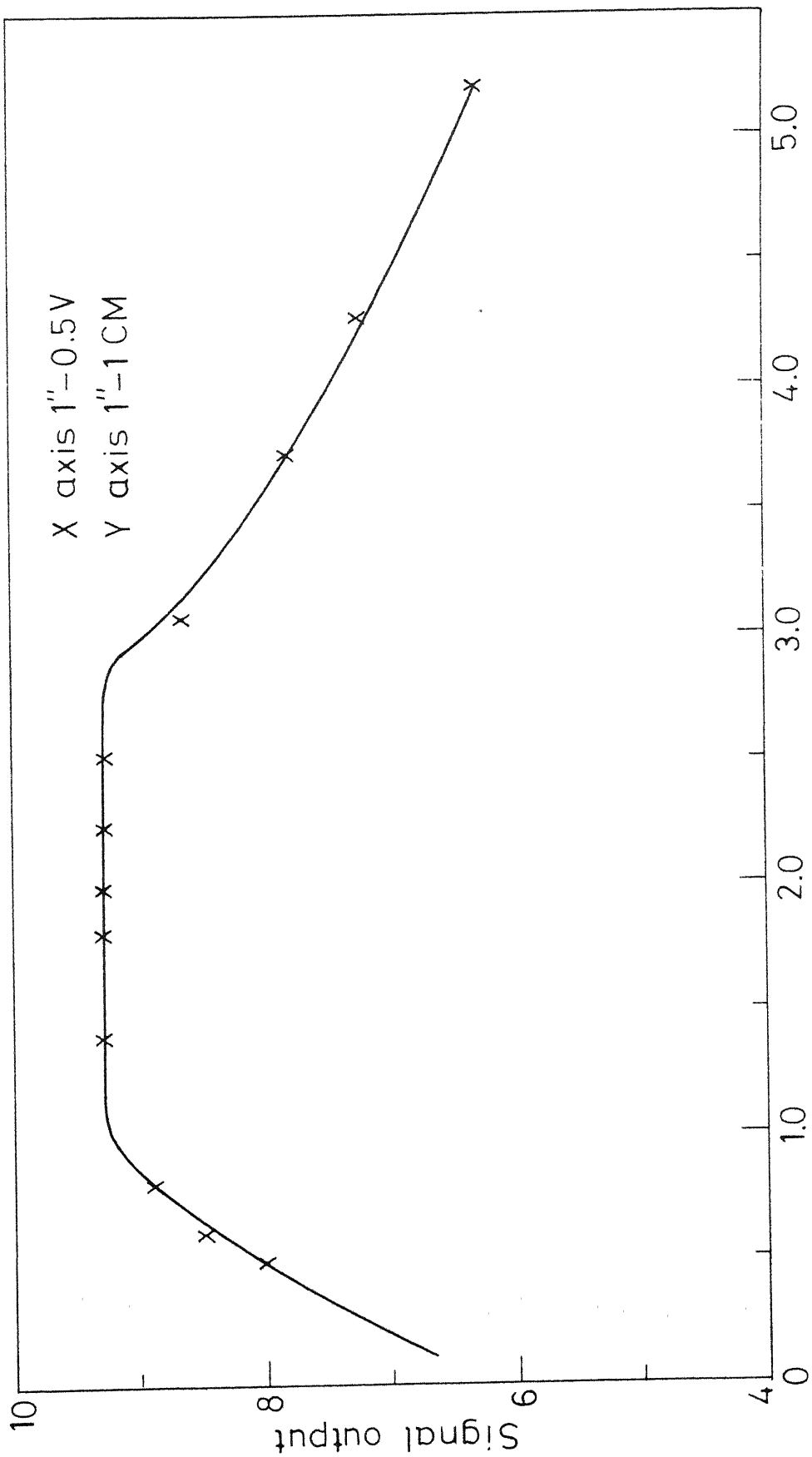

Fig. 5 Diode detector response.

of the spectrometer containing the sample coil is shown in Fig. 6. Depending upon the two different types of measurement in the present work, two separate sample coils were used: one for CH_3Cl where the measurements were confined in the low density region ($0.2 < \rho < 6.5$ amagats) at room temperature and the other for T_1 measurements in the hydrogen-mixtures in which case the densities of the mixtures went as high as 70 amagats and the temperature varied from 300K to 600K. In order to improve the signal to noise ratio for weak signals in the low density region a sample coil of bigger dimensions was made. The sample holder carrying this bigger coil did not leave any space between the pole pieces of the magnet to incorporate a heater. So, for high temperature work (H_2 mixtures), a smaller sample holder was used. The details of the coils and sample holders are given below.

(a) <u>For measurements at low pressures</u> (<u>CH_3Cl as sample</u>)

The coil used in this case was of length 3.5" and diameter 0.8" and consisted of 14 turns of 18 SWG copper wire. The enamel insulation was completely stripped off and the wire was thoroughly cleaned before use. The coil was housed in a sample holder (Fig. 7) made of a thick-walled Be-Cu vessel (1.5" o.d., 1" i.d.) with brass plug A sealed to the vessel with a teflon washer. A glass tube which could fit between the coil and the wall of the sample

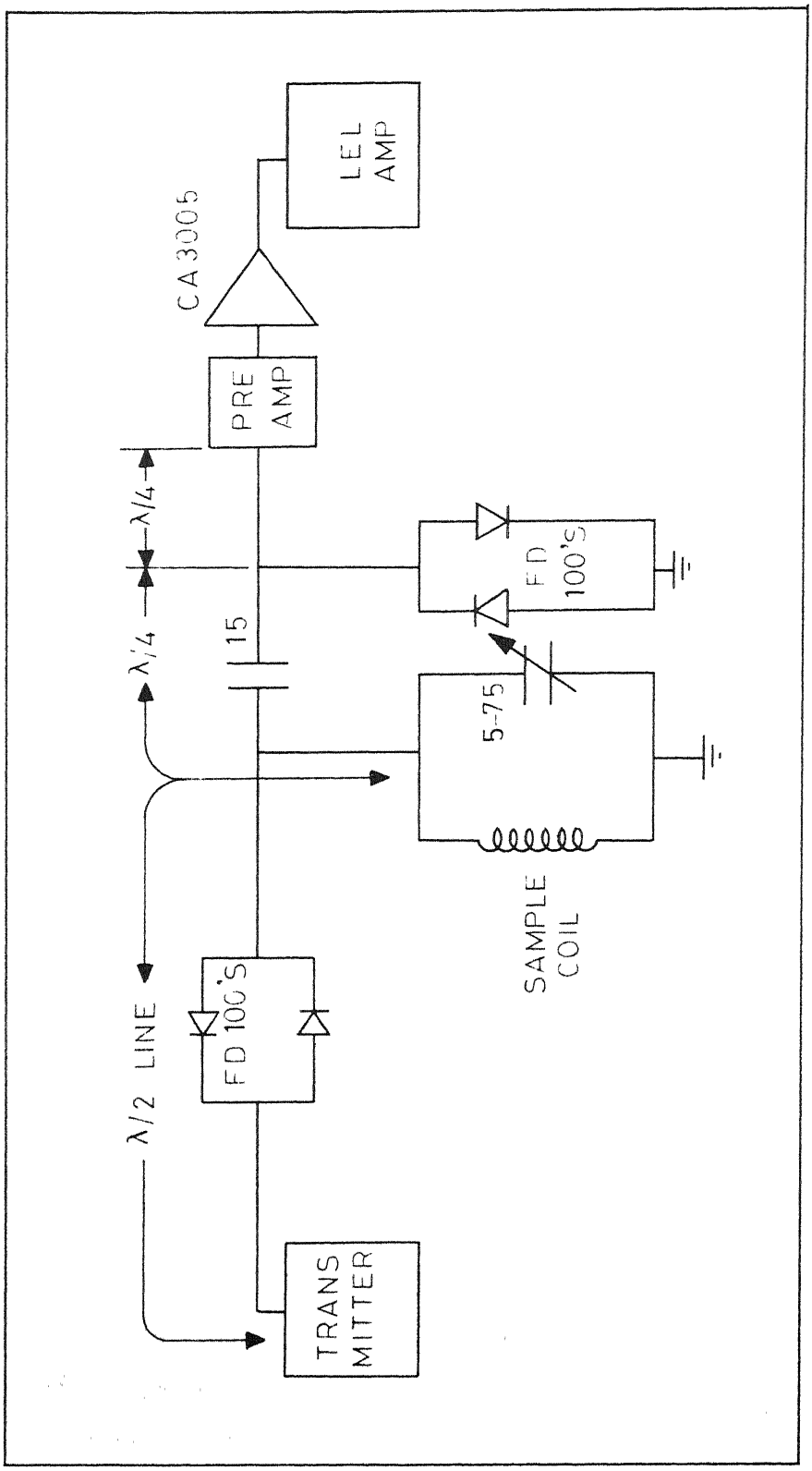

Fig. 6 Schematic : coupling of RF head.

holder was used to insulate the coil from the sample holder. After fixing the return end of the sample coil to the plug A with a screw, the glass tube was put in position such that the other end of the coil came out through the small central hole of the tube as shown in Fig. 7. This end was taken out through a 1/8" bore in the plug B. Thin glass capilliary tubes were used to insulate the wire from the body of the plug. The plug B was then tightened to make pressure seal. The rf head was sealed against pressure using teflon washer. The lead of the coil coming out of the rf head was soldered to a BNC connector.

(b) For measurements at high pressures (H_2 mixtures as sample)

A sample holder made by Rajan et al.[17] was used in this work. The coil was of length 3.8 cm and 0.8 cm diameter and consisted of 15-16 turns of a cleaned 20 SWG copper wire. It was housed in a thick-walled Be-Cu vessel (o.d. 2.7 cm and i.d. 1 cm) with plugs A and B (Fig. 8) sealed to the vessel by using the technique of AE cone fitting. First the return lead of the sample coil was screwed to the plug B. Then B was sealed in its position by tightening the nut E. The other end of the coil was taken out through a bore in A and A was then tightened to make a pressure seal. The rf head was sealed against pressure at room temperature using teflon washer. Glass tubes were used to insulate the coil from the

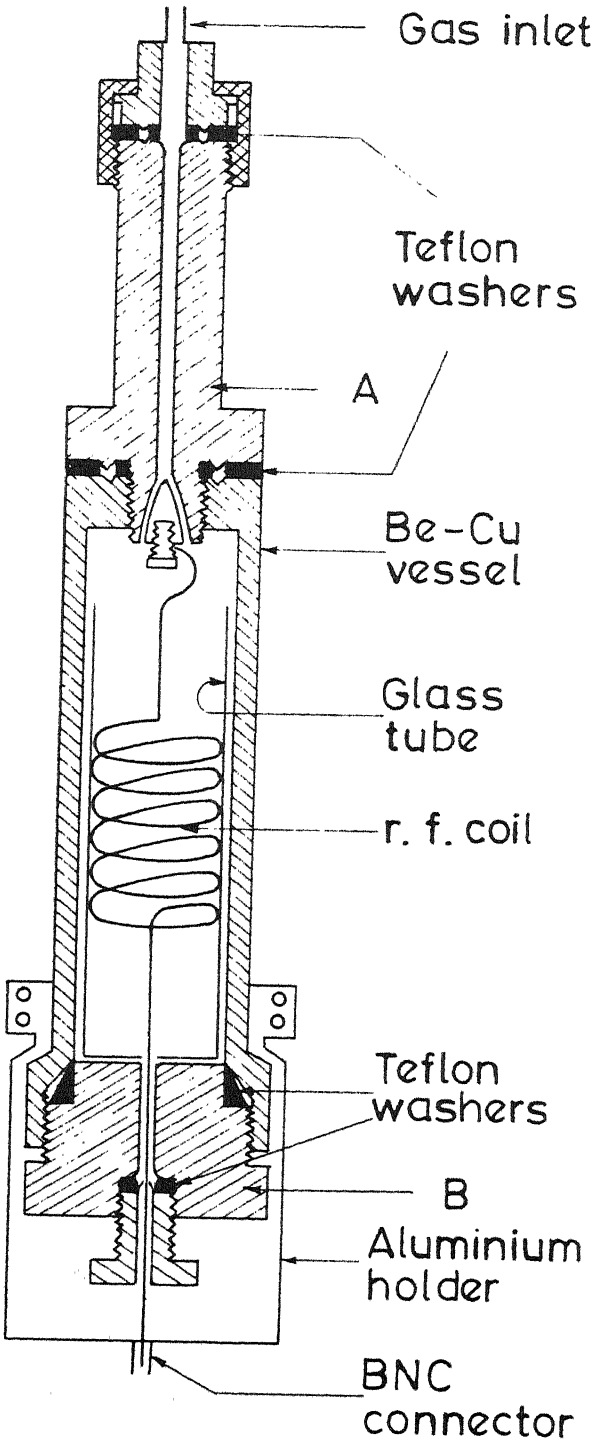

Fig. 7 Sample holder used for CH_3Cl.

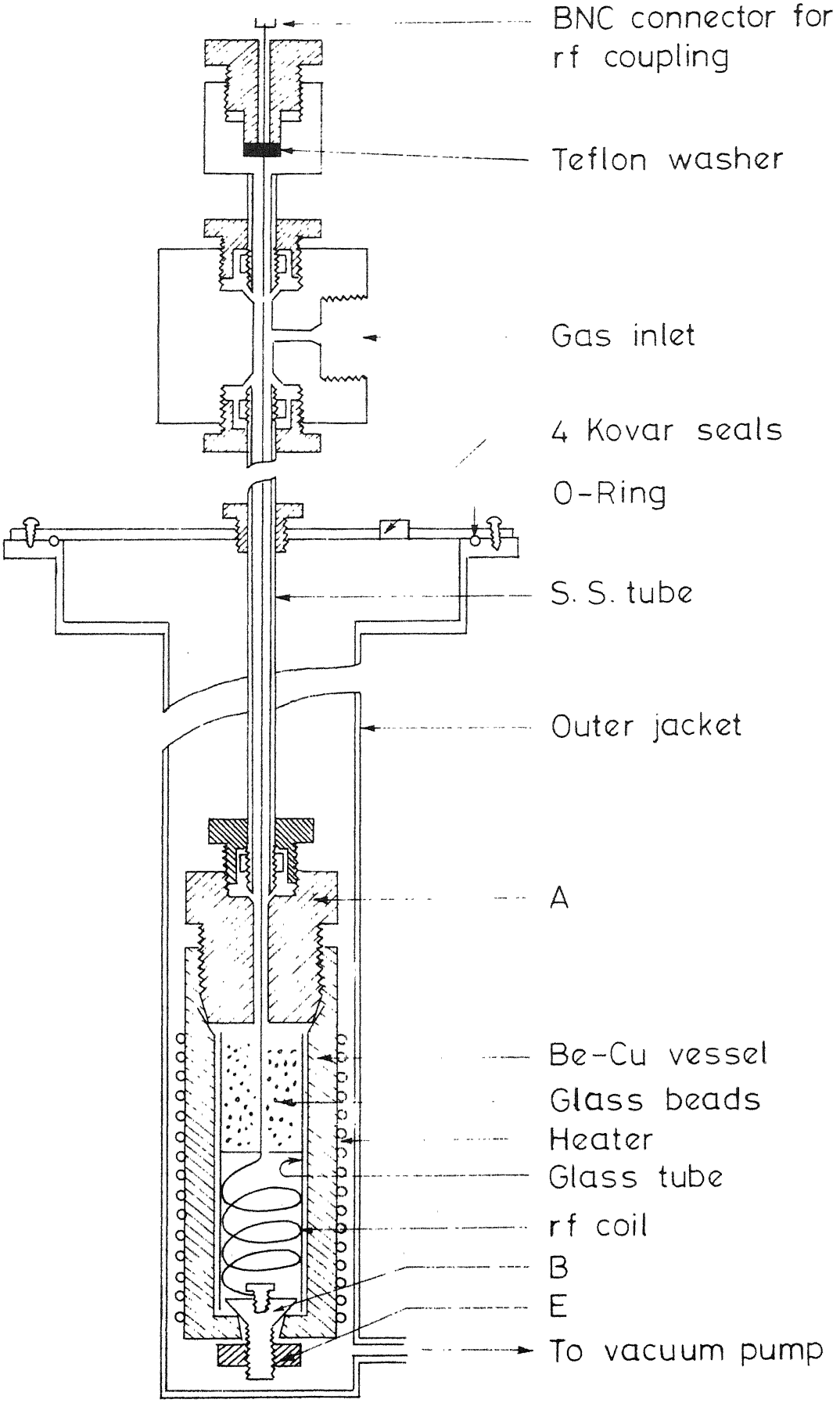

Fig. 8 Sample holder used for H_2 mixtures.

sample holder exactly in the same manner as described in the preceding paragraph in (a).

Pressures above 4 PSIG were measured with Bourdon pressure gauges which were calibrated using a dead weight gauge and below 4 PSIG were measured with a mercury manometer. In the experiments with CH_3Cl the use of rubber was totally avoided since CH_3Cl reacts with rubber.

The schematic of the gas handling system is shown in Fig. 9.

(vii) Temperature measurements

(a) Above room temperature

High temperature work was done only with the smaller sample holder shown in Fig. 8. A commercial 1000 watts non-magnetic spiral heater element was wound on its outside non-inductively. The heater was insulated from the body of the sample holder by a thin mica sheet. The windings of the heater were held in place by using a liquid porcelain called 'sauereisen'. D.C. was used to heat the sample holder since small 50Hz noise was observed when A.C. was used. The high-pressure vessel along with the heater was kept inside a vacuum jacket to keep the convection and conduction current losses to a minimum. In order to maintain the sample holder at 600K about 120 watts of electrical power had to be

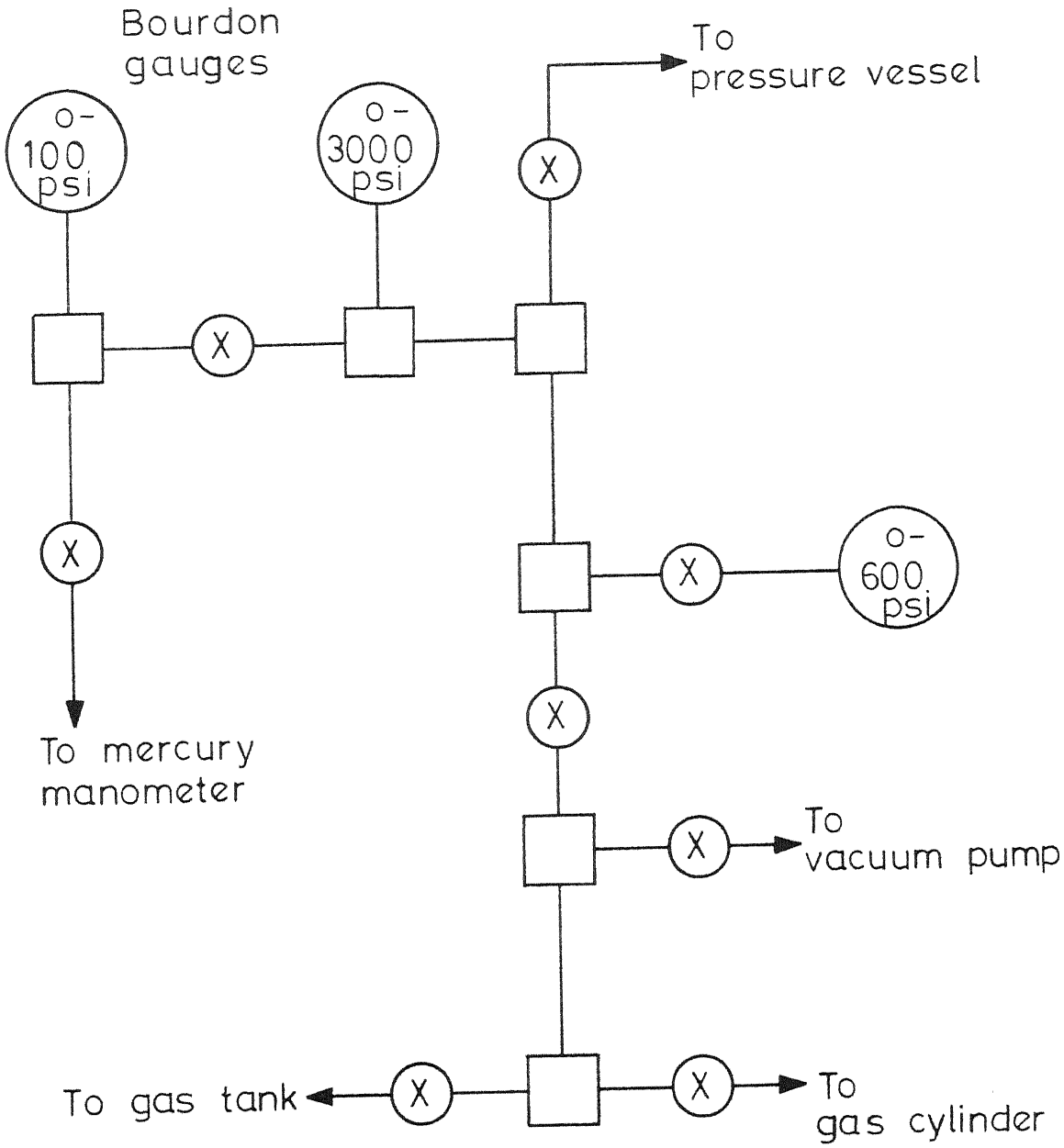

Fig. 9 Gas handling system.

dissipated. The leads from the heater (and the thermocouple also) were taken outside the vacuum jacket through Kovar seals.

A Chromel-Alumel thermocouple was fixed away from the heater on the top plug of the sample holder to measure the temperature. The temperature measurement was done with a Honeywell potentiometer model 2705B which gave an accuracy of $\pm 1^{\circ}$. No special effort was made to control the temperature automatically because once the current was adjusted the temperature was steady within a degree after reaching equilibrium. However, at least 8-10 hours were allowed before starting the T_1 measurements to ensure that the sample was at equilibrium with the sample holder.

(b) Below room temperature

The temperatures in the range 300-200K were produced by using a brine, spirit+liquid nitrogen, the temperature of which depends upon its composition. The more is the liquid nitrogen, the lower is the temperature. Hence by varying the composition a range of temperature from room temperature to the freezing point of spirit can be achieved. The sample holder was put in a Dewar flask filled with the brine and the flask was covered with glass-wool. When the system had attained equilibrium a temperature variation of only 0.5 degrees per hour was observed. The temperature was measured by the Chromel-Alumel thermocouple as described in the preceding paragraph.

(viii) Preparation of sample

(a) Purity of gases

H_2, N_2 and N_2O used in the present work were of research grade and were obtained from Matheson Gas Co. Argon was obtained from Indian Oxygen Ltd. and was of 99.99 percent purity. Methyl chloride gas was supplied by Mettur Chemicals, India and was of 99.95 percent purity. However, it was suspected from the measurements that CH_3Cl contained some impurities. So it was further purified in the following way:

CH_3Cl gas cylinder was connected to a 20 ft. long $\frac{1}{2}$" i.d. copper tubing packed with Zeolite molecular sieve[51] (3A, appropriate for absorbing oxygen and water vapour) and which was made into a coil of 1 ft. diameter. The other end of the coil was connected to a stainless steel container through pressure valves. The copper tubing and the container were thoroughly evacuated. CH_3Cl gas was, then, passed through the copper tubing very slowly and stored in the container. The molecular sieves were regenerated in the beginning as well as intermittantly after some time intervals much shorter than the saturation time of the sieves by heating the coil to 150°C and then cooling it. During the process of regeneration, gas flow was stopped and the coil was continuously evacuated. The oxygen free gas, stored in the container, was further purified by freezing it.

To do this the stainless steel container was put in a dewar containing ethyl alcohol + liquid nitrogen mixture. The composition of the mixture was adjusted to maintain its temperature around -40°C, a temperature below the boiling point of CH_3Cl. The residual gases in the container were pumped out. The container was further cooled to -132°C, a temperature below the melting point of CH_3Cl by adding more liquid nitrogen to the cooling mixture simultaneously pumping out the residual gases from the container. The container having a high purity solid CH_3Cl was then brought to room temperature.

(b) Mixing of gases and composition determination

A mixture H_2-X, where X is Ar, N_2 or N_2O, was prepared in a separate container. First the container was filled with the low concentration component to a pressure which would give approximately the required composition at the total pressure of the container. Then the high concentration component was introduced to bring the total pressure to the desired value. The composition of the mixture was estimated from the partial pressures and was checked by comparing the signal strength (echo-height) of the mixture with that of pure H_2 under identical conditions of pressure, temperature and spectrometer adjustments.

The signal strengths for pure H_2 and H_2-X mixture were corrected for T_2 effects. The height of the spin-echo A (2t'),

where t' is the time between the $\pi/2$ and π pulses, is given by[35]

$$A(2t') = A(0) \exp\left[-\frac{2t'}{T_2}\right] \qquad (2.4)$$

where diffusion effects have been neglected. In terms of the amagat density ρ where an amagat is 2.69×10^{19} molecules/cc, A(0) can be written as,

$$A(0) = C\rho \qquad (2.5)$$

with C as a constant depending upon the number of spins per molecule and temperature. At high densities it can be shown that

$$T_1/\rho = T_2/\rho \qquad (2.6)$$

and eq. (2.4) reduces to

$$A(2t') = C\,\rho \exp(-2t'/T_1) \qquad (2.7)$$

or

$$C\,\rho = A(2t') \exp(2t'/T_1) \qquad (2.8)$$

Thus the quantity $\frac{(C\rho)_{\text{mixture}}}{(C\rho)_{\text{Pure } H_2}}$ gives the fractional concentration of H_2 in the mixture.

It should be noted, as is clear from the eq. (2.7), that for the samples where $T_1 >> 2t_1$, $A(2t') \sim C\,\rho$ but for the cases such as H_2 where $T_1 \sim 2t'$, the exponential factor called the 'T_2 correction' is important.

CHAPTER III

PROTON SPIN-LATTICE RELAXATION IN H_2-Ar, H_2-N_2 AND H_2-N_2O MIXTURES

III.1 General Remarks

The internal degrees of freedom of a H_2 molecule correspond to (i) the electronic (orbital and spin), (ii) vibrational, (iii) rotational and (iv) the nuclear spin states. Since only the ground electronic and vibrational states are occupied up to a temperature 1000K, the H_2 molecule can be considered, below this temperature, as a rigid rotor having an additional degree of freedom corresponding to the nuclear spin states. Thus, the state of H_2 molecule can be described by the rotational quantum number J, m_J and nuclear spin quantum numbers I, m_I.

Further, from the requirement that the total wavefunction of the hydrogen molecule be antisymmetric with respect to the interchange of the two protons, it is concluded that, in general, hydrogen gas consists of two types of molecules, one having the spins of the two nuclei parallel (total spin I=1) and occupying the odd rotational states (J = 1, 3, 5 etc.) and the other having the nuclear spins antiparallel (total spin I=0) and occupying the even rotational states (J = 0, 2, 4 etc.). These two are called

ortho and para modifications respectively. The number of molecules occupying a J state is given by the Boltzmann distribution

$$P_J = g_J \exp(-E_J/kT) \tag{3.1}$$

where P_J is the fraction of the total number of the molecules in the gas occupying the J state, k is the Boltzmann constant and T is the absolute temperature. g_J is the degeneracy of the states

$$g_J = (2I+1)(2J+1) = 3(2J+1) \text{ for } I=1, \text{ i.e. } J \text{ odd (ortho-}H_2\text{)}$$
$$= (2J+1) \text{ for } I=0, \text{ i.e. } J \text{ even (para-}H_2\text{)} \tag{3.2}$$

$$E_J = \frac{J(J+1)\hbar^2}{2I_o} = J(J+1)\, k\theta_R \tag{3.3}$$

and is the energy of the J state. Here I_o = moment of inertia of the H_2 molecule, $\hbar$ = Plank's constant.

$$\theta_R = \frac{\hbar^2}{2I_o k} = 85.3^\circ K \text{ for } H_2 \tag{3.4}$$

The values of P_J for different temperatures are given in table 3.1.

The ratio of ortho- to para-molecules in a sample of hydrogen at thermal equilibrium is given by

$$r = \frac{\sum_{J=odd} 3(2J+1) \exp[-J(J+1)\theta_R/T]}{\sum_{J=even} (2J+1) \exp[-J(J+1)\theta_R/T]} \tag{3.5}$$

Table 3.1. Fractional population of the rotational states for H_2

Temp. K	100% ortho-H_2				100% para-H_2			
	J=1	J=3	J=5	J=7	J=0	J=2	J=4	J=6
150	0.9922	0.0078			0.8584	0.1415		
164	0.9871	0.0129			0.8175	0.1822		
170	0.9848	0.0152			0.8021	0.1976		
185	0.9770	0.0230			0.7588	0.2405		
200	0.9650	0.0350			0.7200	0.2800		
225	0.9499	0.0500			0.6584	0.3385	0.0003	
246	0.9316	0.0682			0.6116	0.3830	0.0054	
250	0.9283	0.0714	0.0003		0.6041	0.3899	0.0059	
267	0.9121	0.0875	0.0004		0.5708	0.4205	0.0087	
300	0.8790	0.1190	0.0020		0.5170	0.4680	0.0150	
350	0.8278	0.1688	0.0033		0.4489	0.5200	0.0309	0.0002
400	0.7780	0.2140	0.0080		0.3970	0.5520	0.0502	0.0007
425	0.7536	0.2363	0.0100	0.0001	0.3752	0.5627	0.0610	0.0011
450	0.7305	0.2561	0.0133	0.0001	0.3557	0.5704	0.0723	0.0016
500	0.6880	0.2900	0.0220	0.0003	0.3220	0.5800	0.0960	0.0030
600	0.6130	0.3430	0.0420	0.0014	0.2710	0.5780	0.1420	0.0090

$$P_J = \frac{3(2J+1)\exp\left[-J(J+1)85.3/T\right]}{\sum_{J_{odd}} 3(2J+1)\exp\left[-J(J+1)85.3/T\right]}$$

$$P_J = \frac{(2J+1)\exp\left[-J(J+1)85.3/T\right]}{\sum_{J_{even}} (2J+1)\exp\left[-J(J+1)85.3/T\right]}$$

From the above expression it is seen that at temperatures $T >> \theta_R$, $r \to 3$, i.e. about 75% of the total number of molecules in the sample are ortho-molecules and the rest are para-molecules. As $T \to 0$, $r \to 0$, i.e. as the temperature goes down the ortho molecules get converted to para form. But this conversion does not occur so quickly because the probability of transition of ortho-H_2 to para-H_2 which involves change of total nuclear spin is very small and it takes a time of the order of years for the equilibrium to be established between the ortho- and para-forms. Therefore, normal H_2 gas is considered as a mixture of two separate gases, namely, ortho-H_2 and para-H_2. A mixture H_2-X, thus, should be treated as a mixture of three species, viz. ortho-H_2, para-H_2 and X.

If ρ_{H_2} and ρ_X is the number of H_2 and X molecules per unit volume respectively and ρ_0 and ρ_p represent the number densities of ortho- and para-H_2 then the density, ρ_T, of the mixture is given by

$$\rho_T = \rho_{H_2} + \rho_X \tag{3.6}$$

where
$$\rho_{H_2} = \rho_0 + \rho_p \tag{3.7}$$

The fractional densities of the components in the mixture can be defined as

$$\tilde{\rho}_X = \frac{\rho_X}{\rho_T} ; \quad \tilde{\rho}_{H_2} = \frac{\rho_{H_2}}{\rho_T} ; \quad \tilde{\rho}_0 = \frac{\rho_0}{\rho_T} \tag{3.8}$$

and for normal H_2

$$\tilde{\rho}_0 = (3/4)\,\tilde{\rho}_{H_2} \qquad (3.9)$$

Only the ortho-H_2 molecules give NMR signal since the para-H_2 does not have a nuclear spin moment. A sample containing N number of H_2 molecules gives a signal having the strength proportional to $\frac{3}{4}NI(I+1) = \frac{3}{2}N$.

III.2 Review of the Theory

The theory of nuclear spin relaxation in H_2 and its mixtures is given in detail elsewhere[1,10] and references cited therein. Bloom and Oppenheim have obtained expressions for the relaxation rates explicitly in terms of the intermolecular interactions by expressing the correlation function of the intramolecular interactions in terms of the correlation functions of the intermolecular interactions. Here, a brief review of Bloom-Oppenheim theory[10] for H_2 is presented and expressions for proton relaxation rates in H_2-X mixtures useful in the analysis of the present data are given.

Correlation functions of the intramolecular interactions

In a sample containing N molecules of hydrogen gas kept in a static magnetic field $\vec{H}_0$ along Z direction, the fluctuating spin-rotational and dipolar intramolecular interactions

produce a small time dependent perturbing term $\mathcal{H}'$ in the total Hamiltonian which is given by[1,10]

$$\mathcal{H}' = \sum_{i=1}^{N} \left[\frac{\gamma\hbar H'}{2} \sum_{m=-1}^{1} L^i_{1m} S^i_{1-m} + \left(\frac{6\pi}{5}\right)^{\frac{1}{2}} \gamma\hbar H'' \sum_{m=-2}^{2} L^i_{2m} S^i_{2-m} \right] \quad (3.10)$$

where the index i denotes the ith molecule and

$\gamma = 2.69 \times 10^4$ sec^{-1} gauss^{-1} is the proton gyromagnetic ratio

$H' = 26.75$ gauss is the coupling constant for intramolecular spin-rotational interaction

$H'' = 33.86$ gauss is the coupling constant for the intramolecular dipolar interaction

and $L_{\ell m}$ and $S_{\ell m}$ ($\ell = 1, 2$) are the functions of molecular rotational operators and nuclear spin operators respectively.

$$L_{10} = \sqrt{2}\, J_z \qquad S_{10} = \sqrt{2}\, I_z$$

$$L_{1\pm1} = J_\pm = J_x \pm i J_y \qquad S_{1\pm1} = I_\pm = I_x \pm i I_y$$

$$L_{20} = Y_{20}(\Omega) \qquad S_{20} = (2/3)^{\frac{1}{2}}[3I_z^2 - I(I+1)]$$

$$L_{2\pm1} = Y_{2\pm1}(\Omega) \qquad S_{2\pm1} = I_z I_\pm + I_\pm I_z$$

$$L_{2\pm2} = Y_{2\pm2}(\Omega) \qquad S_{2\pm2} = I_\pm^2$$

where $Y_{2m}(\Omega)$, $m = 0, \pm1, \pm2$ are the spherical harmonics of order 2 of the orientation Ω of the molecular axis.

By using the general theory[1] the proton spin-lattice relaxation time T_1 can be written as[1,10,36]

$$\frac{1}{T_1} = \frac{\gamma^2 H'^2}{2} J_{11}(\omega_I) + \left(\frac{12\pi}{5}\right) \gamma^2 H''^2 \left[J_{21}(\omega_I) + 4J_{22}(2\omega_I)\right] \tag{3.11}$$

where

$$J_{\ell m} = \int_{-\infty}^{\infty} e^{-i\omega t} G_{\ell m}(t)\, dt \tag{3.12}$$

is the Fourier transform of $G_{\ell m}(t)$ and is known as the spectral density, and

$$G_{\ell m}(t) = \tfrac{1}{2} \left[\overline{L_{\ell m}(0)\, L^{+}_{\ell m}(t)} + \overline{L_{\ell m}(t)\, L^{+}_{\ell m}(0)}\right] \tag{3.13}$$

is the correlation function of $L_{\ell m}$. The bar represents an ensemble average. It was well established by Schwinger[3], Needler and Opechowski[4], Abragam[1] and was also shown experimentally by Hardy[37] that the intramolecular correlation functions can be expressed as exponential functions of time which decay with a time constant τ_c known as correlation time of the intramolecular interaction. Johnson and Waugh[5] pointed out that out of different possible correlation functions only two, G_{1o} and G_{2o}, are important. In the short correlation time limit since the values of the spectral densities of $G_{\ell o}$ evaluated at frequencies ω_I or $2\omega_I$ are the same as those evaluated at zero frequency the eq. (3.11) reduces to

$$\frac{1}{T_1} = \tfrac{1}{2}\gamma^2 H'^2 J_{1o}(0) + 12\pi\, \gamma^2 H''^2 J_{2o}(0) \tag{3.14}$$

The correlation functions $G_{\ell o}$ can be written in terms of the matrix elements of $L_{\ell o}$ between the rotational states, in the following way

$$G_{\ell o}(t) = \sum_{J_o M_o} P_{J_o M_o} (J_o M_o | L_{\ell o} | J_o M_o) \sum_{JM} w(JM;t/J_o M_o;0)(JM|L_{\ell o}|JM)$$

$$= \sum_{J_o M_o} P_{J_o M_o} [f_\ell(J_o)]^{\frac{1}{2}} C(J_o \ell J_o; M_o 0) \sum_{JM} w(JM;t/J_o M_o;0) \times$$

$$[f_\ell(J)]^{\frac{1}{2}} C(J\ell J; M0) \qquad (3.15)$$

where

$$(JM|L_{\ell o}|JM) = [f_\ell(J)]^{\frac{1}{2}} C(J\ell J; M0)$$

is the matrix element of $L_{\ell o}$, $C(J\ell J; M0)$ is a Clebsch-Gordon coefficient (Rose[38])

$$f_1(J) = 2J(J+1)$$

$$f_2(J) = \frac{5}{4\pi} \frac{J(J+1)}{(2J-1)(2J+3)} \qquad (3.16)$$

and $$P_{J_o M_o} = \frac{1}{2J_o+1} P_{J_o} = \frac{\exp(-E_{J_o}/kT)}{\sum_J (2J+1) \exp(-E_J/kT)} \qquad (3.17)$$

is the probability that the molecule is in the state J_o, M_o with energy E_{J_o} while P_{J_o} is the probability that the molecule has the rotational energy $E_{J_o} \cdot w(JM;t/J_o M_o;0)$ is conditional probability that the molecule is in the rotational state J,M at a time t given that it is in the state J_o, M_o at t=0.

G_{1o} and G_{2o} are calculated by assuming that the conditional probability $w(JM;t/J_o M_o;0)$ satisfies a temporally

homogeneous master equation

$$\frac{\partial w}{\partial t} = \dot{w}(JM;t/J_oM_o;0) = \sum_{J'M'} A(JM;J'M')\ w(J'M';t/J_oM_o;0) \qquad (3.18)$$

where $A(JM;J'M')$, $J,M \neq J',M'$, is the transition rate for the transition $J',M' \rightarrow J,M$ that is caused because of the intermolecular anisotropic forces acting during collisions.
For $J=J'$, $M=M'$

$$A(J'M';J'M') = -\sum_{J\neq J'} \sum_{M} A(JM;J'M') - \sum_{M\neq M'} A(J'M;J'M') \qquad (3.19)$$

From eq. (3.18) it is seen that a tensor polarization of order ℓ in the state J for molecules initially in the state J_oM_o and defined as

$$m^{\ell}_{JJ_oM_o}(t) = \sum_{M} C(J\ell J;M0)\ w(JM;t/J_oM_o;0) \qquad (3.20)$$

satisfies the following relation

$$\dot{m}^{\ell}_{JJ_oM_o}(t) = \sum_{J'M'} w(J'M';t/J_oM_o;0) \sum_{M} C(J\ell J;M0)\ A(JM;J'M') \qquad (3.21)$$

The number of coupled equations, eq. (3.18), is equal to the number of rotational states appreciably populated at the temperature of interest.

The transition rates $A(JM;J'M')$ are calculated using 'weak collision approximation' which means that the anisotropic intermolecular potentials are assumed to be weak in the sense that first order perturbation theory may be used to calculate

the transition rates $A(JM;J'M')$. If each term of the intermolecular anisotropic interaction potential be expressed as a product of a lattice operator involving the intermolecular separation and a rotational operator involving the orientations, of the molecular symmetry axes, which can be represented by spherical harmonics $Y_{\lambda\mu}(\Omega)$ of order λ, then the transition probability $A_\lambda(JM;J'M')$ which contains the squares of the matrix elements of the operators between the states J',M' and J,M can be written as

$$A_\lambda(JM;J'M') = Q_\lambda(J,J')\,[C(J'\lambda\, J;M'\mu)]^2\delta_{M,M'+\mu} \qquad (3.22)$$

where $Q_\lambda(J,J')$ depends upon the radial dependence of the anisotropic intermolecular potential and involves the correlation function of the intermolecular interactions. Using eq. (3.22) and the eqs. (6.23a) and (6.24) of Rose[38], it can be shown that

$$\sum_M C(J\ell\, J;M0)A_\lambda(JM;J'M') = C(J'\ell\, J';M'0)B_{\ell\lambda}(J,J') \qquad (3.23)$$

where

$$\left(\frac{2J'+1}{2J+1}\right)B_{\ell\lambda}(J,J') = Q_\lambda(J,J')(-1)^{\lambda+\ell-J-J'}[(2J+1)(2J'+1)]^{\frac{1}{2}} \times W(J,J',J,J';\lambda\ell) - \delta_{JJ'}\sum_{J''}\left(\frac{2J''+1}{2J'+1}\right)Q_\lambda(J'',J') \qquad (3.24)$$

where $W(J,J',J,J';\lambda\ell)$ is a Racah coefficient (Rose[38]). From these expressions and eq. (3.21), it is seen that the tensor

polarization $m^{\ell}_{JJ_oM_o}$ satisfies the following relation in the weak collision approximation

$$\dot{m}^{\ell}_{JJ_oM_o}(t) = \sum_{J'} B_{\ell}(J,J')\ m^{\ell}_{J'J_oM_o}(t) \qquad (3.25)$$

where

$$B_{\ell}(J,J') = \sum_{\lambda} B_{\ell\lambda}\ (J,J') \qquad (3.26)$$

Solving the eq. (3.25) with the initial conditions

$$m^{\ell}_{JJ_oM_o}(0) = C(J_o\ell J_o;M_o0)\ \delta_{JJ_o}$$

and $w(JM;0/J_oM_o;0) = \delta_{JJ_o}\ \delta_{MM_o}$

and using eq. (3.15) the correlation functions $G_{\ell o}(t)$ are obtained in terms of $Q_{\lambda}(J,J')$, i.e. in terms of the correlation functions of the intermolecular interaction.

Correlation functions of the intermolecular interactions

The intermolecular potential between two molecules consists of isotropic and anisotropic parts. The important terms of the anisotropic interaction potential, v_A, between two molecules labelled 1 and 2 can be written as a sum of two terms: one depending upon the orientation of the first molecule and the other depending upon the orientation and the relative position of the second molecule also. If $\vec{r}$ be the vector distance of the centre of mass of 2 from that of the molecule 1 and θ'_1 the angle which the symmetry axis of

molecule 1 makes with $\vec{r}$, then one can write[10]

$$v_A = v_A^{(1)} + v_A^{(2)} \tag{3.27}$$

where $$v_A^{(1)} = b^{(1)}(r)\, P_2(\cos\theta_1') \tag{3.28}$$

and $$v_A^{(2)} = b^{(2)}(r) \sum_{q=-2}^{2} a_q Y_{2q}(\Omega_1') \, Y_{2q}^{*}(\Omega_2') \tag{3.29}$$

in which $P_2(\cos\theta_1')$ is the Legendre polynomial of order 2 of the angle θ_1', $Y_{2q}(\Omega_1')$ and $Y_{2q}(\Omega_2')$ are spherical harmonics of order 2 and Ω_1' and Ω_2', are, respectively, the orientations of the symmetry axes of molecules 1 and 2 with respect to $\vec{r}$. $b^{(1)}(r)$ and $b^{(2)}(r)$ are function of r and a_q are constants. For quadrupole-quadrupole interaction $a_0=6$, $a_1=a_{-1}=-4$, $a_2=a_{-2}=1$ and

$$b^{(2)}(r) = \frac{4\pi Q_1 Q_2}{r^5} \tag{3.30}$$

where Q_1 and Q_2 are the quadrupole moments of the molecules 1 and 2 respectively. The potential written in eq. (3.27) is the most general one if both the molecules are ortho-H_2 molecules in their lowest rotational state. If the molecule 2 is a para-H_2 or inert gas molecule, $v_A^{(1)}$ represents the interaction potential. If the molecule 1 is an ortho-H_2 molecule in any J state and the molecule 2 is another molecule having permanent quadrupole moment, such as N_2, v_A, as written in eq. (3.27), gives the leading terms of the anisotropic intermolecular potential.

In the laboratory reference frame, in which the Z axis is along $\vec{H}_o$, $v_A^{(1)}$ and $v_A^{(2)}$ are written as[10]

$$v_A^{(1)} = \frac{4\pi}{5} b^{(1)}(r) \sum_{\mu=-2}^{2} Y_{2\mu}(\Omega_1) Y^*_{2\mu}(\Omega) \qquad (3.31)$$

$$v_A^{(2)} = \left(\frac{56\pi}{45}\right)^{\frac{1}{2}} b^{(2)}(r) \sum_{m_\mu m'} (-1)^\mu C(224; m, m', \mu) Y_{2m}(\Omega_1) Y_{2m'}(\Omega_2) \cdot$$

$$\times Y_{4-\mu}(\Omega) \qquad (3.32)$$

where Ω_1, Ω_2 and Ω are the orientations of the molecules 1, 2 and the vector $\vec{r}$, respectively, in the laboratory frame. Since $v_A^{(1)}$ involves rotational operators of the molecule 1 only and $v_A^{(2)}$ involves rotational operators for both the molecules, it is seen that there is no interference between the contributions, from $v_A^{(1)}$ and $v_A^{(2)}$, to $Q_\lambda(J, J')$, so that one can write

$$Q_\lambda(J, J') = Q_\lambda^{(1)}(J, J') + Q_\lambda^{(2)}(J, J'), \lambda = 2 \text{ for } H_2 \qquad (3.33)$$

where $Q_\lambda^{(1)}(J, J')$ and $Q_\lambda^{(2)}(J, J')$ arise from $v_A^{(1)}$ and $v_A^{(2)}$ respectively. The effect of $v_A^{(1)}$ is to produce transitions from the state J',M' to J,M in the molecule 1 and that of $v_A^{(2)}$ is to produce transitions in the molecule 1 from J',M' to J,M while the molecule 2 simultaneously undergoes transition from the state J''',M''' to J'', M'' . The transition rates $A^{(1)}(JM, J'M')$ and $A^{(2)}(JM, J'M')$, for the molecule 1, produced by $v_A^{(1)}$ and $v_A^{(2)}$ respectively can be written using the first

order perturbation theory as

$$A^{(1)}(JM;J'M') = \frac{1}{\hbar^2}\int_{-\infty}^{\infty} e^{i\omega_{JJ'}t}\,\overline{(J'M'|v_A^{(1)}(0)|JM)(JM|v_A^{(2)}(t)|J'M')}\,dt \tag{3.34}$$

$$= \frac{4\pi}{5}\left(\frac{2J'+1}{2J+1}\right)[C(J'2J;00)]^2[C(J'2J;M'\mu)]^2 j^{(1)}(\omega_{JJ'})$$

where $$j^{(1)}(\omega_{JJ'}) = \frac{1}{\hbar^2}\int_{-\infty}^{\infty} e^{i\omega_{JJ'}t}\,k^{(1)}(t)\,dt \tag{3.35}$$

$$\hbar\omega_{JJ'} = E_J - E_{J'}$$

in which

$$k^{(1)}(t) = (N-1)\,\overline{b^{(1)}(r(0))\,Y_{2-\mu}(\Omega(0))\,b^{(1)}(r(t))Y_{2\mu}(\Omega(t))} \tag{3.36}$$

is the correlation function of $b^{(1)}(r)\,Y_{2-\mu}(\Omega)$;

$$A^{(2)}(JM;J'M') = \sum_{J''J'''}\sum_{M''M'''} A[(JM;J'M')(J''M'';J'''M''')] \tag{3.37}$$

where

$$A[(JM;J'M')(J''M'';J'''M''')] = \sum_{mm'}\left(\frac{56\pi}{45}\right) j^{(2)}(\omega_{JJ';J''J'''})$$

$$\times [C(224;m,m')]^2\,\frac{P_{J'''}}{2J'''+1}\,|(JM|Y_{2m}(\Omega_1)|J'M')|^2$$

$$\times\,|(J''M''|Y_{2m'}(\Omega_2)|J'''M''')|^2 \tag{3.38}$$

and represents the rate of simultaneous transitions produced, in the molecules, by $v_A^{(2)}$.

Here $\hbar\omega_{JJ';J''J'''} = (E_J - E_{J'}) + (E_{J''} - E_{J'''})$ (3.39)

and $j^{(2)}(\omega_{JJ';J''J'''})$ is the Fourier transform of the correlation function $k^{(2)}(t)$ of $b^{(2)}(r)Y_{4-\mu}(\Omega)$, where

$$k^{(2)}(t) = (N-1)\,\overline{b^{(2)}(r(0))Y_{4-\mu}(\Omega(0))\; b^{(2)}(r(t))\; Y_{4\mu}(\Omega(t))} \tag{3.40}$$

values of $j^{(q)}(\omega)$, $q = 1,2$, have been calculated by Bloom et al.[10] using Constant Acceleration Approximation (CAA)[10]. Summations in eq. (3.37) are performed by the method given by Rose.[38]

Using these expressions for $A^{(1)}(JM;J'M')$ and $A^{(2)}(JM;J'M')$ and eq. (3.22) where $\lambda = 2$ for H_2, $Q_2^{(1)}(JJ')$ and $Q_2^{(2)}(JJ')$ are obtained, in terms of the spectral densities of the correlation functions $k^{(1)}(t)$ and $k^{(2)}(t)$ of the intermolecular interaction, as

$$Q_2^{(1)}(J,J') = \frac{4\pi}{5}\left(\frac{2J'+1}{2J+1}\right)[C(J'2J;00)]^2 j^{(1)}(\omega_{JJ'}) \tag{3.41}$$

and $$Q_2^{(2)}(J,J') = \frac{7}{10\pi}[C(J2J';00)]^2 \sum_{J''',J''} F_{J'''}$$

$$\times\,[C(J'''2J'';00)]^2\, J^{(2)}(\omega_{JJ';J''J'''}) \tag{3.42}$$

Using these expressions and the relations that preceded $G_{\ell o}$ are obtained which with the help of eq. (3.14) yield an expression for T_1 in terms of the spectral densities $j^{(1)}(\omega_{JJ'})$

and $j^{(2)}(\omega_{JJ';J''J'''})$ of the intermolecular correlation functions.

In the present work, mixtures of H_2 with Ar, N_2 and N_2O have been studied. H_2-Ar collisions cannot cause any transitions in the J states of ortho-H_2 because Ar is a spherically symmetric atom. H_2-N_2 and H_2-N_2O collisions also cannot produce any inter J transitions in the rotational states of ortho-H_2 because of the energy mismatch between the J levels of H_2 and N_2 (or N_2O) for allowed transitions. Hence the case of infrequent transitions between J states of H_2 will be considered in detail and expression for T_1 will be given.

Case of infrequent transitions between states of different J

For the case where the transitions between different rotational states occur much less frequently than those between the states with different M within the same J manifold, it can be shown that

$$Q_2(J,J') << Q_2(J,J) \qquad J \neq J' \tag{3.43}$$

and

$$j^{(1)}(\omega_{JJ'}) = j^{(1)}(0)\,\delta_{JJ'} \tag{3.44}$$

$$j^{(2)}(\omega_{JJ';J''J'''}) = j^{(2)}(0)\,\delta_{JJ'}\delta_{J''J'''} \tag{3.45}$$

Eqs. (3.41) and (3.42), then reduce to

$$Q_2^{(1)}(J,J) = \frac{4\pi}{5}\,\frac{J(J+1)}{(2J-1)(2J+3)}\,j^{(1)}(0) \tag{3.46}$$

and $$Q_2^{(2)}(J,J) = \frac{7}{25\pi} \frac{J(J+1)}{(2J-1)(2J+3)} \; C \; j^{(2)}(0) \qquad (3.47)$$

where $$C = \frac{5}{2} \sum_{J''} P_{J''} \frac{J''(J''+1)}{(2J''-1)(2J''+3)} = \frac{5}{2} \left\langle \frac{J(J+1)}{(2J-1)(2J+3)} \right\rangle' \qquad (3.48)$$

and the prime indicates that the average is taken over the rotational states of the molecules 2 which collide with the ortho-H_2 molecule (molecule 1).

Bloom and Oppenheim[9,10] have evaluated expressions for $j^{(q)}(0)$ using constant Acceleration Approximation[10] as

$$j^{(q)}(0) = \frac{\rho a^4 (2\pi\beta\mu)^{\frac{1}{2}}}{\hbar^2} \; I^{(q)}(p) \qquad (3.49)$$

where ρ is the number density of the gas, μ is the reduced mass of the colliding pair and a is a length parameter which is a measure of the range of the isotropic intermolecular potential. The index p is determined by the angular variation of the anisotropic interaction. When q=1, p=2 and when q=2, p=4 for H_2.

If the radial dependence of the anisotropic intermolecular potentials $v_A^{(q)}$ (see eqs. (3.27)-(3.30)) could be written in the form

$$b^{(q)}(ax) = \frac{a_1(q)}{x^{n'}} - \frac{a_2(q)}{x^n} \qquad (3.50)$$

where r = ax and x is a dimensionless variable, then one can write[9]

Substituting eq. (3.49) into eqs. (3.46) and (3.47), one obtains

$$Q_2^{(1)}(J,J) = \left(\frac{4\pi}{5\hbar^2}\right) \rho a^4 (2\pi\beta\mu)^{\frac{1}{2}} I^{(1)}(2) \left[\frac{J(J+1)}{(2J-1)(2J+3)}\right] \quad (3.57)$$

and $$Q_2^{(2)}(J,J) = \left(\frac{7}{25\pi\hbar^2}\right) \rho a^4 (2\pi\beta\mu)^{\frac{1}{2}} I^{(2)}(4) \left[\frac{J(J+1)}{(2J-1)(2J+3)}\right] C \quad (3.58)$$

Using eqs. (3.57), (3.58), (3.33) and (3.24), $B_\ell(JJ)$ are obtained as

$$B_1(J,J) = \frac{-12\pi}{5\hbar^2} \frac{\rho a^4 (2\pi\beta\mu)^{\frac{1}{2}}}{(2J-1)(2J+3)} \left[I^{(1)}(2) + \frac{7}{20\pi^2} C I^{(2)}(4)\right] \quad (3.59)$$

and $$B_2(J,J) = \frac{3(4J^2 + 4J - 7)}{(2J-1)(2J+3)} B_1(J,J) \quad (3.60)$$

which, in turn, can be expressed in terms of quantities k_o and k_1 defined as

$$k_o = \frac{6\pi}{5\hbar^2} I^{(1)}(2) \quad (3.61)$$

$$k_1 = \frac{21}{50\pi\hbar^2} I^{(2)}(4) \quad (3.62)$$

in the following manner

$$B_1(J,J) = -\frac{2\rho a^4 (2\pi\beta\mu)^{\frac{1}{2}}}{(2J-1)(2J+3)} (k_o + C k_1) \quad (3.63)$$

and $B_2(J,J)$ is given by eq. (3.60).

Using these expressions for $B_\ell(J,J)$ and eqs. (3.15), (3.20), (3.21), (3.22)-(3.26) and (3.43), G_{1o} and G_{2o} are obtained

whose Fourier transforms are given by[10]

$$J_{\ell o} = \frac{2}{2\ell+1} \sum_J P_J f_\ell(J) \frac{1}{|B_\ell(J,J)|}, \quad \ell = 1, 2 \tag{3.64}$$

and T_1 is, then, written with the help of eq. (3.14) as

$$\frac{\rho a^4 (2\pi\beta\mu)^{\frac{1}{2}} (k_o + Ck_1)}{T_1} = \sum_J P_J \left[\frac{1}{3} \gamma^2 H'^2 \{J(J+1)(2J-1)(2J+3)\} \times \{1 + \frac{3H''^2}{H'^2} \frac{1}{4J^2+4J-7}\}\right] \tag{3.65}$$

$$\text{or} \quad \frac{1}{T_1} = \frac{1.02 \times 10^{13} \langle D(J) \rangle}{\rho a^4 (2\pi\beta\mu)^{\frac{1}{2}} (k_o + Ck_1)} \tag{3.66}$$

where

$$D(J) = \frac{J(J+1)(2J-1)(2J+3)}{57.4} \cdot \{1 + \frac{4.74}{4J^2 + 4J - 7}\}. \tag{3.67}$$

and $\langle\ \rangle$ represents an average over all the rotational states of the ortho-H_2 molecule (molecule 1). The numerical values of γ, H', and H'' for H_2 have been used to find out the numerical factors in eqs. (3.66) and (3.67).

H_2-X mixtures (X = Ar, N_2 and N_2O)

The total interaction potential between ortho-H_2 and X molecules consists of an isotropic part $v_o(r)$ and an anisotropic part $v_A(r,\theta')$, where r is the intermolecular separation and θ' represents the orientations of the molecular symmetry

axes with respect to $\vec{r}$ (i.e. in body fixed frame). It is assumed that $v_o(r)$ is given by Lennard-Jones potential

$$v_o(r) = 4\varepsilon \left[\left(\frac{a}{r}\right)^{12} - \left(\frac{a}{r}\right)^{6}\right] \qquad (3.68)$$

where ε and a are the Lennard Jones energy and distance parameters appropriate for H_2-X pair.

The anisotropic part of the interaction potential between H_2 and Ar molecules depends upon the orientation of H_2 molecule only, since Ar is a spherically symmetric atom, and hence can be written in the form of $v_A^{(1)}$ as given in eq. (3.27). For H_2-N_2 and H_2-N_2O pairs the interaction potential v_A contains both $v_A^{(1)}$ and $v_A^{(2)}$ because N_2 and N_2O have permanent quadrupole moments.

The long range attractive parts, $v_{att}(r,\theta')$, of the anisotropic intermolecular potentials between H_2 and X can be written in terms of their polarizabilities, following Buckingham's results [10], as

$$\left[v_{att}(r,\theta')\right]_{X=Ar} = -\frac{3U_1U_2}{2(U_1+U_2)}\,\alpha_2\left[\frac{\alpha_1}{r^6} + \frac{1}{3}\,\frac{(\alpha_{\parallel}-\alpha_{\perp})_1}{r^6}\,P_2(\cos\theta_1') + \ldots\ldots\right] \qquad (3.69)$$

$$\left[v_{att}(r,\theta')\right]_{\substack{X=N_2\\ \text{or } N_2O}} = -\frac{3U_1U_2}{2(U_1+U_2)}\left[\frac{\alpha_1\alpha_2}{r^6} + \frac{1}{3}\,\alpha_2\,\frac{(\alpha_{\parallel}-\alpha_{\perp})_1}{r^6}\,P_2(\cos\theta_1') + \frac{1}{3}\,\alpha_1\,\frac{(\alpha_{\parallel}-\alpha_{\perp})_2}{r^6}\,P_2(\cos\theta_2') + \ldots\right] \qquad (3.70)$$

where only the leading terms have been retained and θ_1' and θ_2' are respectively the orientation of the molecular symmetry axes of molecules 1 and 2 with respect to $\vec{r}$. α_1 and α_2 are the total polarizabilities of the molecules 1 and 2 while $\alpha_{\parallel}$ and $\alpha_{\perp}$ are the polarizabilities parallel and perpendicular to the molecular axes. U_1 and U_2 have the units of energy and it was suggested by Buckingham[10] that they might be taken as the first ionization potentials of the molecules. The first terms in eqs. (3.69) and (3.70) are the isotropic parts of the long range interaction and hence must be identical with the attractive part in eq. (3.68). Therefore it was chosen to fix

$$\frac{3U_1U_2}{2(U_1+U_2)} \alpha_1\alpha_2 = 4\varepsilon a^6 \qquad (3.71)$$

It should be noted here that the values of $U_1U_2/(U_1+U_2)$ obtained for H_2-X pairs using the above equation are approximately twice of those obtained following Buckingham's suggestion. This difference is due to the fact that the r^{-6} term is only the leading term of the potential derived by Buckingham while in 12-6 potential it is the only term.

It is assumed that the anisotropic interaction potentials contain repulsive terms also which vary as r^{-12} and have the same angle dependence as that of the attractive parts. Thus, the intermolecular anisotropic potential for H_2-X can be written as

$$[v_A(r,\theta')]_{H_2\text{-}Ar} = b_1(r)\ P_2(\cos\theta_1') \tag{3.72}$$

$$[v_A(r,\theta')]_{\substack{H_2\text{-}N_2 \\ H_2\text{-}N_2O}} = b_1(r)\ [P_2(\cos\theta_1') + P_2(\cos\theta_2')] + b_2(r) \sum_{q=-2}^{2}{}' a_q\ Y_{2q}(\Omega_1')\ Y_{2q}(\Omega_2') \tag{3.73}$$

(where the terms have the meaning as given in eq. (3.28) and eq. (3.29))

where

$$b_1(r) = \frac{a_1}{x^{12}} - \frac{a_2}{x^6}, \qquad x = r/a \tag{3.74}$$

$$b_2(r) = \frac{b_1}{x^{12}} - \frac{b_2}{x^5} \text{ where } b_2 = \frac{4\pi Q_{H_2} Q_X}{5\, a_{H_2\text{-}X}^5}, \quad X = N_2 \text{ or } N_2O$$

$$x = r/a \tag{3.75}$$

As described earlier, H_2-Ar collisions cannot produce transitions in the J states of the ortho-H_2 molecule since Ar is a spherically symmetric atom. H_2-N_2 and H_2-N_2O collisions also cannot produce any J transitions due to the mismatch in the energy differences between the J states of N_2, N_2O and H_2. Evaluating $Q_2(J,J)$ etc. for ortho-H_2 and X interactions and proceeding in the same way as done for H_2 for the case of infrequent transitions between J states, the relaxation rate, $(\rho/T_1)^{O\text{-}X}$, due to ortho-H_2 and X collisions only, are obtained as

$$\left(\frac{\rho}{T_1}\right)^{H_2\text{-}X} = \frac{1.02 \times 10^{13} \langle D(J)\rangle}{\rho_1\, a_{H_2\text{-}X}^4\, (2\pi\beta\mu_{H_2\text{-}X})^{\frac{1}{2}} (k_o + C_X k_1)^{H_2\text{-}X}} \tag{3.76}$$

for $X = N_2$, N_2O or any molecule having dominant quadrupole moment and

$$\left(\frac{\rho}{T_1}\right)^{H_2-X} = \frac{1.02 \times 10^{13} \langle D(J) \rangle}{\rho_1 \, a^4_{H_2-X} \, (2\pi\beta\mu_{H_2-X})^{\frac{1}{2}} (k_o)^{H_2-X}} \qquad (3.77)$$

for X = Ar or any spherically symmetric atom. In eqs. (3.76) and (3.77), D(J) has the same meaning as given earlier in eq. (3.67), a_{H_2-X} and μ_{H_2-X} are the parameters (see eq. (3.49)) corresponding to H_2-X pair and C_X is a quantity defined in eq. (3.48) in which average is taken over the rotational states of X. Values of C_X are obtained as 5/2 for N_2 and N_2O[9]. ρ is the density in amagats and $\rho_1 = 2.69 \times 10^{19}$ molecule/cc is the number density corresponding to one amagat.

III.3 Experimental Results and Interpretation

III.3.1 H_2-Ar mixtures

The proton spin-lattice relaxation times T_1 were measured in H_2-Ar mixtures as a function of density and composition in the temperature range of 300-600K. Typical plots of T_1 versus ρ at different temperatures are shown in Figs. 10 and 11.

The values of T_1/ρ for different compositions and temperatures are shown in Fig. 12. The data did not show any non-linearity in T_1/ρ versus composition and so $(T_1/\rho)^{O-Ar}$ values

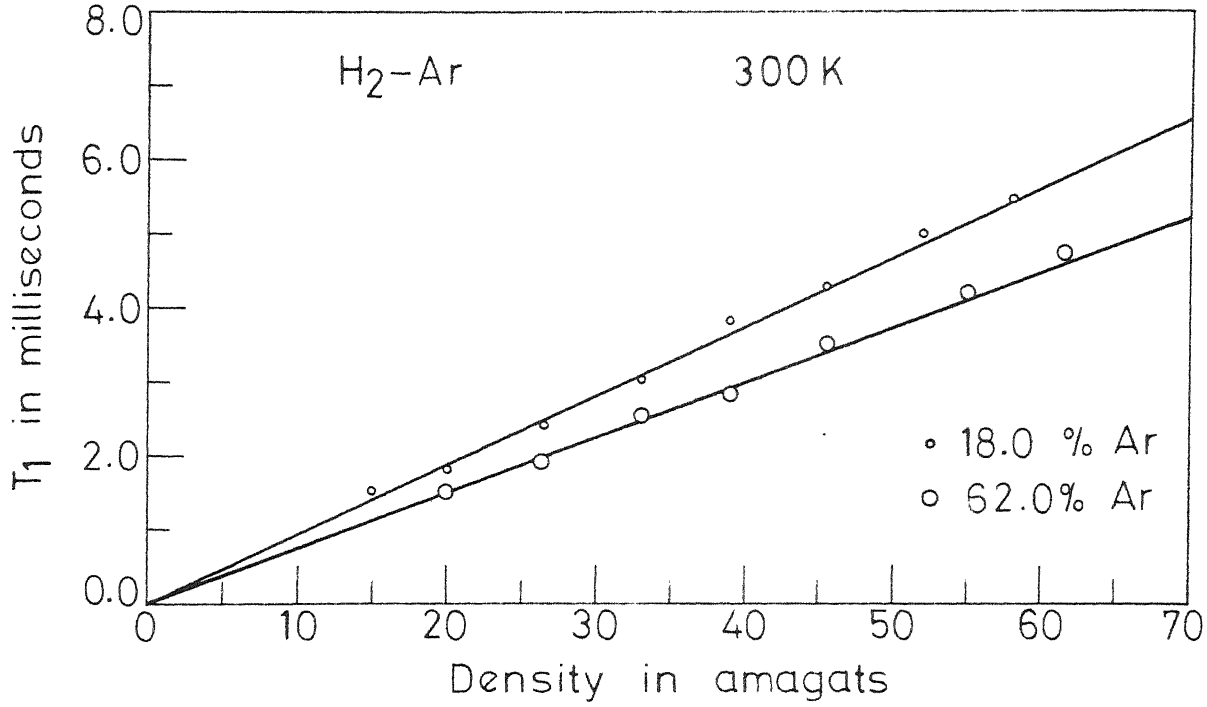

Fig. 10 T_1 vs density at 300K in H_2-Ar mixtures.

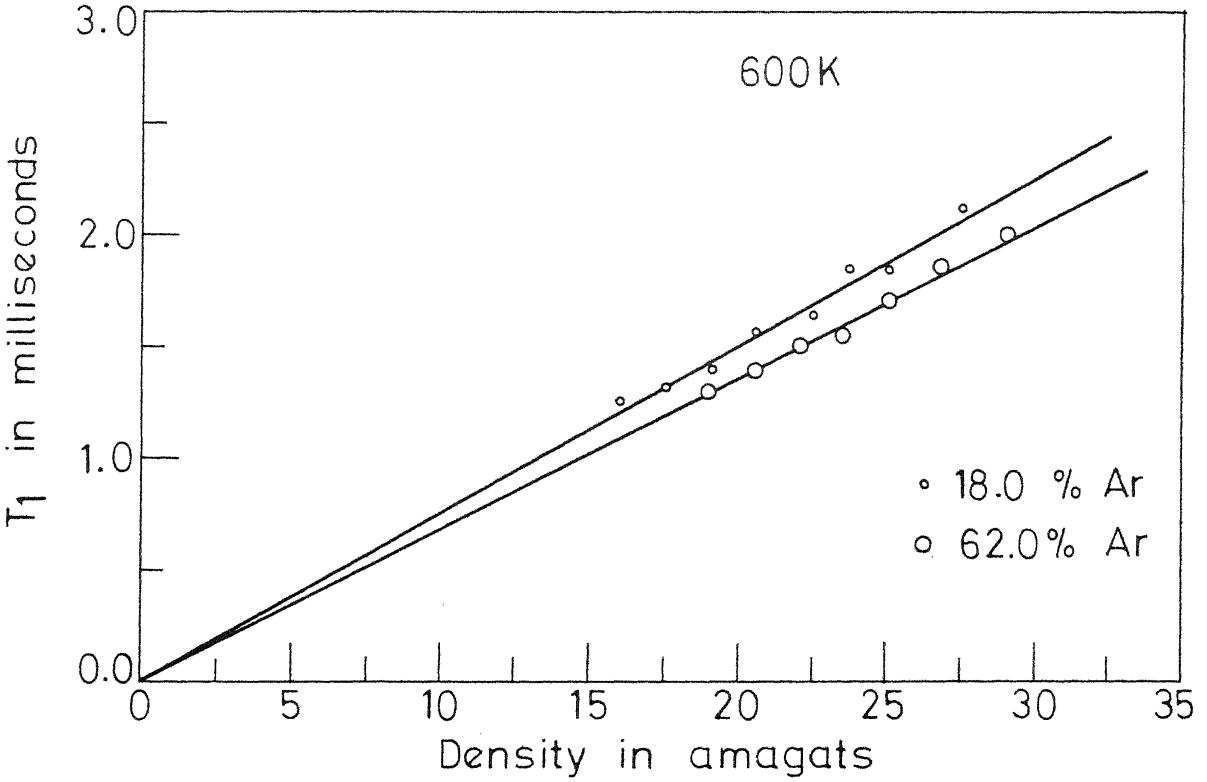

Fig. 11 T_1 vs density at 600K in H_2-Ar mixtures.

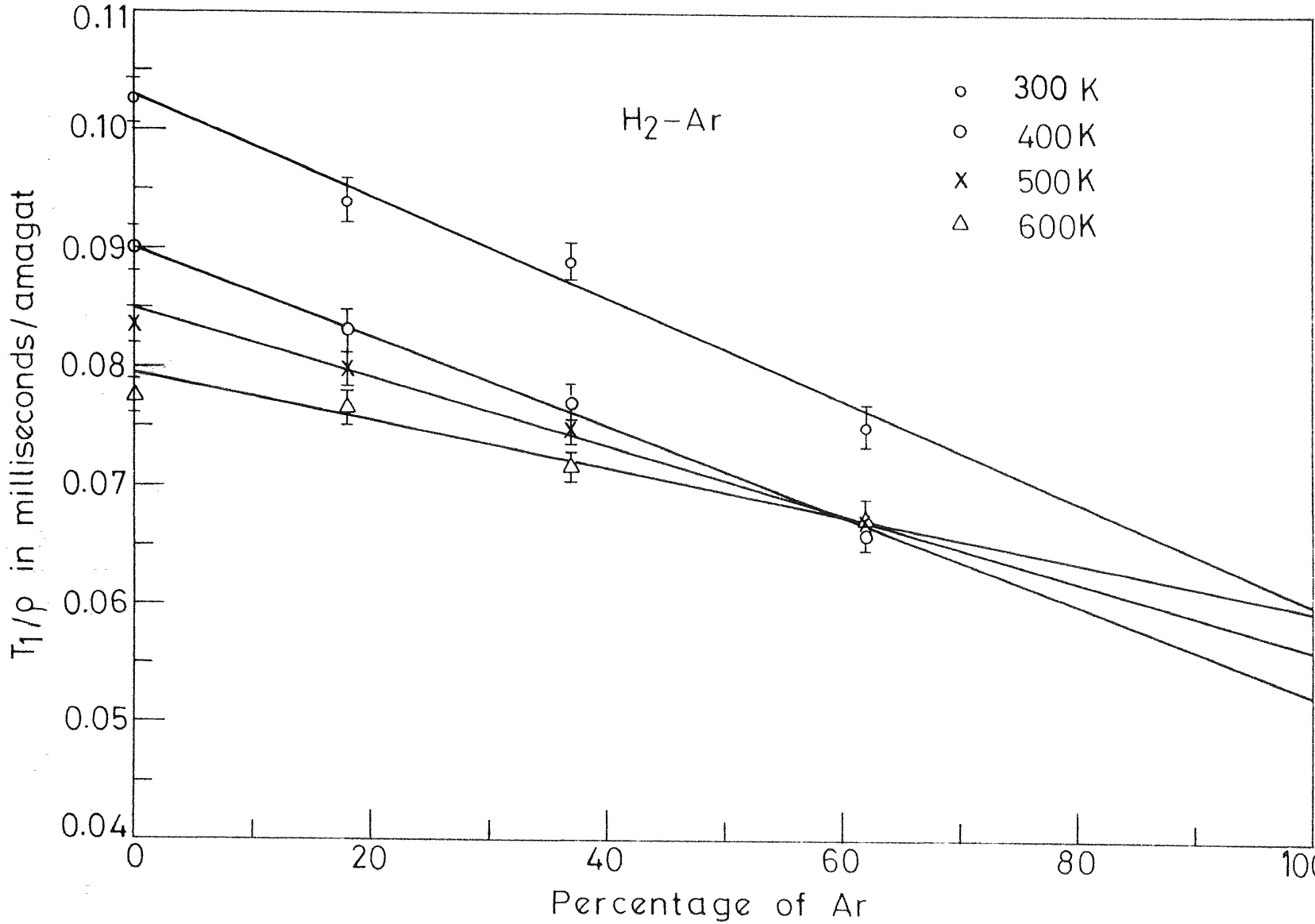

Fig. 12 Dependence of T_1/ρ on Argon concentration at different temperatures.

for ortho-H_2 and Ar collisions alone were obtained by using a linear extrapolation of the plot to 100% Ar. The solid line represents linear fits of the data using method of least squares. The error bars show the standard deviations. However, a non-linear behaviour for T_1/ρ versus composition is predicted by the Bloom-Oppenheim two level theory[20] which takes into account the transitions between different J states and assumes that only the rotational states J=1 and J=3 for ortho-H_2 and the states J=0, 2 and 4 for para-H_2 are populated. This theory, however, cannot be used satisfactorily at temperatures above 450K since the fractional populations in the states higher than the first two for ortho-H_2 become appreciable. At present no theory which takes more than two levels into consideration including inter J state transitions is available. Hence to take into account any nonlinearity effects, if present at all, the T_1/ρ data were fitted to an empirical relation of the form,

$$T_1/\rho = A_o + A_1 X_x + A_2 X_x^2 \qquad (3.78)$$

where X_x denotes the fractional concentration of the component X in H_2-X mixture, as has already been done for H_2-He mixtures by Lalita and Bloom[21]. $(T_1/\rho)^{0-X}$ is obtained by putting $X_x = 1$ in eq. (3.78).

Foster et al.[12] have obtained $(T_1/\rho)^{0-Ar}$ values in the temperature range of 160-270K using a linear variation of

T_1/ρ versus composition. These values as well as the values of $(T_1/\rho)^{O-Ar}$ obtained by the linear and empirical fits above room temperature are shown in Fig. 13 as a function of temperature. From the data it can be seen that the difference in the values of $(T_1/\rho)^{O-Ar}$ obtained from linear fit and empirical fit is maximum at room temperature and negligible at 600K. Hence it may be inferred that the deviation from the linear dependence of T_1/ρ on composition is most prominent around room temperature. The values of $(k_o)^{O-Ar}$ are obtained from the experimental values of $(T_1/\rho)^{O-Ar}$ using eq. (3.77), and are shown in Fig. 14 and given in table 3.2 as a function of temperature. These values are referred to as $(k_o)^{O-Ar}_{exptl}$ and the corresponding $(T_1/\rho)^{O-Ar}$ values as $(T_1/\rho)^{O-Ar}_{exptl}$.

Interpretation

The intermolecular interaction potential between H_2 and Ar can be written in the following form (see eqs. (3.68), (3.69), (3.72) and (3.74)).

$$V = v_o(r) + v_A(r,\theta')$$

$$= 4\varepsilon \left(\frac{1}{x^{12}} - \frac{1}{x^6}\right) + \left(\frac{a_1}{x^{12}} - \frac{a_2}{x^6}\right) P_2(\cos\theta_1'), \quad x = \frac{r}{a} \qquad (3.79)$$

where orientations are with respect to $\vec{r}$ (i.e. in molecule fixed frame whose Z axis is along $\vec{r}$). One can then write using eqs. (3.61), (3.77) and (3.51)

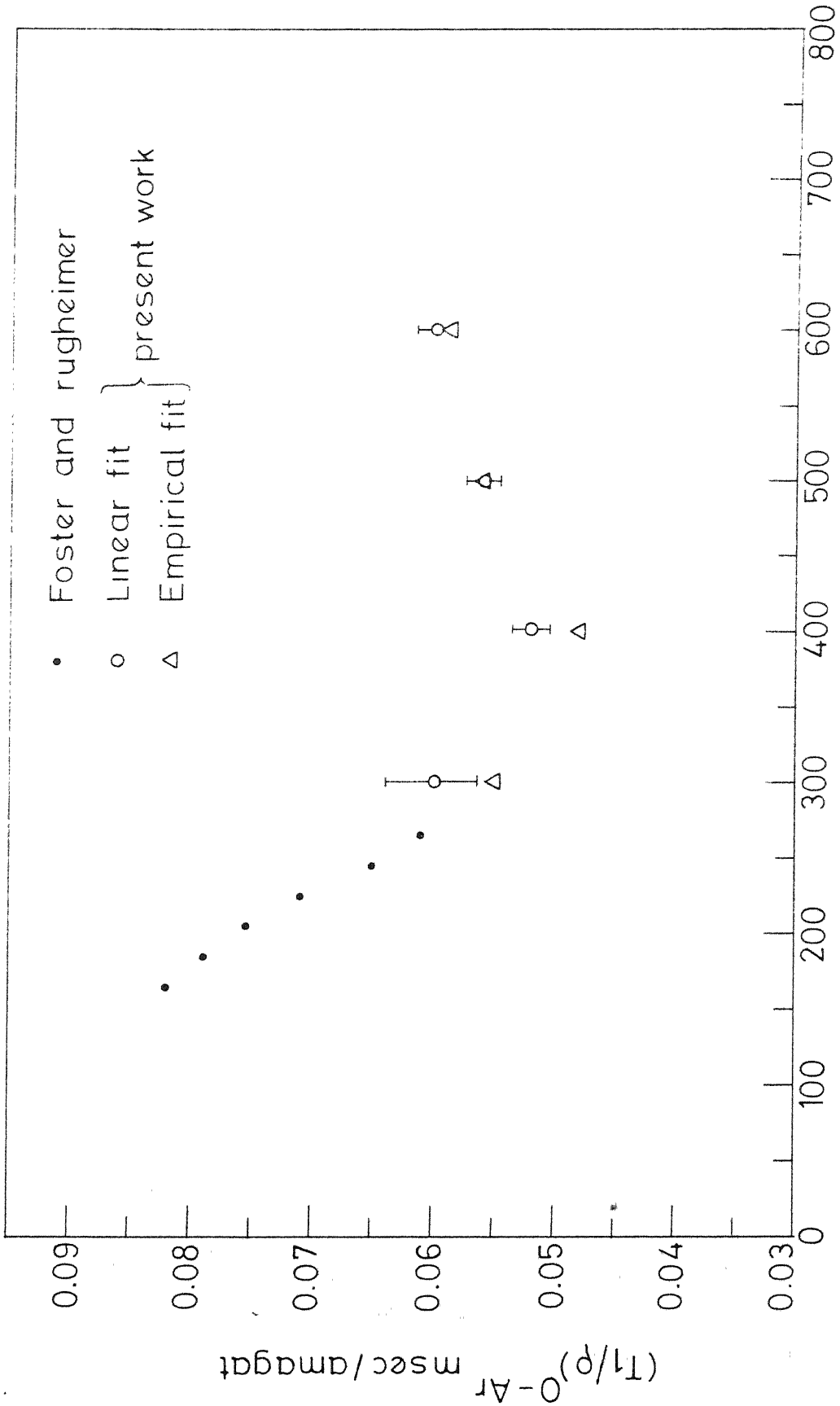

Fig. 13 Plot of $(T_1/\rho)^{O\text{-}Ar}$ vs temperature.

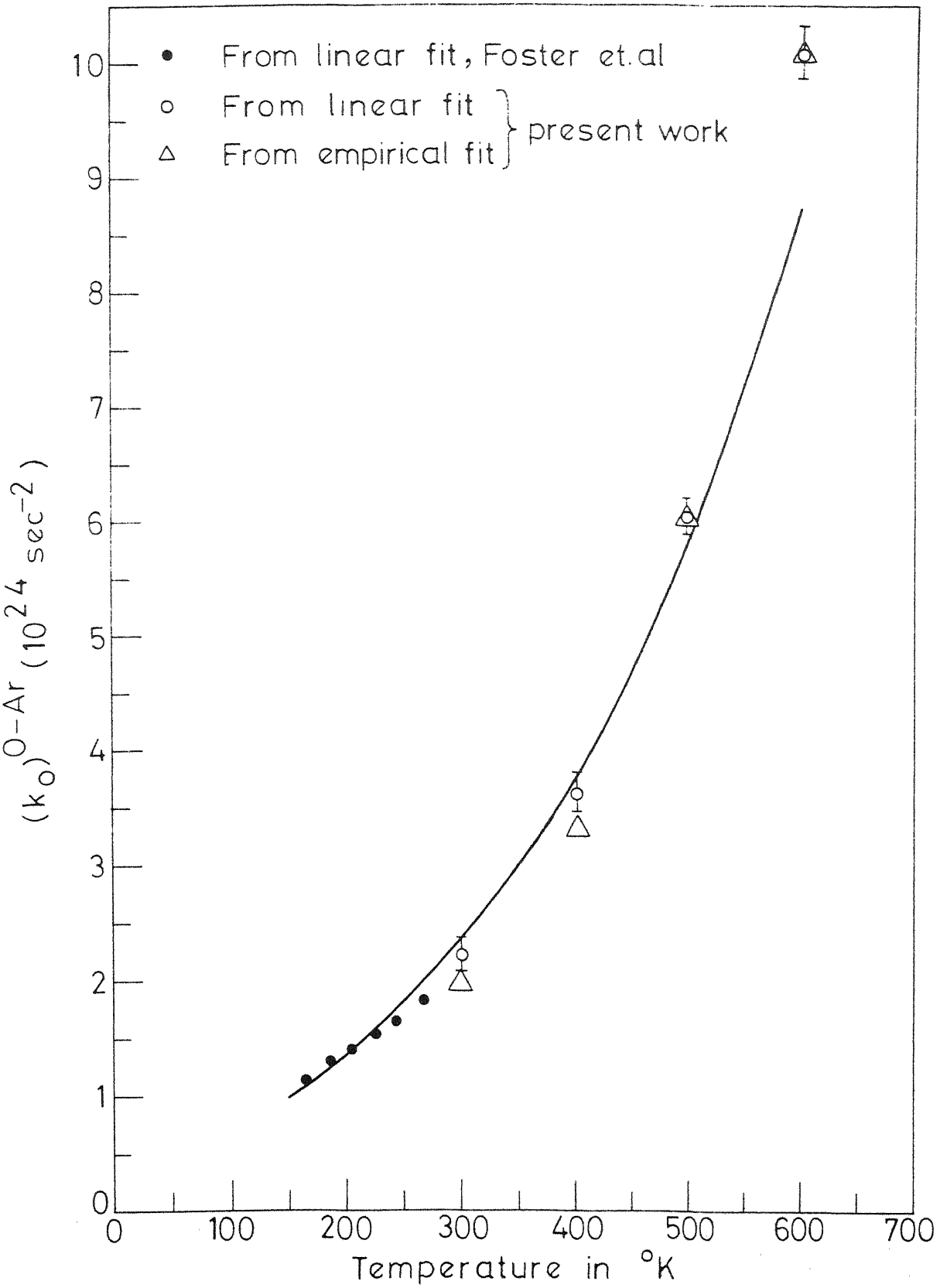

Fig. 14 Temperature dependence of $(k_o)^{O-Ar}$.

$$(k_o)^{O-Ar} = \frac{6\pi}{5\hbar^2} [I^{(1)}(2)]_{H_2-Ar}$$

$$= \frac{6\pi}{5\hbar^2} [a_1{}^2 I(2,12) + a_2{}^2 I(2,6) - 2a_1 a_2 I(2,6,12)] \quad (3.80)$$

where I(2,12) etc. are certain integrals defined in eqs. (3.52) and (3.53). These integrals were evaluated on IBM 1401 and 7044 computers at the I.I.T. Kanpur Computer Centre using Gaussian Quadrature Technique. Values of these integrals for H_2-Ar are listed in table 3.3.

The constants a_1 and a_2, which are the strengths of the repulsive and attractive terms in the intermolecular anisotropic potential, were calculated from the above relation using the method of least squares. The values of a_1 and a_2 are obtained by fitting the values of $(k_o)^{O-Ar}_{exptl}$ corresponding to two different sets of $(T_1/\rho)^{O-Ar}_{exptl}$ obtained from linear and empirical fits and are given in table 3.4. The solid lines in Fig. 14 represent the calculated values of $(k_o)^{O-Ar}$ using the eq. (3.80) and the values of a_1 and a_2 obtained for linear fit.

The relative anisotropy, $a_2/4\varepsilon$, in the attractive term of the intermolecular potential was obtained as 0.137 for the linear fit and as 0.135 for the empirical fit. It may be seen from the eq. (3.69) that $a_2/4\varepsilon = \frac{1}{3}((\alpha_{\parallel} - \alpha_{\perp})/\alpha)_{H_2}$. Using the polarizability data its value is obtained as 0.128 [47].

Table 3.2. Values of $(T_1/\rho)^{O-Ar}$ and $(k_o)^{O-Ar}_{exptl}$ as obtained by fitting the T_1/ρ vs. composition data by a linear relation and by the empirical relation (eq. (3.78))

Temp. ^oK	T_1/ρ versus composition fitted by a linear relation		T_1/ρ versus composition fitted by the empirical relation	
	$(T_1/\rho)^{O-Ar}$ in msec/amagat	$(k_o)^{O-Ar}_{exptl}$ $(10^{24} sec^{-2})$	$(T_1/\rho)^{O-Ar}$ in msec/amagat	$(k_o)^{O-Ar}_{exptl}$ $(10^{24} sec^{-2})$
164	0.082	1.14		
185	0.079	1.27		
204	0.076	1.39		
225	0.071	1.53		
246	0.065	1.65		
267	0.061	1.79		
300	0.060	2.21	0.055	1.95
400	0.052	3.63	0.048	3.33
500	0.056	6.05	0.056	6.02
600	0.060	10.10	0.059	9.92

Table 3.3. Values of I(2,12), I(2,6) and I(2,6,12) for dilute H_2-Ar mixture including the first quantum correction for a Lennard-Jones isotropic potential [$(\varepsilon/k)_{H_2\text{-Ar}} = 75.118^{\circ}K$, $(a)_{H_2\text{-Ar}} = 3.169\text{Å}$, $(\mu)_{H_2\text{-Ar}} = 1.919$ amu]

$\beta\varepsilon$	I(2,12)	I(2,6)	I(2,6,12)
0.45516	0.03427	0.05823	0.04113
0.41723	0.03639	0.05844	0.04240
0.37551	0.03934	0.05896	0.04421
0.34137	0.04244	0.05965	0.04612
0.31292	0.04566	0.06045	0.04809
0.28340	0.04979	0.06156	0.05064
0.25720	0.05458	0.06287	0.05350
0.18590	0.07602	0.06867	0.06575
0.15170	0.09537	0.07348	0.07602
0.12520	0.11941	0.07891	0.08799

Table 3.4. Values of the strengths a_1 and a_2 of the repulsive and attractive terms of the anisotropic part of the potential (eq. (3.79)) when T_1/ρ versus composition is fitted by linear as well as by empirical relation (eq. (3.78)) for H_2-Ar.

When $(T_1/\rho)^{O-Ar}$ is obtained by	$a_1 \times 10^{15}$ (ergs)	$a_2 \times 10^{15}$ (ergs)	$a_2/4\varepsilon$
Linear fit	8.19 ± 0.01	5.68 ± 0.01	0.137
Empirical fit	8.11 ± 0.01	5.59 ± 0.01	0.135

In Fig. 14 the point corresponding to the $(k_o)^{O-Ar}_{exptl}$ value at 600K lies slightly higher than the calculated value using the a_1 and a_2 obtained from the least square fit. In order to get a better fit of the entire data, anisotropic potentials as given in the eq.(3.79) but having repulsive terms with radial dependence other than r^{-12} were tried (namely, $\bar{r}^{n'}$ where n' = 14, 15, 16, 17, 18 and 19. Higher values of n' were chosen since the temperature dependence of the integrals I(p) becomes more steeper as n' increases). It was found that the model potential containing the repulsive term varying as $\bar{r}^{12}$ represented the data best. (These different fits are not shown in Fig. 14 for clarity.) The large difference in $(k_o)^{O-Ar}$ values at 600K might be due to the fact that in obtaining the values of $(T_1/\rho)^{O-Ar}_{exptl}$ for 100% Ar in H_2-Ar mixtures a linear (or an empirical relation given by eq. (3.78)) has been used whereas a theory taking into account all the populated J states and the inter J transitions in a H_2-Ar mixture might yield some other dependence of T_1/ρ on the composition which should be used to obtain $(T_1/\rho)^{O-Ar}_{exptl}$.

The value of $a_2/4\varepsilon$ obtained using Bloom-Oppenheim theory and the model potential given in eq. (3.79) is close to the value obtained by polarizability data. From the agreement of the two values of the relative anisotropy, $a_2/4\varepsilon$, in the attractive term of anisotropic intermolecular potential,

obtained from the present analysis over a wide temperature range and the discussion presented above it may be concluded that a model potential written as

$$V = 4\varepsilon \left[\frac{1}{x^{12}} - \frac{1}{x^{6}}\right] + \left(\frac{8.11\times10^{-15}}{x^{12}} - \frac{5.59\times10^{-15}}{x^{6}}\right) P_2 (\cos\theta_1')$$

or,

$$V = 41.46\times10^{-15} \text{ erg } \left[\left(\frac{a}{r}\right)^{12} - \left(\frac{a}{r}\right)^{6}\right] + 5.59\times10^{-15} \text{ erg}$$

$$\times \left[1.45\left(\frac{a}{r}\right)^{12} - \left(\frac{a}{r}\right)^{6}\right] P_2 (\cos\theta_1') \qquad (3.81)$$

where $a = 3.169$ Å for H_2--Ar pair represents the NMR data well and also that the polarizability data can be used to estimate the strength of the attractive anisotropic intermolecular potentials.

Foster et al.[12] analysed their T_1/ρ data in H_2-Ar and other H_2-inert gas mixtures at low temperatures using Quantum Scattering theory and assuming an intermolecular potential of the form as given in eq. (3.79). They obtained values of the relative anisotropy, $a_2/4\varepsilon$, in the anisotropic attractive potential which are twice of that obtained by polarizability data whereby they suspected that perhaps the radial dependence of the repulsive part of the anisotropic potential might be other than $\bar{r}^{12}$. But Riehl et al.[11] have fitted the H_2-He data in low temperature range using an exp(-6) potential and obtained a value of $a_2/4\varepsilon$ which is again twice of that obtained by polarizability data. So it may be concluded that

the Quantum Scattering theory does not give a value for $a_2/4\varepsilon$ consistent with polarizability data.

III.3.2 H_2-N_2 Mixtures

T_1 in H_2-N_2 mixtures were measured as a function of density and composition in the temperature range of 300-600K. The plots of T_1 versus ρ and T_1/ρ versus composition are shown in Figs. 15, 16 and 17. The solid lines represent linear fits. The error bars denote the standard deviations. Where these are not shown, the standard deviations are less than 2%.

In this case also non-linearity of T_1/ρ versus composition was not observed and thus values of $(T_1/\rho)^{0-N_2}$ were obtained by using linear extrapolation. But the two level theory and a recent work by Kalechstein and Armstrong[49] predict a non-linearity. Hence $(T_1/\rho)^{0-N_2}$ values were also found out by fitting the data to the empirical relation as given by eq. (3.78) in a manner described for H_2-Ar mixtures. It was observed that the values of $(T_1/\rho)^{0-N_2}$ obtained from the empirical relation are very close to those obtained by a linear fit within the experimental error. These values of $(T_1/\rho)^{0-N_2}$ together with those obtained by Williams[24] in the temperature range 150-295K, which they have obtained by assuming a linear variation of T_1/ρ versus composition are shown in Fig. 18. Williams' data were also fitted to the

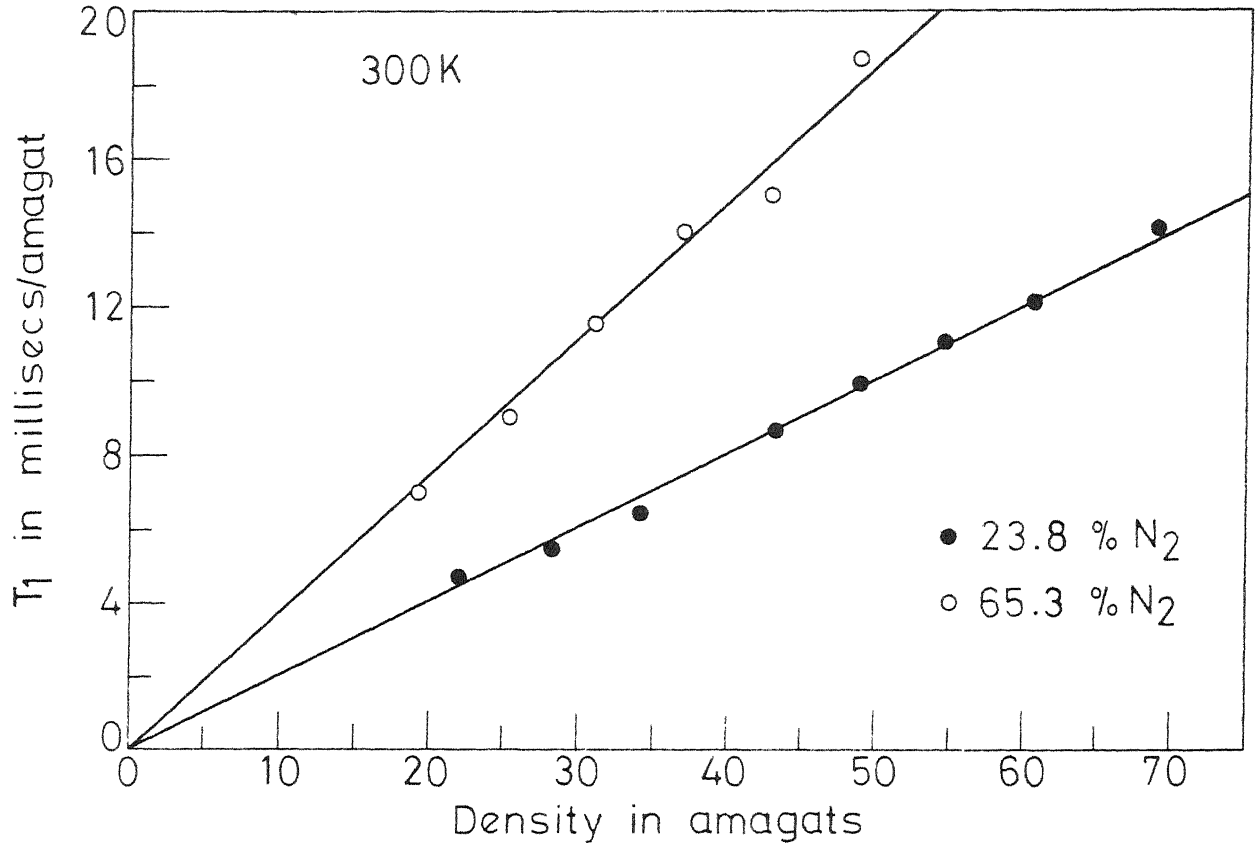

Fig. 15 Plots of T_1 versus ρ in H_2–N_2 mixtures.

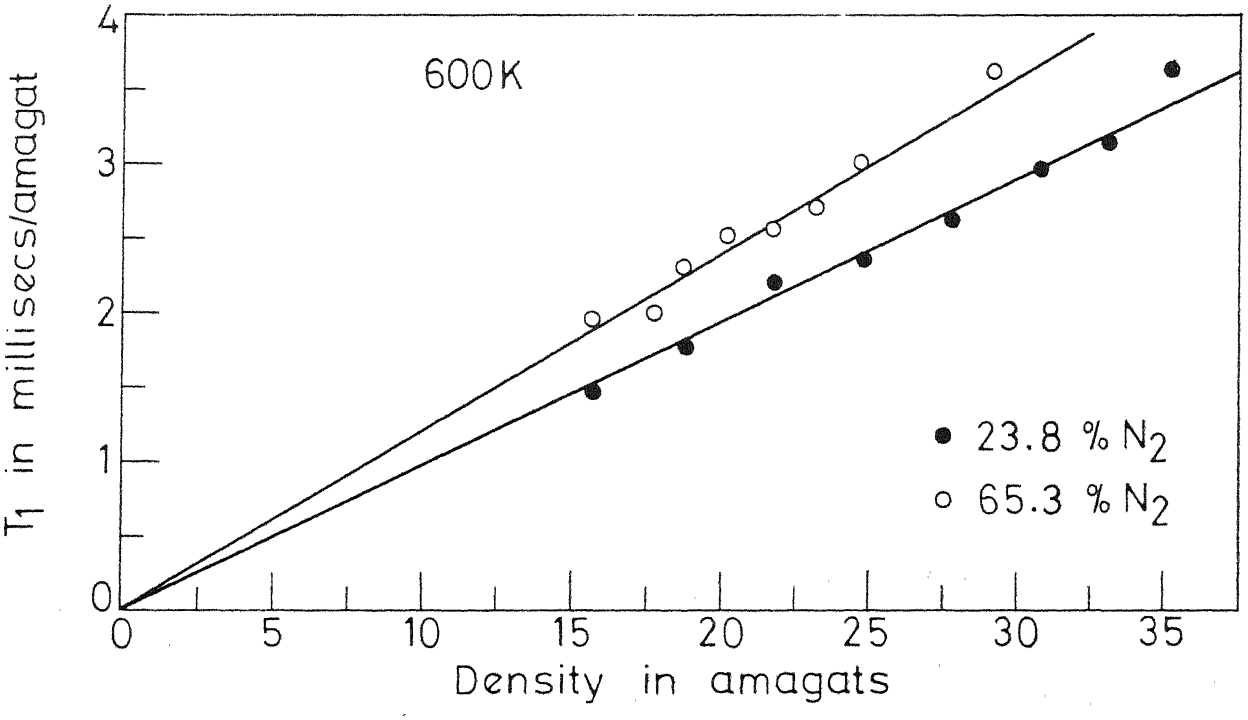

Fig. 16 Plots of T_1 versus ρ in H_2–N_2 mixtures.

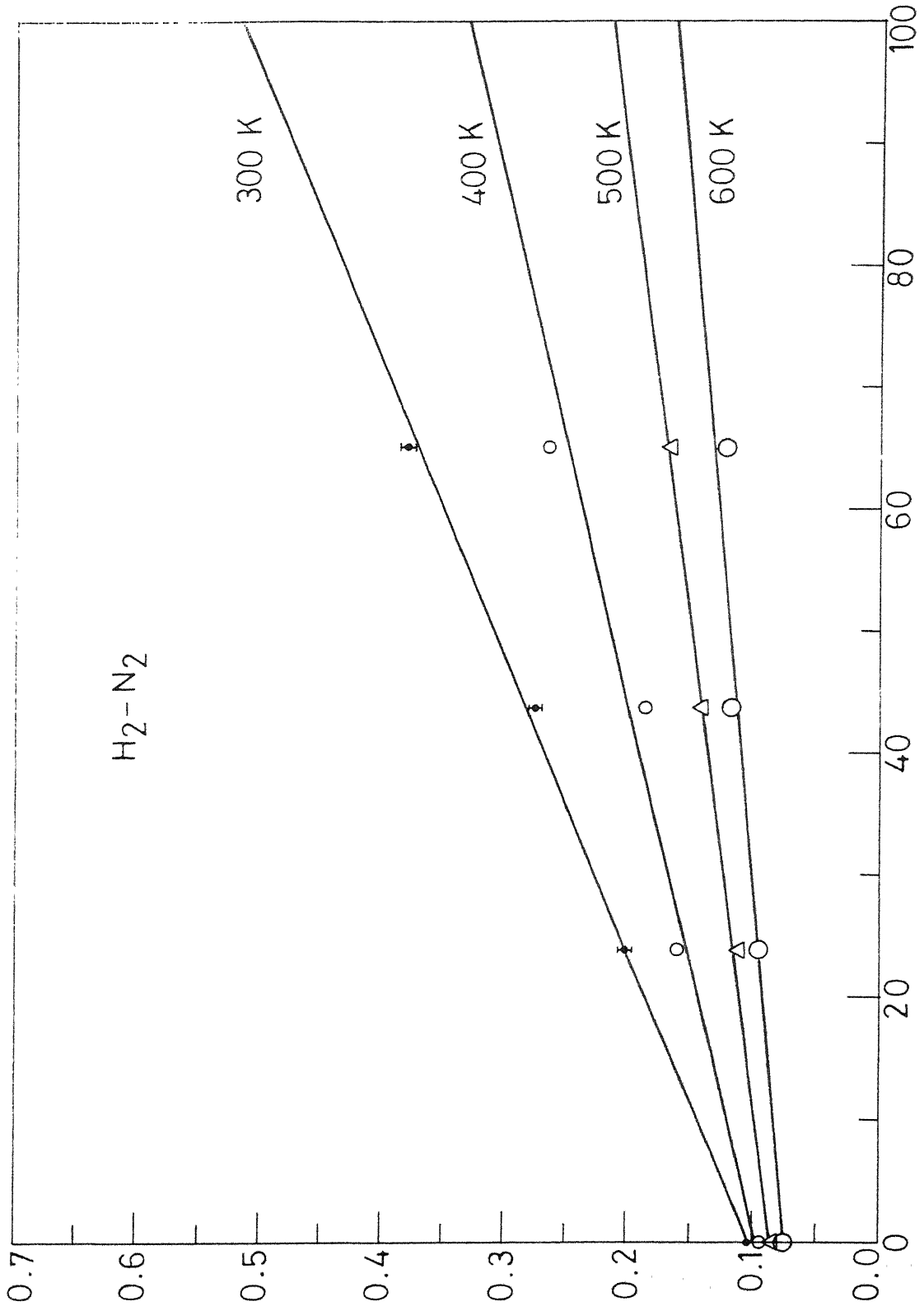

Fig. 17 Dependance of T_1/ρ on Nitrogen concentration at different temperatures.

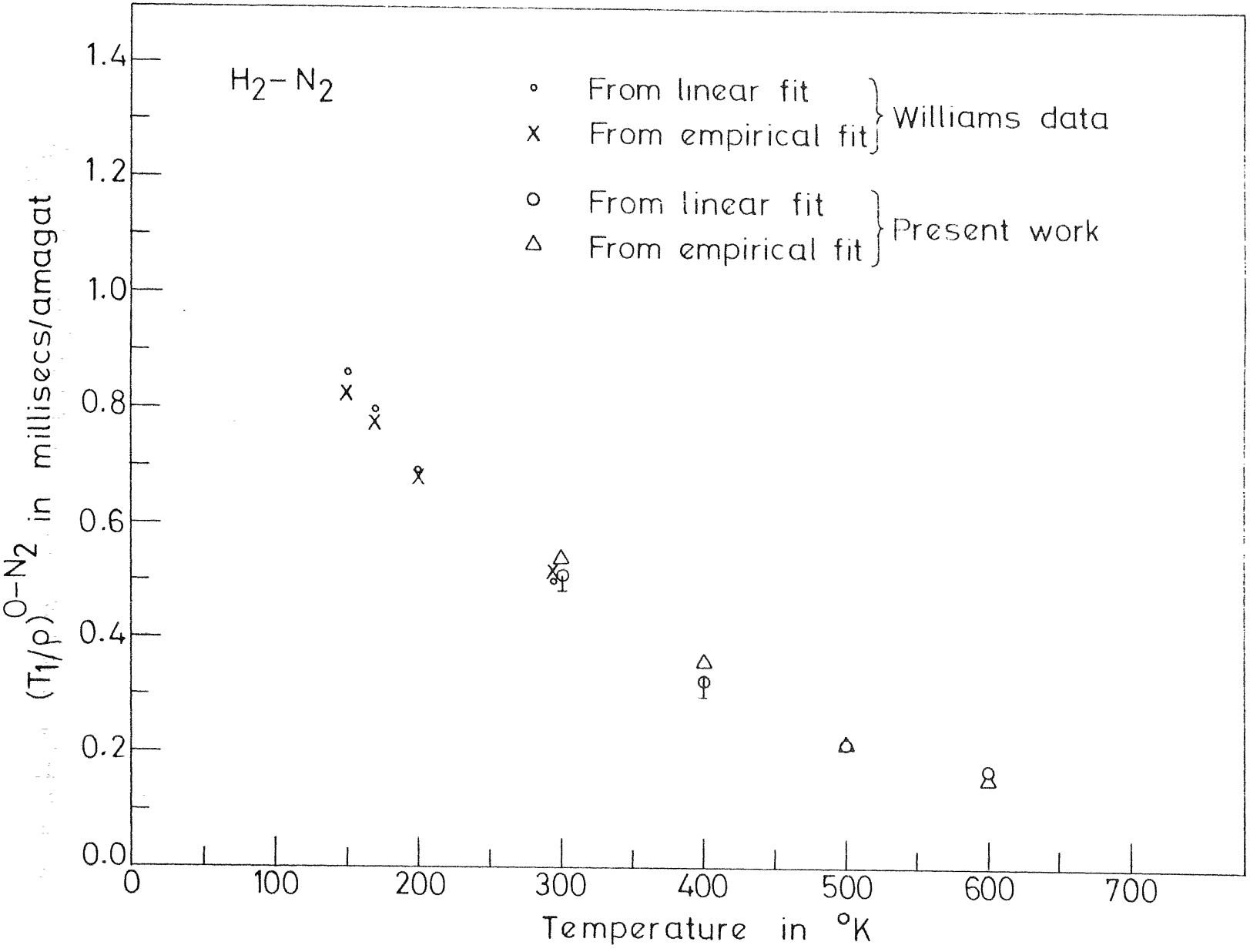

Fig. 18 Plot of $(T_1/\rho)^{O-N_2}$ versus temperature.

empirical relation. The values of $(T_1/\rho)^{O-N_2}$ are shown in Fig. 18. All these values of $(T_1/\rho)^{O-N_2}$ were used to calculate $(k_o + C_{N_2} k_1)^{O-N_2}$ using eq. (3.76). The values of $(T_1/\rho)^{O-N_2}$ and of $(k_o+C_{N_2} k_1)^{O-N_2}$ are also given in table 3.5. Fig. 19 shows the values of $(k_o+C_{N_2} k_1)^{O-N_2}$ obtained from the values of $(T_1/\rho)^{O-N_2}$ evaluated by a linear fit of T_1/ρ versus composition data. The error bars represent standard deviations.

Interpretation

The intermolecular potential between H_2 and N_2 can be written as (see eqs. (3.68), (3.70), (3.73) and (3.75))

$$V = 4\varepsilon\left[\frac{1}{x^{12}} - \frac{1}{x^6}\right] + \left(\frac{a_1}{x^{12}} - \frac{a_2}{x^6}\right)\left[P_2(\cos\theta_1') + P_2(\cos\theta_2')\right]$$

$$+ \left(\frac{b_1}{x^{12}} - \frac{b_2}{x^5}\right) \sum_{q=-2}^{2} a_q Y_{2q}(\Omega_1') \, Y_{2q}(\Omega_2') \qquad (3.82)$$

with $x = r/a$.

For this form of potential one can write, using eqs. (3.76), (3.61), (3.62) and (3.51)

$$(k_o+C_{N_2} k_1)^{O-N_2} = \left(\frac{6\pi}{5\hbar^2}\right)\left[a_1^2 \, I(2,12) + a_2^2 \, I(2,6) - 2a_1 a_2 I(2,6,12)\right]$$

$$+ C_{N_2}\left(\frac{21}{50\pi\hbar^2}\right)\left[b_1^2 \, I(4,12) + b_2^2 I(4,5) - 2b_1 b_2 I(4,5,12)\right] \qquad (3.83)$$

where $C_{N_2} = 5/2$ and $I(4,12)$ etc are certain integrals as defined in eqs. (3.52) and (3.53). The values of the integrals

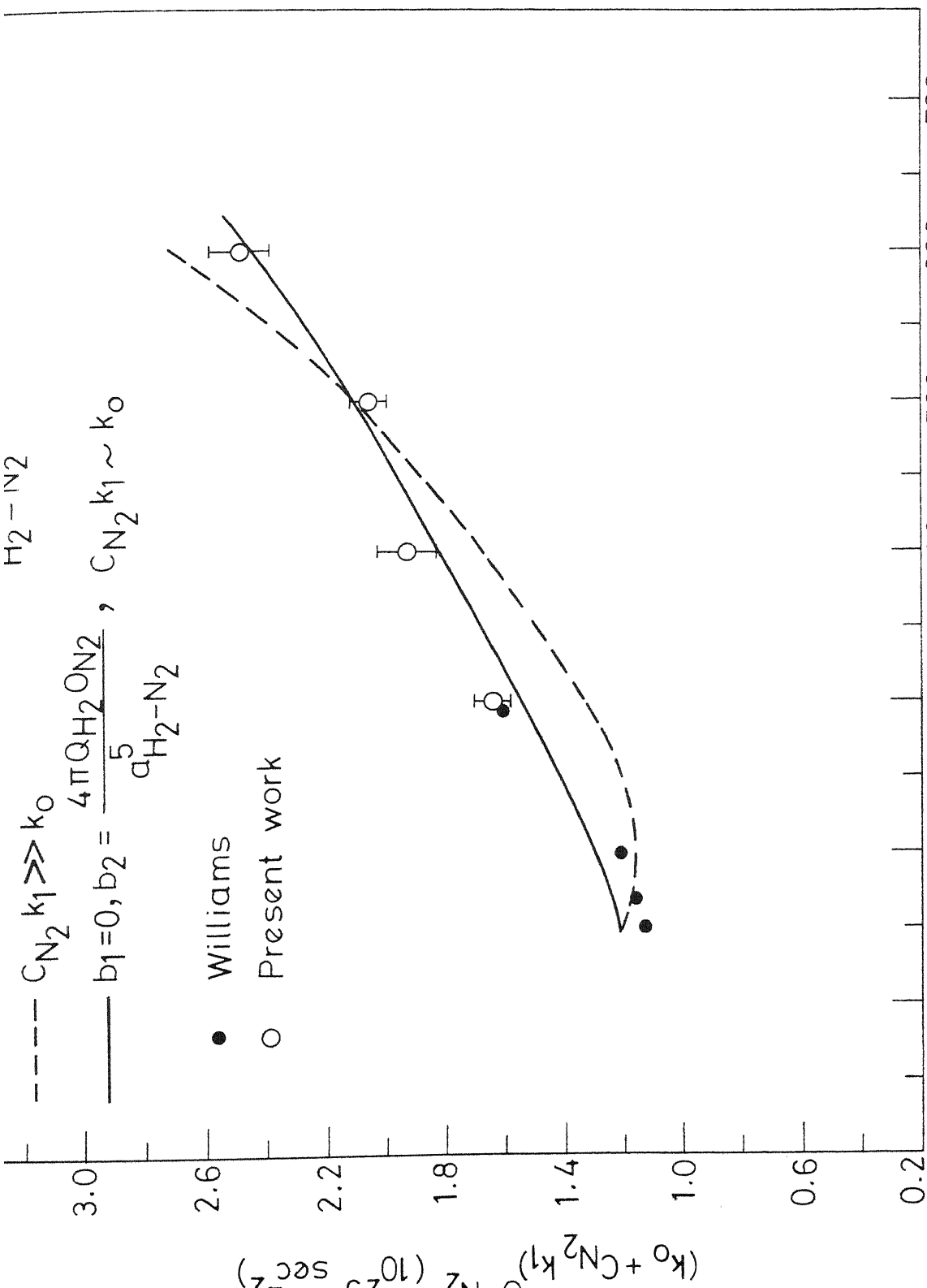

Fig. 19 Plot of $(k_o + C_{N_2} k_1)^{O-N_2}$ versus temperature. Curves show least square fits.

Table 3.5. Values of $(T_1/\rho)^{O-N_2}$ and $(k_o+C_{N_2}k_1)^{O-N_2}$ as obtained by fitting the T_1/ρ versus composition data by a linear relation and by the empirical relation (eq. (3.78)).

Temp. (°K)	T_1/ρ versus composition fitted by a linear relation		T_1/ρ versus composition fitted by the empirical relation	
	$(T_1/\rho)^{O-N_2}$ (msec/amagat)	$(k_o+C_{N_2}k_1)^{O-N_2}$ (10^{25} sec^{-2})	$(T_1/\rho)^{O-N_2}$ (msec/amagat)	$(k_o+C_{N_2}k_1)^{O-N_2}$ (10^{25} sec^{-2})
150	0.860	1.11	0.822	1.07
170	0.793	1.15	0.785	1.14
200	0.687	1.20	0.680	1.19
295	0.500	1.62	0.520	1.68
300	0.510	1.66	0.540	1.76
400	0.330	1.95	0.350	2.06
500	0.215	2.05	0.212	2.00
600	0.170	2.47	0.163	2.39

Table 3.6. Values of I(2,12), I(2,6) and I(2,6,12) for dilute H_2-N_2 mixture including the first quantum correction for Lennard-Jones isotropic potential. [$(\varepsilon/k)_{H_2-N_2}=59.44^{\circ}K$, $(a)_{H_2-N_2}=3.314\text{Å}$, $(\mu)_{H_2-N_2}$ = 1.881 amu][48]

$\beta\varepsilon$	I(2,12)	I(2,6)	I(2,6,12)
0.39624	0.03780	0.05867	0.04326
0.34962	0.04164	0.05946	0.04562
0.29717	0.04779	0.06101	0.04940
0.20148	0.06975	0.06702	0.06227
0.19812	0.07101	0.06735	0.06297
0.14712	0.09879	0.07429	0.07777
0.12007	0.12554	0.08021	0.09094
0.09906	0.15899	0.08678	0.10631

Table 3.7. Values of I(4,12), I(4,5) and I(4,5,12) for dilute H_2-N_2 mixture including the first quantum correction for Lennard-Jones isotropic potential

$\beta\varepsilon$	I(4,12)	I(4,5)	I(4,5,12)
0.39624	0.02757	0.05016	0.03170
0.34962	0.03031	0.05018	0.03314
0.29717	0.03479	0.05066	0.03550
0.20148	0.05059	0.05330	0.04357
0.19812	0.05150	0.05346	0.04399
0.14712	0.07155	0.05686	0.05316
0.12007	0.09087	0.05990	0.06143
0.09906	0.11463	0.06322	0.07061

are given in Tables 3.6 and 3.7.

From the eq. (3.76) it can be seen that the experimental observation of the proton spin-lattice relaxation times T_1 in H_2-N_2 mixtures gives information on $(k_o + C_{N_2} k_1)^{O-N_2}$ and not on k_o and $C_{N_2} k_1$ separately. Therefore to extract information about the attractive and repulsive parts of the anisotropic intermolecular potential (eq. (3.82)) the $(k_o + C_{N_2} k_1)^{O-N_2}$ values were fitted to eq. (3.83) using the method of least squares and considering the cases where k_o is assumed to be much smaller than $C_{N_2} k_1$ and hence neglected as was done for H_2-CO_2 mixtures by previous workers[21] and when the effect of k_o is also taken into account. The values of b_1, b_2 and a_1, a_2, b_1, b_2 for these two cases were calculated. Neither of these two models gave satisfactory fit of the experimental data. Hence slight variations of these models were tried in which b_2 was taken to be equal to the strength of the quadrupole-quadrupole interaction between the molecules H_2 and N_2. The repulsive term in k_o was excluded and the constants a_2, b_1 were evaluated. This also did not give a good fit of the experimental data nor it gave a value of a_2 consistent with the polarizability data. Another model was tried in which the repulsion in k_1 was excluded and a_1 and a_2 were evaluated using the method of least squares. It was found that this model represented the data best as can be seen from the Fig. 19. a_1 and a_2 for this model are obtained as

$(6.98\pm0.01)\times10^{-15}$ ergs and $(4.25\pm0.01)\times10^{-15}$ ergs respectively. The relative anisotropy, $a_2/4\varepsilon$, in the attractive $\bar{r}^6$ term of the anisotropic part of the potential was obtained as 0.131 which is close to the value, 0.128, obtained from polarizability data.

Thus it may be concluded that a potential written as

$$V = 4\varepsilon\left(\frac{1}{x^{12}} - \frac{1}{x^6}\right) + \left(\frac{6.98\times10^{-15}}{x^{12}} - \frac{4.25\times10^{-15}}{x^6}\right)\left[P_2(\cos\theta_1') + P_2(\cos\theta_2')\right]$$

$$- \frac{4\pi Q_{H_2} Q_{N_2}}{a^5 x^5} \sum_{q=-2}^{2}{}' a_q \, Y_{2q}(\Omega_1') \, Y_{2q}^{*}(\Omega_2')$$

or,

$$V = 32.81\times10^{-15}\ \text{erg}\left[\left(\frac{a}{r}\right)^{12} - \left(\frac{a}{r}\right)^6\right] + 4.25\times10^{-15}\ \text{erg}\left[1.64\left(\frac{a}{r}\right)^{12} - \left(\frac{a}{r}\right)^6\right]$$

$$\times\left[P_2(\cos\theta_1') + P_2(\cos\theta_2')\right]$$

$$- 27.73\times10^{-15}\ \text{erg}\left(\frac{a}{r}\right)^5 \sum_{q=-2}^{2}{}' a_q \, Y_{2q}(\Omega_1') \, Y_{2q}^{*}(\Omega_2') \qquad (3.84)$$

where the values $\varepsilon = 8.203 \times 10^{-15}$ ergs, $a = 3.314$ Å for H_2-N_2 pair for Lennard-Jones potential and $Q_{H_2} = 0.63 \times 10^{-26}$ e.s.u. cm^2 [52], and $Q_{N_2} = 1.4 \times 10^{-26}$ e.s.u. cm^2 [52] are used, represents the N.M.R. data well and also that the polarizability data can be used to get an estimate of the strength of the attractive $\bar{r}^6$ term of the anisotropic intermolecular potential.

III.3.3 H_2-N_2O Mixtures

Proton spin-lattice relaxation times T_1 were measured in H_2-N_2O mixtures as a function of temperature, density and composition in the temperature range of 200-400K. The measurements were done up to 400K only since some chemical reaction was observed to occur in the mixture inside the Be-Cu pressure vessel at higher temperatures. Typical plots of the values of T_1 as a function of ρ and of T_1/ρ as a function of composition are shown in Figs. 20, 21 and 22.

In this case also T_1/ρ was found to vary linearly with composition. The analysis was done exactly in the same way as was done for H_2-N_2 mixtures. It was observed here also that values of $(T_1/\rho)^{0-N_2O}$ obtained by empirical and linear fits are close to each other (see table 3.8) and thus one can consider T_1/ρ to be a linear function of composition. Values of $(T_1/\rho)^{0-N_2O}$ obtained using a linear fit and the empirical fit are shown in Fig. 23 along with the data obtained by Johnson and Waugh[5] at room temperature. The values of $(k_o+C_{N_2O}k_1)^{0-N_2O}$ were calculated using these values of $(T_1/\rho)^{0-N_2O}$ and eq. (3.76) and are given in table 3.8. Values of $(k_o+C_{N_2O}k_1)^{0-N_2O}$ corresponding to the $(T_1/\rho)^{0-N_2O}$ obtained by linear fit are shown in Fig. 24.

Interpretation

The intermolecular potential for H_2 and N_2O molecules

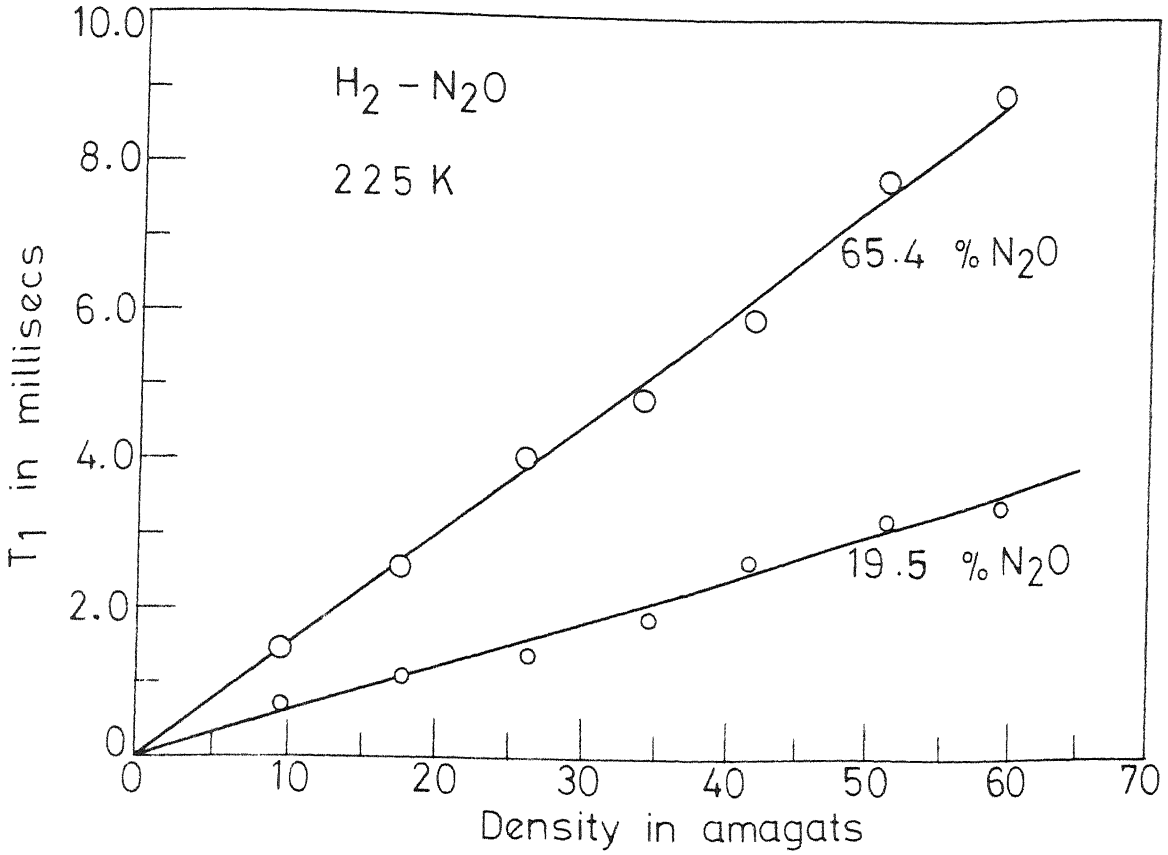

Fig. 20 Plots of T_1 vs ρ in H_2-N_2O mixtures.

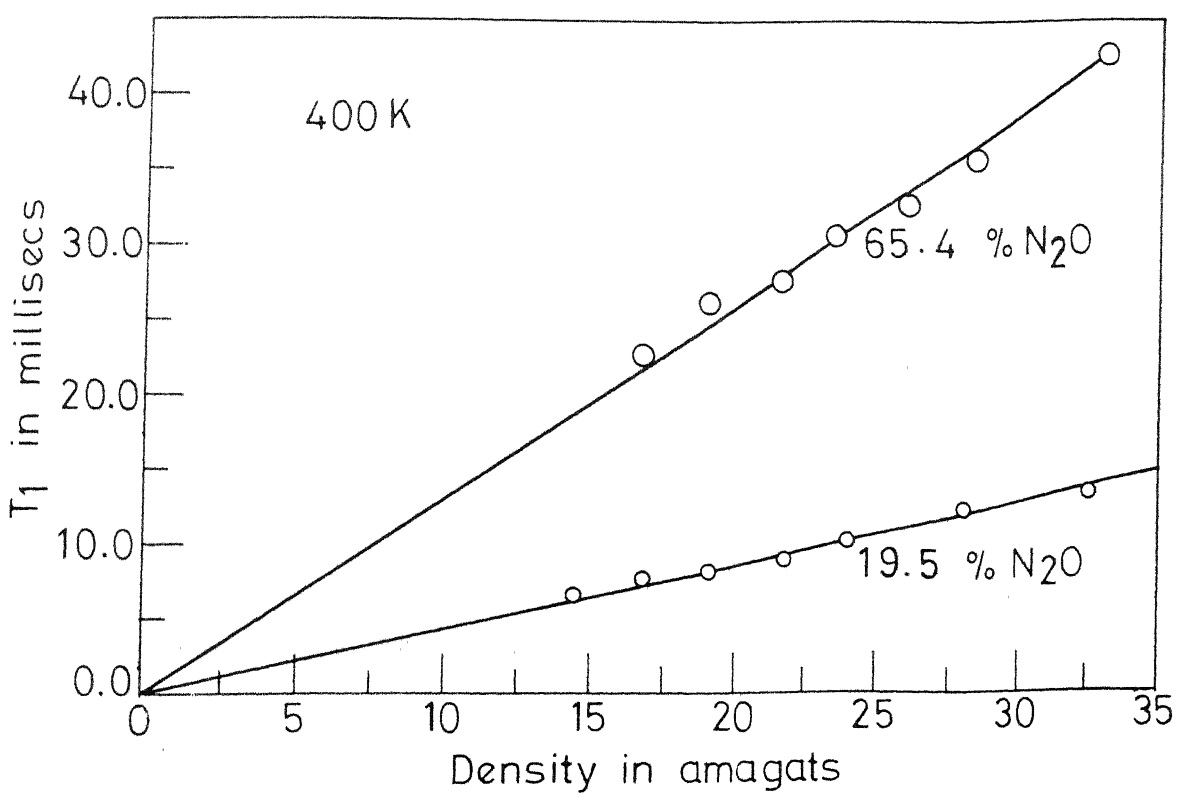

Fig. 21 Plots of T_1 vs ρ in H_2-N_2O mixtures.

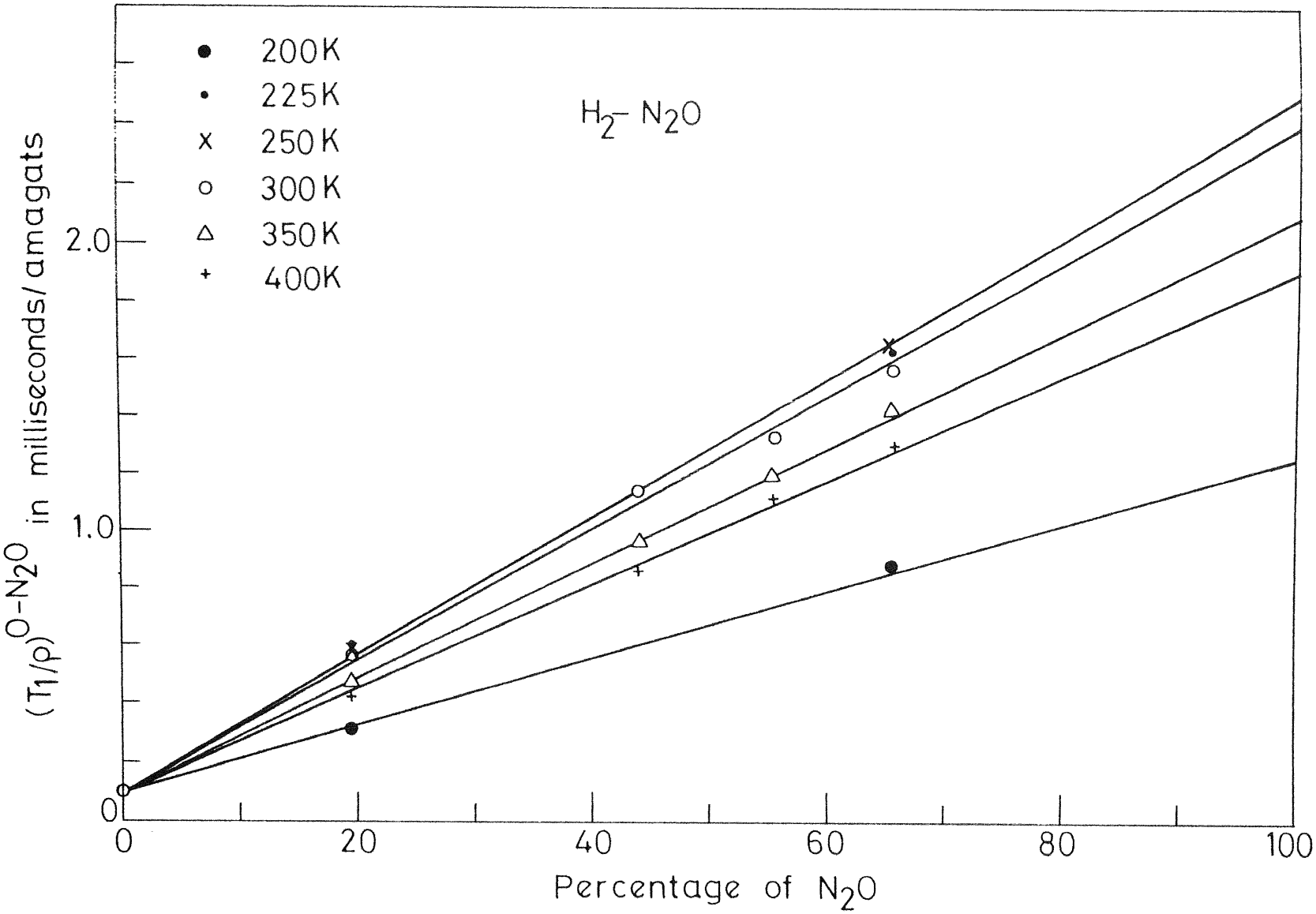

Fig. 22 Dependence of T_1/ρ on the composition of H_2–N_2O mixture.

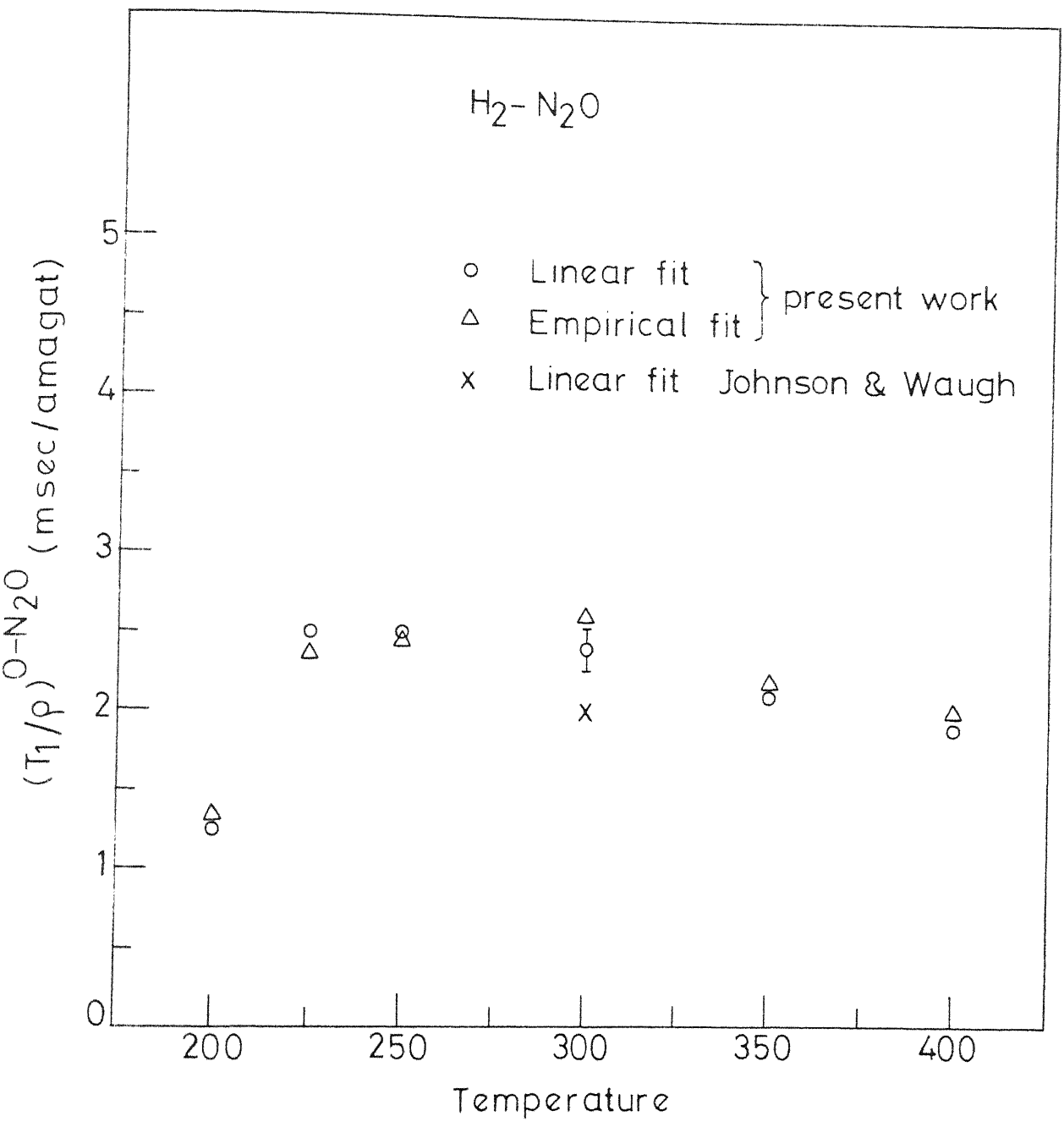

Fig. 23 Values of $(T_1/\rho)^{O-N_2O}$ as a function of temperature.

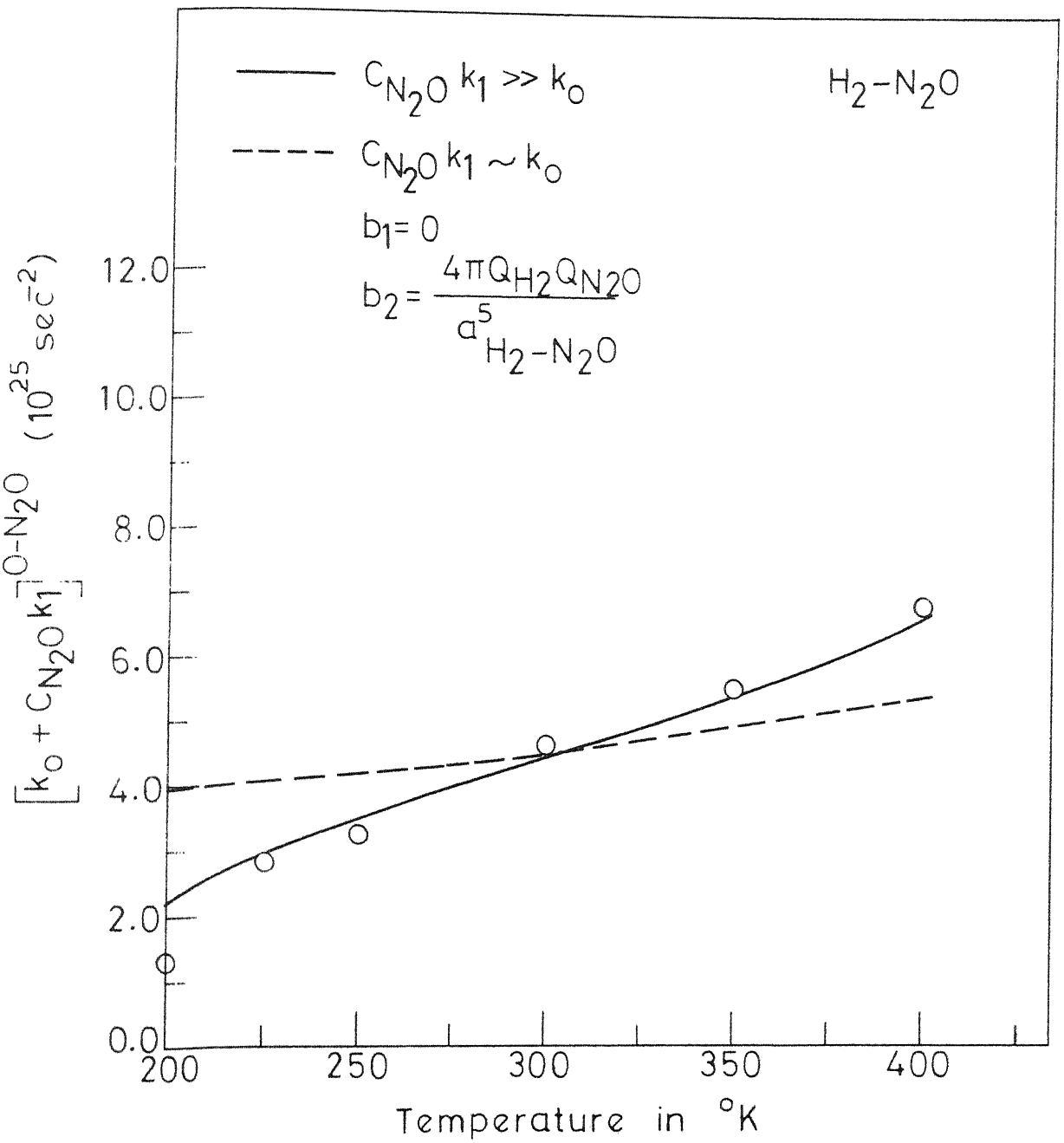

Fig. 24 Plot of $(k_o + C_{N_2O} k_1)^{O-N_2O}$ versus temperature. Curves show least square fits

can be written, neglecting, the small dipole moment on N_2O, in the form of eq. 3.82, whence $(k_o+C_{N_2O}k_1)^{O-N_2O}$ can be written in the form of eq. (3.83). The values of the constants a_1, a_2, b_1 and b_2 were calculated using the method of least squares. (The values of integrals I(2,12) etc. occurring in eq. (3.83) are given in Tables 3.9 and 3.10.) Different model potentials were tried to fit the data best, as was done for H_2-N_2, for the cases when $k_o \ll C_{N_2O}k_1$ and when $k_o \sim C_{N_2O}k_1$. It was found that a potential of the form of eq. (3.82) with

$$\left.\begin{aligned} a_1 &= 0 \\ a_2 &= 0 \end{aligned}\right\} \text{ i.e. } \quad k_o \ll C_{N_2O}k_1$$

represents the data best as can be seen from the Fig. 24 (fits with other forms are not shown in this figure for clarity). b_1 and b_2 obtained in this way are $(10.33\pm0.01)\times10^{-14}$ ergs and $(4.93\pm0.09)\times10^{-14}$ ergs respectively. The model potential (eq. (3.82)) then can be expressed as

$$V = 4\varepsilon\left[\frac{1}{x^{12}} - \frac{1}{x^6}\right] + \left(\frac{10.33\times10^{-14}}{x^{12}} - \frac{4.93\times10^{-14}}{x^5}\right) \sum_{q=-2}^{2} a_q Y_{2q}(\Omega_1') Y_{2q}^{*}(\Omega_2') \text{ erg} \qquad (3.85)$$

with $x = r/a$ and $\varepsilon = 11.54\times10^{-15}$ ergs for H_2-N_2O pair. The quadrupole moment Q_{N_2O} of N_2O was obtained using the relation

Table 3.8. Values of $(T_1/\rho)^{O-N_2O}$ and $(k_o+C_{N_2O}k_1)^{O-N_2O}$ as obtained by fitting the T_1/ρ vs composition data by a linear relation and by the empirical relation (eq. (3.78))

Temp. (°K)	T_1/ρ versus composition fitted by a linear relation		T_1/ρ versus composition fitte by the empirical relation	
	$(T_1/\rho)^{O-N_2O}$ (msec/amagat)	$(k_o+C_{N_2O}k_1)^{O-N_2O}$ (10^{25} sec^{-2})	$(T_1/\rho)^{O-N_2O}$ (msec/amagat)	$(k_o+C_{N_2O}k_1)^{O-N_2O}$ (10^{25} sec^{-2})
200	1.25	1.17	1.34	1.26
225	2.51	2.77	2.37	2.63
250	2.48	3.24	2.45	3.19
300	2.40	4.68	2.65	5.15
350	2.10	5.50	2.18	5.70
400	1.91	6.80	2.01	7.15

Table 3.9. Values of I(2,12), I(2,6) and I(2,6,12) for dilute H_2-N_2O mixture including the first quantum correction for Lennard-Jones isotropic potential.

$[(\varepsilon/k)_{H_2\text{-}N_2O} = 83.624^{\circ}K,\ (a)_{H_2\text{-}N_2O} = 3.759\text{Å},$
$(\mu)_{H_2\text{-}N_2O} = 1.928$ amu.$]$[48].

$\beta\varepsilon$	I(2,12)	I(2,6)	I(2,6,12)
0.41812	0.03627	0.05833	0.04242
0.37166	0.03971	0.05907	0.04445
0.33450	0.04322	0.05988	0.04662
0.27875	0.05080	0.06196	0.05130
0.24030	0.05864	0.06422	0.05602
0.20648	0.06807	0.06662	0.06136

Table 3.10. Values of I(4,12), I(4,5) and I(4,5,12) for dilute H_2-N_2O mixture including the first quantum correction for Lennard-Jones isotropic potential.

βε	I(4,12)	I(4,5)	I(4,5,12)
0.41812	0.02658	0.05030	0.03124
0.37166	0.02890	0.05013	0.03239
0.33450	0.03139	0.05026	0.03371
0.27875	0.03685	0.05098	0.03660
0.24030	0.04235	0.05188	0.03944
0.20648	0.04934	0.05309	0.04295

$$b_2 = \frac{4\pi Q_{H_2} Q_{N_2O}}{a^5_{H_2\text{-}N_2O}}, \qquad Q_{H_2} = 0.63 \times 10^{-26} \text{ esu cm}^2$$

$$a_{H_2\text{-}N_2O} = 3.755 \text{ Å}$$

as $(4.65 \pm 0.09) \times 10^{-26}$ esu cm^2. This value is higher than the recommended value which is 3.0×10^{-26} esu cm^2 [52], though it is in agreement with the value obtained earlier by NMR method ($Q_{N_2O} = 4.25 \times 10^{-26}$ esu cm^2)[9] using the data at room temperature. It is quite likely that the form of the repulsive part of the anisotropic potential used here needs to be improved.

CHAPTER IV*

PROTON SPIN-LATTICE RELAXATION IN CH_3Cl GAS

IV.1 General

CH_3Cl is a symmetric top molecule having C_{3v} symmetry. Its rotational states can be described by the quantum numbers J, K, and M which correspond to the total angular momentum $\vec{J}$, the projection of $\vec{J}$ on the symmetry axis of the molecule and the projection of $\vec{J}$ on a space-fixed Z-axis respectively. If $\mathcal{H}_J$ denotes the rotational Hamiltonian for a symmetric top molecule, one can write

$$\mathcal{H}_J \, |JKM\rangle = \hbar \omega_{JK} |JKM\rangle$$

where

$$\hbar\omega_{JK} = \frac{\hbar^2}{2I_o} J(J+1) + \frac{\hbar^2}{2} \left(\frac{1}{I_A} - \frac{1}{I_o}\right) K^2 \qquad (4.1)$$

$$= hBJ(J+1) + h(A-B) K^2 \qquad (4.2)$$

where I_A and I_o are the moments of inertia of the molecule parallel and perpendicular to the symmetry axis and their

---

*A paper entitled 'Proton spin-lattice Relaxation in Low Density CH_3Cl Gas' based on the material presented in this chapter was published in Chemical Physics Letters, Vol. 58, page 375-378 (1978).

values for CH_3Cl are[39] 5.49 x 10^{-40} gm cm^2 and 57 x 10^{-40} gm cm^2 respectively. In writing the eq. (4.1) it has been assumed that the molecule is in ground electronic and vibrational states.

IV.2 Review of the Spin-relaxation Theory

The dominant intramolecular interactions that contribute to the spin-lattice relaxation in dilute gases are the intramolecular dipolar and spin-rotational interactions. Assuming that the contribution from the intramolecular dipolar interaction is negligible for CH_3Cl as was found for many symmetric top molecules BF_3, CHF_3, CH_3F, PH_3, NH_3 by Dong and Bloom[44] and Armstrong and Courtney[45], the proton spin-lattice relaxation rate can be written as (see eq.(1.22)),

$$\frac{1}{T_1} = R_C$$

The theory of nuclear spin relaxation due to spin-rotation interaction was first discussed by Hubbard[40] and Blicharski[42] and was extended by Bloom et al.[43] for the case of dilute polyatomic gases. They have obtained expressions for T_1 in terms of the Fourier transforms of the correlation functions of the spin-rotation interaction. A brief review is presented below.

The Hamiltonian describing the spin-rotation interaction can be written, in general, as

$$\mathcal{H}_{s.r.} = -h \vec{I} \cdot \tilde{C} \cdot \vec{J} \tag{4.3}$$

where $\vec{I}$ is the nuclear spin angular momentum, $\vec{J}$ is the molecular rotational angular momentum and $\tilde{C}$ is the spin-rotation tensor. In polyatomic molecules, the spin-rotation interaction is in general characterized by six independent parameters, viz., the three principal values of the spin-rotation tensor and the three Euler angles required to specify the orientation of the principal axis coordinate system. For symmetric top molecules of symmetry C_{3v} (such as molecules of the form YX_3 or CX_3Y) the spin-rotation tensor for the Y nucleus which is on the body symmetry axis is of the form[45]

$$\tilde{C} = \begin{bmatrix} C_{\perp} & 0 & 0 \\ 0 & C_{\perp} & 0 \\ 0 & 0 & C_{\parallel} \end{bmatrix} \tag{4.4}$$

where $C_{\perp}$ and $C_{\parallel}$ are proportional to the magnetic fields per unit angular momentum produced at Y site by rotations of the molecule about axes perpendicular and parallel to the symmetry axis respectively. Thus, only two independent parameters, namely, $C_{\perp}$ and $C_{\parallel}$ are needed to characterize the spin-rotation tensor. It is customary to represent the spin-

rotation tensor in terms of quantities C_a and C_d defined as

$$C_a = \frac{1}{3}(C_{\parallel} + 2C_{\perp}), \quad C_d = C_{\perp} - C_{\parallel} \tag{4.5}$$

C_a is the spin-rotation coupling constant for the isotropic part of the interaction whereas C_d is for the anisotropic part of the interaction. The Hamiltonian for the spin-rotation interaction for the Y nuclei may be written as [40]

$$h^{-1}\mathcal{H}_{s.r.} = C_a \sum_{k=-1}^{1} (-1)^k I'_k J'_{-k} - C_d\left(I'_o J'_o - \frac{1}{3}\sum_{k=-1}^{1}(-1)^k I'_k J'_{-k}\right) \tag{4.6}$$

where

$$I_o = I_z$$
$$I_{\pm} = \mp \frac{1}{\sqrt{2}}(I_x \pm i\, I_y)$$

and

$$J_o = J_z$$
$$J_{\pm} = \mp \frac{1}{\sqrt{2}}(J_x \pm i\, J_y)$$

The primes in eq. (4.6) denote that the components are taken in molecule-fixed coordinate frame with its Z axis along the molecular symmetry axis. For one of the off-axis X nuclei, $\tilde{C}$ can be written as [44,45]

$$\tilde{C} = \begin{bmatrix} 0 & C_{xx}-C_{yy} & 0 \\ C_{xx}-C_{yy} & 0 & 0 \\ 0 & 0 & 0 \end{bmatrix} +$$

$$+\begin{bmatrix} \frac{1}{2}(C_{xx}-C_{yy}) & 0 & 0 \\ 0 & -\frac{1}{2}(C_{xx}-C_{yy}) & 0 \\ 0 & 0 & 0 \end{bmatrix}$$

$$+\begin{bmatrix} \frac{1}{2}(C_{xx}+C_{yy}) & 0 & 0 \\ 0 & \frac{1}{2}(C_{xx}+C_{yy}) & 0 \\ 0 & 0 & C_{zz} \end{bmatrix} \qquad (4.7)$$

where C_{xx}, C_{yy} and C_{zz} are the diagonal components of the spin-rotation tensor for one of the X nuclei. The first two terms have matrix elements connecting the states for which $\Delta K = \pm 1, \pm 2$ and the last term for $\Delta K = 0$. For dilute gases, it can be shown[44,45] that the matrix elements between different K states can be neglected. $\tilde{C}$, then, contains only the last term in eq. (4.7) and only the parameters $C_\perp$ and $C_\parallel$ defined as,

$$C_\perp = \tfrac{1}{2}(C_{xx} + C_{yy}) \qquad (4.8)$$

$$\text{and} \qquad C_\parallel = C_{zz}$$

are required to describe the spin-rotation tensor. The spin-rotation tensor for X nuclei also, thus, reduces to the form of eq. (4.4). The Hamiltonian for the spin-rotation interaction for the X nuclei, therefore, can be written in the form of eq. (4.6) where C_a and C_d would be given by eqs. (4.8) and (4.5).

In space fixed frame the eq. (4.6) becomes

$$h^{-1}\mathcal{H}_{s.r.} = \sum_{m} I_m K_{1m} \tag{4.9}$$

where

$$K_{1m} = (-1)^m C_a J_{-m} - \left(\frac{2}{3}\right)^{\frac{1}{2}} C_d \sum_{\mu} (-1)^{\mu} C(112; m\mu) D^2_{o,-(m+\mu)} J_{\mu} \tag{4.10}$$

in which D are the rotational matrices (Rose[38]).

Using the general theory[1], R_C is written as,

$$R_C = 4\pi^2 J_{1m}(\omega_o) \tag{4.11}$$

where $J_{1m}(\omega_o)$ is the Fourier transform of $G_{1m}(\tau)$

$$J_{1m}(\omega_o) = \int_{-\infty}^{\infty} G_{1m}(\tau)\, e^{-i\omega_o \tau}\, d\tau \tag{4.12}$$

and $G_{1m}(\tau)$ is the correlation function of K_{1m}

$$G_{1m}(\tau) = R_e \langle K_{1m}(0)\, K^{\dagger}_{1m}(\tau) \rangle \tag{4.13}$$

where the symbol $\langle\ \rangle$ represents an ensemble average. For a freely rotating molecule $[G_{1m}(\tau)]_{free}$ comes out to be independent of m. Hardy[37] has shown that under quite general conditions, one can write

$$G_{1m}(\tau) = G_{10}(\tau) \exp(im\omega_J \tau) \tag{4.14}$$

where ω_J is the Larmor frequency for the molecule. Thus, in order to evaluate $G_{1m}(\tau)$ only $G_{10}(\tau)$ need to be evaluated which, with the help of eq. (4.13), can be written as,

$$G_{10}(\tau) = R_e[C_a^2 \langle J_o(0)\ J_o(\tau)\rangle$$

$$-2(\tfrac{2}{3})^{\frac{1}{2}} C_a C_d \sum_{\mu} (-1)^{\mu} C(112;0\mu)\ \langle D^2_{o,-\mu}(0) J_{\mu}(0) J_o(\tau)\rangle$$

$$+ \tfrac{2}{3} C_d^2 \sum_{\mu,\mu'} (-1)^{\mu+\mu'} C(112;0\mu)\ C(112,0\mu')$$

$$\times \langle D^2_{o,-\mu}(0)\ J_{\mu}(0) J^{\dagger}_{\mu'}(\tau)\ D^{2\dagger}_{o,-\mu'}(\tau)\rangle] \qquad (4.15)$$

Due to collisions between molecules the time dependence of $G_{10}(\tau)$ is affected. For polyatomic molecules it was assumed by Bloom, Bridges and Hardy[43] that the effect of collisions could be adequately described by writing

$$G_{1m}(\tau) = [G_{1m}(\tau)]_{free}\ g_2(\tau) \qquad (4.16)$$

where $g_2(0) = 1$ and $g_2(\tau)$ is a function which decreases monotonically to zero as τ is increased and is called the reduced correlation function. So, to take into account the effect of collisions on G_{1m} and hence on G_{10} all the correlation functions occurring in the right hand side of eq. (4.15) are expressed as products of corresponding free molecular correlation functions with monotonically decreasing functions of time $g_1(\tau)$, $g_2(\tau)$ and $g'_{12}(\tau)$ respectively, i.e.

$$\langle J_o(0) J_o(\tau)\rangle = [\langle J_o(0) J_o(\tau)\rangle]_{free}\ g_1(\tau) \qquad (4.17)$$

$$\langle D^2_{o,-\mu}(0)\ J_{\mu}(0)\ J_o(\tau)\rangle = [\langle D^2_{o,-\mu}(0)\ J_{\mu}(0)\ J_o(\tau)\rangle]_{free}\ g_{12}(\tau) \qquad (4.18)$$

$$\langle D^2_{0,-\mu}(0)\ J_\mu(0)\ J^\dagger_{\mu'}(\tau)\ D^{2\dagger}_{0,-\mu'}(\tau)\rangle$$

$$= [\langle D^2_{0,-\mu}(0)\ J_\mu(0) \qquad J^\dagger_{\mu'}(\tau)\ D^{2\dagger}_{0,-\mu'}(\tau)\rangle]_{free}\ g'_{12}(\tau) \tag{4.19}$$

where $g_1(\tau)$, $g_2(\tau)$ and $g'_{12}(\tau)$ are the 'reduced correlation functions' with $g_1(0) = g_2(0) = g'_{12}(0) = 1$. After evaluating the free-molecular correlation functions it is seen that they contain terms that are time independent as well as terms that oscillate at frequencies corresponding to rotational transitions $\Delta J = \pm 1$. For dilute gases it can be shown that the oscillating terms do not contribute appreciably to the spectral density at the Larmor frequency and, hence, can be neglected. Then with the help of eqs. (4.17), (4.19) and (4.15) one gets

$$G_{10}(\tau) = \tfrac{1}{3}\, C_a^2 \sum_{J=0}^{\infty} \sum_{K=-J}^{J} (2J+1)J(J+1)\ P_{JKM}$$

$$\times \{g_1(\tau) - \frac{2}{3}\frac{C_d}{C_a}\left[\frac{3K^2-J(J+1)}{J(J+1)}\right] g_{12}(\tau)$$

$$+ \frac{1}{9}\left(\frac{C_d}{C_a}\right)^2 \left[\frac{3K^2-J(J+1)}{J(J+1)}\right]^2 g'_{12}(\tau)\} \tag{4.20}$$

The spectral density $J_{10}(\omega)$ is obtained using eqs. (4.15) and (4.12) as

$$J_{10}(\omega) = p(\omega)\ \tfrac{1}{3}\, C_a^2\ \langle J(J+1)\rangle\ j_1(\omega) \tag{4.21}$$

where $j_1(\omega) = \int_{-\infty}^{\infty} g_1(\tau)\, e^{-i\omega\tau}\, d\tau$; $\omega = \omega_o - \omega_J$

and

$$p(\omega) = 1 - \frac{2}{3}\left(\frac{C_d}{C_a}\right) \frac{\langle 3K^2 - J(J+1)\rangle}{\langle J(J+1)\rangle} \frac{j_{12}(\omega)}{j_1(\omega)}$$

$$+ \frac{1}{9}\left(\frac{C_d}{C_a}\right)^2 \frac{\left\langle \frac{9K^4}{J(J+1)} - 6K^2 + J(J+1)\right\rangle}{\langle J(J+1)\rangle} \frac{j'_{12}(\omega)}{j_1(\omega)} \qquad (4.22)$$

and $j_{12}(\omega)$ and $j'_{12}(\omega)$ are the spectral densities of $g_{12}(\tau)$ and $g'_{12}(\tau)$ respectively. Using eqs. (4.21), (4.22) and (4.11) and assuming that $\omega_o >> \omega_J$, R_C is obtained as

$$R_C = \frac{4\pi^2}{3} p(\omega_o)\, C_a^2 \langle J(J+1)\rangle\, j_1(\omega_o) \qquad (4.23)$$

If all the 'reduced correlation functions' occurring in eq. (4.20) are assumed to decay with the same time constant τ_1, i.e.

$$g(\tau) = \exp(-\tau/\tau_1) \qquad (4.24)$$

then $j_1(\omega) = j_{12}(\omega) = j'_{12}(\omega) = \frac{2\tau_1}{1 + \omega^2 \tau_1^2}$.

Defining quantity α as,

$$\alpha = \frac{\hbar^2}{2I_o kT} \qquad (4.25)$$

and evaluating the averages and using eq. (4.22), the eq. (4.23) reduces to[45]

$$R_C = \frac{2\pi^2}{\alpha}\left[I_{01}C_a^2 - 2\left(I_{10} - \frac{1}{3}I_{01}\right)C_a C_d + \left(I_{2-1} - \frac{2}{3}I_{10} + \frac{1}{9}I_{01}\right)C_d^2\right]$$

$$\times \frac{\tau_1}{1 + \omega^2 \tau_1^2} \qquad (4.26)$$

where

$$I_{01} = \frac{2\alpha}{3} \langle J(J+1) \rangle = 1 - \frac{y^2}{3}$$

$$I_{10} = \frac{2\alpha}{3} \langle K^2 \rangle = \frac{1 - y^2}{3} \qquad (4.27)$$

$$I_{2-1} = \frac{2\alpha}{3} \left\langle \frac{K^4}{J(J+1)} \right\rangle = \left(\frac{1-y^2}{y^2}\right)^2 \left(-1 - \frac{y^2}{3} + s\right)$$

$$I_{1-1} = \left\langle \frac{K^2}{J(J+1)} \right\rangle = -\left(\frac{1-y^2}{y^2}\right)(1 - s)$$

where

$$y = \left(1 - \frac{I_A}{I_o}\right)^{\frac{1}{2}} = \left(\frac{\beta}{\alpha+\beta}\right)^{\frac{1}{2}}$$

$$s = \frac{1}{2y} \ln \left(\frac{1+y}{1-y}\right) \quad \text{for} \quad \beta > 0$$

$$= \frac{1}{|y|} \tan^{-1} |y| \quad \text{for} \quad \beta < 0.$$

Eq. (4.26) can be written, in short, as

$$R_C = \frac{4\pi^2}{\alpha} C_{eff}^2 \frac{\tau_1}{1 + (\omega_o - \omega_J)^2 \tau_1^2} \qquad (4.28)$$

where

$$C_{eff}^2 = \left(1 - \frac{y^2}{3}\right) C_a^2 + \frac{4}{9} y^2 C_a C_d$$

$$+ \frac{1}{9} \left[9\left(\frac{1-y^2}{y^2}\right)^2 \left(-1 - \frac{y^2}{3} + s\right) - 1 + \frac{5}{3} y^2\right] C_d^2 \qquad (4.29)$$

The spin-lattice relaxation time T_1 due to spin-rotation interaction is then given by

$$\frac{1}{T_1} = \frac{4\pi^2}{\alpha} C_{eff}^2 \frac{\tau_1}{1 + (\omega_0 - \omega_J)^2 \tau_1^2} \qquad (4.30)$$

IV.2 Results and Interpretation

The proton spin-lattice relaxation time T_1 was measured in CH_3Cl in the density range of 0.2-6.5 amagats at room temperature (298K). The dependence of T_1 on the density is shown in Fig. 25. Long relaxation times coupled with low signal to noise ratio made it difficult to take data below 0.2 amagat. The details of sample purification and preparation are given in Chapter II.

Assuming that the spin-rotation interaction is the dominant mechanism of relaxation in CH_3Cl the relaxation rate can be given by eq. (4.30). From this equation it is seen that the plot of T_1 versus ρ goes through a characteristic minimum at $\omega\tau = 1$ while for $\omega\tau_1 >> 1$, $T_1 \propto \tau_1$. Using the kinetic theory the correlation time may be taken as

$$\tau_1 = \frac{1}{\rho \langle \sigma v \rangle} \qquad (4.31)$$

where ρ is the number density of the gas and $\langle \sigma v \rangle$ is the velocity averaged collision cross-section for molecular reorientation. Since τ_1 is inversely proportional to ρ, it is obvious that in the region $\omega\tau_1 >> 1$, T_1 decreases as the frequency of collision (and hence ρ) increases but in

the region $\omega\tau_1 \ll 1$, $T_1 \propto \rho$ (phenomenon called as pressure narrowing). From eqs. (4.30) and (4.31) and following Armstrong et al.[45] T_1 can be written as

$$\frac{T_1}{\rho} = A + B/\rho^2 \qquad (4.32)$$

with $$A = \frac{\alpha}{4\pi^2} \frac{1}{C_{eff}^2} \frac{\omega_o}{\rho_{min}} \quad , \ \omega_o \gg \omega_J \qquad (4.33)$$

$$B = \frac{\alpha}{4\pi^2} \frac{1}{C_{eff}^2} \omega_o \rho_{min} \qquad (4.34)$$

where ρ_{min} is the density at which T_1 minimum occurs.

The experimental data between 0.2 to 6.5 amagats was fitted to eq. (4.32) using the method of least squares. The fitted curve is shown in Fig. 25 by solid line. The values of A and B obtained are given below along with their standard deviations,

$$A = 371.12 \pm 4.09 \quad \text{msec/amagat}$$

$$B = 27.55 \pm 4.03 \quad \text{msec.amagat.}$$

The values of ρ_{min} and $T_{1\,min}$ were obtained as 0.273 amagat and 202.23 msecs. respectively.

Using eq. (4.33) and the values of A and ρ_{min}, the value of C_{eff}^2 was obtained as 0.1 MHz neglecting ω_J in comparison to ω_o.

The minimum value of T_1 occurs at $(\omega_o - \omega_J)\tau_1 = 1$. Since $\tau_1^{-1} = \rho \langle\sigma v\rangle$ at constant temperature

$$\langle\sigma v\rangle = \frac{\omega_o - \omega_J}{\rho_{min}} \qquad (4.35)$$

Defining an effective cross-section, σ_{eff}, for molecular reorientation as $\langle\sigma v\rangle / \bar{v}$, where $\bar{v} = (8kT/\pi\mu)^{\frac{1}{2}}$ in which k is the Boltzmann constant and μ is the reduced mass of CH_3Cl, it was found that $\sigma_{eff} = 4.01$ Å^2. Comparing this value with the kinetic crosssection, $\sigma_{kin} = \pi a^2_{CH_3Cl}$ where the value of the Lennard-Jones parameter a_{CH_3Cl} for methyl chloride is 4.15 Å [48], one get $\sigma_{kin}/\sigma_{eff} \simeq 14$, which indicates that it takes about 14 collisions on the average to randomize the rotational angular momentum.

CHAPTER V

ANALYSIS OF T_1 DATA IN HCl, F_2, NH_3 AND BF_3

V.1 General

The general theory of spin-relaxation[1] expresses the relaxation rates in terms of the correlation functions of the intramolecular interactions. Using Bloom-Oppenheim theory[10] the correlation functions for intramolecular interactions can be written in terms of the correlation functions of intermolecular interactions. Rigorous expressions for the relaxation rates for simple systems like H_2, where the number of rotational states populated at ordinary temperatures is one or two, were obtained by Bloom et al.[10] and the T_1 data were interpreted to obtain information about the anisotropic intermolecular potential. For systems of diatomic and polyatomic molecules where the number of populated rotational states is large, no such theory is available in literature. Hence, Rajan et al.[17] proposed a model according to which the correlation time corresponding to a state for the intramolecular interactions is taken to be equal to the lifetime of the molecule in that J state. The lifetime is calculated

using the first order perturbation theory assuming that the collisions are weak. They applied this model to obtain the intermolecular potentials in spherical top molecules, CH_4, CF_4 and SiF_4 and in mixtures of CH_4 with He, Ne, Ar, N_2 and CO_2. From the analysis of T_1 data, they obtained values of hyperpolarizability of CH_4 and the octopole moments of CH_4, CF_4 and SiF_4 which are in good agreement with the values that are obtained from other methods. Hence, one can conclude that this model worked well in these systems.

The purpose of the present investigation is to test the validity of this model in some linear and symmetric top molecules. Two linear molecules having dipole and quadrupole moments, viz. HCl and F_2 respectively and two symmetric top molecules having dipole and quadrupole moments viz., NH_3 and BF_3 were chosen for this purpose. For all these molecules, the spin-rotation interaction is the dominant mechanism of relaxation [25-27].

The Hamiltonian corresponding to the intramolecular spin-rotational interaction for the nuclei can be written, in general, as[1]

$$\mathcal{H} = -h\vec{I}\cdot\tilde{C}\cdot\vec{J} \qquad (5.1)$$

where $\vec{I}$ and $\vec{J}$ are the nuclear spin and molecular rotational angular momentum operators respectively and $\tilde{C}$ represents the

spin-rotation coupling constant which is a tensor for symmetric top molecules and a scaler for linear molecules.

Using the general theory[1], T_1 is given by

$$\frac{1}{T_1} = \left\langle \frac{1}{T_1^J} \right\rangle \tag{5.2}$$

where

$$\frac{1}{T_1^J} = \frac{8\pi^2}{3} C^2 J(J+1) \tau_1^J \tag{5.3}$$

for linear molecules, in the short correlation time limit. Here τ_1^J is the correlation time for the spin-rotation interaction corresponding to the J state. For a symmetric top molecule eq. (5.2) reduces to

$$\frac{1}{T_1} = \frac{4\pi^2}{\alpha} C_{eff}^2 \tau_1 \tag{5.4}$$

where α and C_{eff}^2 are defined earlier in eqs. (4.25) and (4.29), respectively, in Chapter IV.

According to Rajan's model[17], $T_1^{J'}$ for a state J'M' can be written as

$$\frac{1}{\tau_1^{J'}} = \frac{1}{2J'+1} \sum_{M'=-J'}^{J'} \sum_{J} \sum_{M=-J}^{J} A(JM;J'M') \tag{5.5}$$

$$M \neq M' \text{ for } J=J',$$

for linear molecules and

$$\frac{1}{\tau_1^{J'}} = \frac{1}{(2J'+1)^2} \sum_{M'=-J'}^{J'} \sum_{J} \sum_{M=-J}^{J} \left\{ \sum_{KK'} A(JKM;J'K'M') \right\} \tag{5.6}$$

$$M' \neq M \text{ for } J'=J$$

for symmetric top molecules.

Here $A(JM;J'M')$ and $A(JKM;J'K'M')$ are the transition rates for the transitions $J'M' \rightarrow JM$ and $J'K'M' \rightarrow JKM$ for the linear and symmetric top molecules respectively and are evaluated in terms of the intermolecular interactions using first order perturbation theory (weak collision approximation).

The intermolecular potential between two molecules can be written as

$$V = v_o(r) + v_A(r,\theta) \tag{5.7}$$

The isotropic part, $V_o(r)$, is assumed to be a Lennard-Jones potential

$$V_o(r) = 4\varepsilon \left[\left(\frac{a}{r}\right)^{12} - \left(\frac{a}{r}\right)^{6}\right], \quad \varepsilon \text{ and } a \text{ are the Lennard-Jones parameters,} \tag{5.8}$$

and the anisotropic part, $v_A(r,\theta)$, can be expressed in terms of the multipole interactions between them.

The anisotropic attractive interaction potential between two molecules having axially symmetric charge distribution is, in general, written as[50] a summation of terms of the form

$$V_\lambda = 4\pi\, \varepsilon_\lambda(r) \sum_{m_1,m_2} C(\ell_1 \ell_2 \ell; m_1 m_2 m)\, Y_{\ell_1 m_1}(\Omega_1)\, Y_{\ell_2 m_2}(\Omega_2)\, Y^{*}_{\ell m}(\Omega) \tag{5.9}$$

with $$\varepsilon_\lambda(r) = C_\lambda \frac{Q_{\ell_1} Q_{\ell_2}}{r^{\ell+1}}$$

where Ω_1, Ω_2 and Ω are the orientations of the vectors shown in Fig. 26 related to a space-fixed frame (SFF). In this figure e_1 and e_2 are elementary charge distributions on the molecules 1 and 2 respectively. The molecules have been considered as having rigid non-overlapping charge distributions centered around origins O_1 and O_2. The vector connecting O_1 and O_2, denoted by $\vec{r} = (r, \Omega)$ where $\Omega = (\theta, \phi)$, is along the intermolecular axis. $\lambda = \ell_1 \ell_2$, $\ell = \ell_1 + \ell_2$, ℓ_1 and ℓ_2 indicate the order of the electric moment: for dipole $\ell_1 = 1$, the quadrupole $\ell_1 = 2$ etc.

$$C_\lambda = C_{\ell_1, \ell_2} = \frac{(-1)^{\ell_2}}{(2\ell+1)} \left[\frac{4\pi\,(2\ell+1)!}{(2\ell_1+1)!\,(2\ell_2+1)!} \right]^{\frac{1}{2}} \qquad (5.10)$$

The quantity Q_{ℓ_1} denotes the scaler magnitude of the multipole moment of order ℓ_1 for the axially symmetric charge distribution. $C(\ell_1 \ell_2 \ell;\ m_1 m_2 m)$ is a Clebsch-Gordon coefficient as defined by Rose[38] and $Y_{\ell m}$ are the spherical harmonics of order ℓ of the corresponding angles.

The repulsive part of the anisotropic potential was assumed to vary as r^{-12} having the same angle dependence as that of the attractive part.

V.2 Linear Molecules

1. Molecules having dipole moment

The anisotropic part of the intermolecular potential between two molecules having permanent dipole moments, such

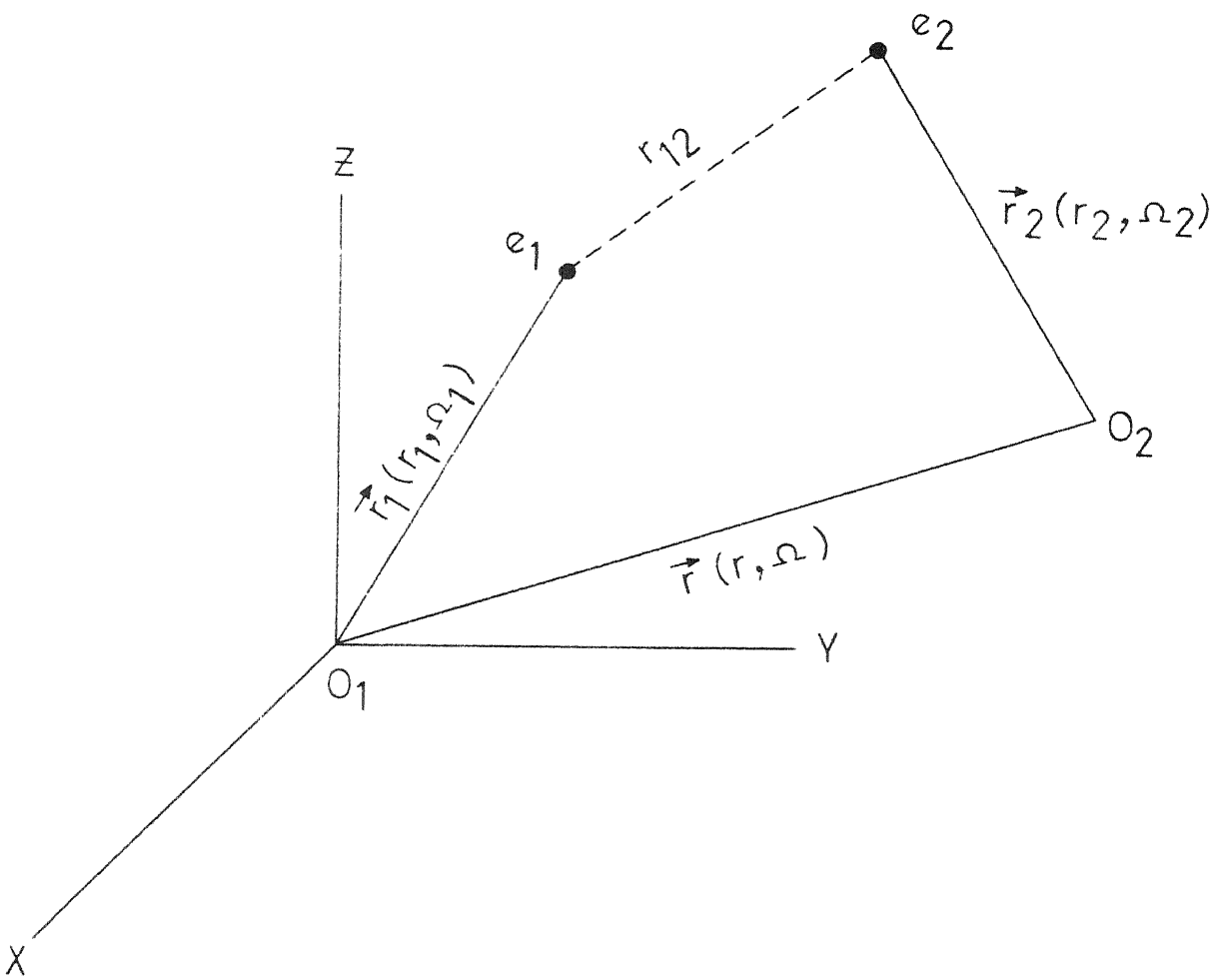

Fig. 26 Orientation of Ω_1, Ω_2 and Ω relative to SFF.

as HCl, can be written using eq. (5.9), neglecting higher order interactions, as

$$v_A(r,\theta) = \left(\frac{8\pi}{15}\right)^{\frac{1}{2}} b(ax) \sum_{m_1 m_2} C(112; m_1 m_2 m)\, Y_{1m_1}(\Omega_1)\, Y_{1m_2}(\Omega_2)\, Y^{*}_{2m}(\Omega) \tag{5.11}$$

$$\text{where} \quad b(ax) = \frac{a_1}{x^{12}} - \frac{a_2}{x^{3}} \tag{5.12}$$

$$\text{with} \quad x = r/a \quad \text{and} \quad a_2 = 4\pi\mu^2/a^3 \tag{5.13}$$

The effect of the anisotropic potential is to produce transitions in molecule 1 (e.g., HCl) from the state J',M' to the state J,M while the molecule 2 (e.g., another HCl molecule) simultaneous undergoes a transition from J''', M''' to J'', M''. Denoting the transition rate for this process by $A[(JM;J'M')(J''M'';J'''M''')]$, one can write[10] the transition rate for the transition $J',M' \rightarrow JM$ for the molecule 1 as (see eqs. (3.37) and (3.38)).

$$A(JM;J'M') = \sum_{J''J'''M'M'''} A[(JM;J'M')(J''M'';J'''M''')] \tag{5.14}$$

where

$$A[(JM;J'M')(J''M'';J'''M''')] = \sum_{m_1 m_2} \left(\frac{8\pi}{15}\right) j(\omega_{JJ';J''J'''}) \times [C(112; m_1 m_2 m)]^2 P_{J'''M'''} \left|(JM \mid Y_{1m_1}(\Omega_1) \mid J'M')\right|^2 \times \left|(J''M'' \mid Y_{1m_2}(\Omega_2) \mid J'''M''')\right|^2 \tag{5.15}$$

where $\hbar\omega_{JJ';J''J'''} = (E_J - E_{J'}) + (E_{J''} - E_{J'''})$ (5.16)

$P_{J'''M'''} = \frac{P_{J'''}}{2J''' + 1}$, $P_{J'''}$ being the probability that the molecule has the rotational energy $E_{J'''}$.

and $j(\omega_{JJ';J''J'''})$ is given by

$$j(\omega_{JJ';J''J'''}) = \frac{1}{\hbar^2} \int_{-\infty}^{\infty} e^{i\omega_{JJ';J''J'''}t}\, k(t)\,dt \qquad (5.17)$$

where

$$k(t) = (N-1)\left\langle b[r(0)]\, Y^{*}_{2m}[\Omega(0)]\, b[r(t)]\, Y_{2m}[\Omega(t)] \right\rangle \qquad (5.18)$$

and is the correlation function of $b(r)Y^{*}_{2m}(\Omega)$, N being the total number of molecules. If the spacing between the rotational levels of the molecule is small, as is the case for molecules having large moment of inertia, it can be assumed that

$$j(\omega_{JJ';J''J'''}) \simeq j(0) \qquad (5.19)$$

The function $j(0)$ has been evaluated by Bloom and Oppenheim[10] using Constant Acceleration Approximation and an expression for this corresponding to dipole-dipole interaction is obtained by putting p=2 in eq. (3.49) of Chapter III of this thesis, as

$$j(0) = \frac{\rho a^4 (2\pi\beta\mu)^{\frac{1}{2}}}{\hbar^2} I(2) \qquad (5.20)$$

where ρ is the number density of the gas, a is the Lennard-

Jones distance parameter, $\beta = 1/kT$ and μ is the reduced mass of the colliding pair and

$$I(2) = a_1^2 I(2,12) + a_2^2 I(2,3) - 2a_1 a_2 I(2,3,12) \qquad (5.21)$$

where I(2,12) etc. are certain integrals as defined in eqs. (3.52) and (3.53) in Chapter III.

Using eq. (4.34) of Rose to evaluate the matrix elements occurring in eq. (5.15) and then using eqs. (5.14), one gets

$$A(JM,J'M') = \frac{1}{6\pi}\, j(0)\, \frac{2J'+1}{2J+1} \left[C(J'1J;\, M',\, M-M')\right]^2 \left[C(J'1J,00)\right]^2 \qquad (5.22)$$

The average life time $\tau_1^{J'}$ in the state J' is obtained from eqs. (5.5) and (5.22) as

$$\frac{1}{\tau_1^{J'}} = \frac{1}{6\pi}\, j(0) \qquad (5.23)$$

The spin-lattice relaxation time T_1 is then, given by (using eqs. (5.3) and (5.2))

$$(T_1)^{-1} = \frac{8\pi^2 C_{eff}^2}{3}\, 6\pi\, \frac{1}{j(0)} \cdot \langle J(J+1) \rangle \qquad (5.24)$$

$$\text{or} \quad \frac{T_1}{\rho} = \frac{3}{8\pi^2 C_{eff}^2}\, \frac{1}{6\pi}\, \frac{1}{\langle F \rangle}\, \frac{\rho_1 a^4 (2\pi\beta\mu)^{\frac{1}{2}}}{\hbar^2} \left[a_1^2 I(2,12) + a_2^2 I(2,3) - 2a_1 a_2 I(2,3,12) \right] \qquad (5.25)$$

where $F = J(J+1)$, $\rho_1 = 2.69 \times 10^{19}$ molecules/cc and $\langle\rangle$ represents an average over the rotational states appreciably populated at the temperature of interest.

2. Molecules having quadrupole moment

For this group of molecules (e.g. F_2) an expression for anisotropic attractive intermolecular potential is obtained from eq. (5.9) by putting $\ell_1 = \ell_2 = 2$. The total intermolecular anisotropic potential is, then given by

$$v_A(r,\theta) = \left(\frac{56\pi}{45}\right)^{\frac{1}{2}} b(ax) \sum_{m_1 m_2} C(224;\, m_1 m_2 m)\, Y_{2m_1}(\Omega_1) \times Y_{2m_2}(\Omega_2)\, Y^{*}_{4m}(\Omega) \qquad (5.26)$$

$$\text{where} \quad b(ax) = \frac{a_1}{x^{12}} - \frac{a_2}{x^5} \qquad (5.27)$$

$$\text{and} \quad x = r/a \qquad \text{and} \qquad a_2 = 4\pi Q^2/a^5 \qquad (5.28)$$

where Q is the quadrupole moment of the molecule.

Proceeding in the same way as for the previous case the following relations are obtained

$$A(JM;J'M') = \frac{7}{10\pi}\, j(0)\, \frac{2J'+1}{2J+1} \left[C(J'2J;\, M',\, M-M')\right]^2 \left[C(J'2J;00)\right]^2 \qquad (5.29)$$

$$\frac{1}{\tau_1}_J = \frac{7}{10\pi}\, j(0) \left[1 - \frac{1}{5}\, \frac{J(J+1)}{(2J-1)(2J+3)}\right] \qquad (5.30)$$

$$\text{and} \quad \frac{T_1}{\rho} = \frac{3}{8\pi^2 C_{eff}^2} \quad \frac{7}{10\pi} \quad \frac{1}{\langle F \rangle} \quad \frac{\rho_1 \, a^4 (2\pi\beta\mu)^{\frac{1}{2}}}{\hbar^2} \, I(4) \qquad (5.31)$$

where

$$F = \frac{J(J+1)}{1 - \frac{J(J+1)}{5(2J-1)(2J+3)}} \qquad (5.32)$$

$$I(4) = a_1^2 I(4,12) + a_2^2 I(4,5) - 2a_1 a_2 I(4,5,12) \qquad (5.33)$$

V.3 Symmetric Top Molecules

1. Molecules having dipole moments

Since these molecules (e.g., NH_3) have axially symmetric charge distribution, the intermolecular potential between two molecules is given by eq. (5.11). The transition rates are evaluated in the same way as was done for the case V.2.1, the only difference being that the rotational states of a symmetric top molecule are described by the quantum numbers J, K, M and the factor P_{JKM} is used, in the place of P_{JM}, to evaluate the averages. The matrix elements are evaluated using normalized symmetric top wave functions[38]

$$|JKM\rangle = \left(\frac{2J+1}{8\pi^2}\right)^{\frac{1}{2}} D^{J\,*}_{MK}(\alpha\beta\gamma)$$

and the relation (see eq. (4.30) of Rose[38]) $Y^{*}_{2m}(\beta,\alpha) = \left(\frac{5}{4\pi}\right)^{\frac{1}{2}} \times D^{2}_{M0}(\alpha\beta 0)$. After evaluating the matrix elements and carrying out the summations the following expression is obtained for the transition rate A(JKM, J'K'M')

$$A(JKM, J'K'M') = \left(\frac{1}{6\pi}\right) j(0) \frac{2J'+1}{2J+1} [C(J'1J;M', M-M']^2$$

$$\times [C(J'1J;K', 0, K)]^2 \delta_{K',K} \quad (5.34)$$

Using eq. (5.6) and then eq. (5.4), τ_1^J and T_1 are obtained as

$$\frac{1}{\tau_1^J} = \frac{4}{27\pi} j(0) \quad (5.35)$$

$$\frac{T_1}{\rho} = \frac{\alpha}{4\pi^2} \frac{1}{C_{eff}^2} \left(\frac{4}{27\pi}\right) \frac{\rho_1 a^4 (2\pi\beta\mu)^{\frac{1}{2}}}{\hbar^2}$$

$$\times [a_1^2 I(2,12) + a_2^2 I(2,3) - 2a_1 a_2 I(2,3,12)] \quad (5.36)$$

where $$\alpha = \frac{\hbar^2}{2I_o k} \quad (5.37)$$

I_o being the moment of inertia of the molecule about an axis perpendicular to the symmetry axis.

2. Molecules having quadrupole moment

For molecules having quadrupole moment and axially symmetric charge distribution (e.g., BF_3) the interaction potential $v_A(r,\theta)$ is given by eq. (5.26). Evaluating the matrix elements etc. in the same way as done for the previous case one gets,

$$A(JKM, J'K'M') = \frac{56\pi}{45} \frac{9}{125} \left(\frac{5}{4\pi}\right)^2 j(0) \frac{2J'+1}{2J+1}$$

$$\times [C(J'2J;\ M', M-M')]^2 [C(J'2J, K'0K)]^2 \delta_{K',K} \quad (5.38)$$

$$\frac{1}{\tau_1^J} = \left(\frac{84}{125\pi}\right) j(0) \quad (5.39)$$

$$\frac{T_1}{\rho} = \frac{\alpha}{4\pi^2}\,\frac{1}{C_{eff}^2}\left[\frac{84}{125\pi}\right]\frac{\rho_1\, a^4(2\pi\beta\mu)^{\frac{1}{2}}}{h^2}\left[a_1^{\,2}I(4,12)\right. \qquad (5.40)$$
$$\left. + a_2^{\,2}I(4,5) - 2a_1 a_2 I(4,5,12)\right]$$

where all the quantities are corresponding to the molecules of interest.

V.4 T_1 data and Interpretation

The T_1 data as a function of density and temperature are available in literature, for hydrogen nuclei in HCl[27] and NH_3[25] and for the fluorine nuclei in F_2[26] and BF_3[25] and are given in table 5.1. The values of the strengths, a_1 and a_2, of the repulsive and attractive terms of the anisotropic intermolecular potentials for these molecules were obtained by the help of eqs. (5.25), (5.36), (5.31) and (5.40) respectively by the method of least squares. The integrals I(2,12) etc. occurring in these equations were evaluated in the manner described in Chapter III and their values are given in tables 5.3 and 5.4. The values of other factors i.e., C_{eff}^2, I_o, a and ε/k for these molecules are given in table 5.2. From the values obtained for a_2 the dipole and quadrupole moments were calculated using relations (5.13) and (5.28) using appropriate values of the parameter a for the molecule under consideration. The values of the electric moments thus obtained together with the values reported from other methods are given in table 5.5.

Table 5.1. Experimental T_1/ρ values for HCl, F_2, NH_3 and BF_3.

System	Temperature (°K)	T_1/ρ (msec/amagat)
NH_3	300	51.3
	348	40.0
BF_3	220	7.13
	277	5.43
	300	4.89
	337	3.98
HCl	228	24.7
	240	22.2
	263	19.9
	316	17.5
	338	14.8
F_2	222	18.0×10^{-3}
	290	12.7×10^{-3}
	333	9.7×10^{-3}

Table 5.2. Values of I_o, C^2_{eff}, ε/k and a for HCl etc.

System	I_o (10^{-40} gm cm^2)	C^2_{eff} (MHz)	ε/k* (°K)	a* (Å)
HCl	2.71[52]	41x41[53]	360	3.305
F_2	31.7[26]	157x157[26]	112	3.653
NH_3	2.82[25]	217[45]	255	2.6
BF_3	78.9[25]	42[45]	178	4.38

*Values taken from Hirschfelder [48].

Table 5.3. Values of integrals I(2,12), I(2,3) and I(2,3 for a dilute classical gas

$\beta\varepsilon$	I(2,12)	I(2,3)	I(2,3,12)
0.73368	0.02718	0.20623	0.05433
0.85107	0.02631	0.21669	0.05561
1.06509	0.02618	0.23908	0.05972
1.13924	0.02644	0.24787	0.06160
1.36882	0.02801	0.27871	0.06880
1.50000	0.02936	0.29904	0.07385
1.57895	0.03032	0.31231	0.07726

Table 5.4. Values of integrals I(4,12), I(4,5) and I(4,5,12) for a dilute classical gas

$\beta\varepsilon$	I(4,12)	I(4,5)	I(4,5,12)
0.33630	0.03125	0.05024	0.03363
0.38620	0.02805	0.05009	0.03193
0.50450	0.02345	0.05082	0.02967
0.52819	0.02288	0.05111	0.03572
0.59333	0.02156	0.05205	0.02943
0.64260	0.02088	0.05295	0.02879
0.80909	0.01947	0.05678	0.02909

Table 5.5. Values of the electric multipole moments for HCl etc.

System	Dominant electric multipole moment	Values of the moments obtained From NMR data	From other methods
HCl	μ (10^{-18} esu cm)	1.25±0.01	1.18[54]
F_2	Q (10^{-26} esu cm^2)	0.99±0.01	0.886[54]
NH_3	μ (10^{-18} esu cm)	0.29±0.02	1.47[54]
BF_3	Q (10^{-26} esu cm^2)	1.32±0.01	7.99[*]

[*] A value estimated following the method used by P. W. Anderson, Phys. Rev., 80, 511 (1950).

It is observed that the value of quadrupole moment Q for F_2 and the dipole moment μ for HCl are close to the reported values while the values of Q for BF_3 and μ for NH_3 are quite different. This leads to a conclusion that Rajan's model for the correlation time of the intramolecular correlation function works well in some cases, especially, for spherical top molecules such as CH_4 etc. as discussed by them and also in linear molecules as found in the present work. Perhaps the model does not work well in symmetric top molecules.

It may be noted that Armstrong et al.[45] obtained the values of C^2_{eff} from the T_1 minimum studies in many symmetric top molecules. They found that the values obtained for C^2_{eff} from N.M.R. data are in good agreement with those obtained from other methods only for BF_3 and CHF_3 whereas there is a wide descrepancy in the values for CH_3F, PH_3 and NH_3. They concluded that the theory for spin-relaxation in symmetric top molecules should be reassessed. The present analysis also shows a descrepancy only for symmetric top molecules. This may be due to the inadequacy of the model proposed by Rajan et al. or due to the inadequacy of the spin-relaxation theory for symmetric top molecules itself as pointed out by Armstrong et al.

CHAPTER VI

CONCLUSIONS

The work presented in this thesis consists of three types of investigations, viz: (1) obtaining information about the intermolecular potentials in the mixtures of H_2 with mono-, di- and tri-atomic molecules, namely, Ar, N_2 and N_2O, (2) obtaining the value of spin-rotation coupling constant for protons in CH_3Cl from the study of T_1 minimum, and (3) application of a model first proposed by Rajan et al. for estimating the correlation time for intramolecular spin-rotational interaction. The details of the findings are summarized in the following paragraphs:

(1) Proton spin-lattice relaxation time T_1 in the mixtures H_2-X, where X is Ar, N_2 or N_2O, were measured as a function of temperature (300-600K for H_2-Ar and H_2-N_2 and 200-400K for H_2-N_2O), density and composition with a 30 MHz spin-echo spectrometer using phase sensitive detection. A π-$\pi/2$-π pulse sequence was used to produce the echo. The T_1/ρ versus composition data in H_2-X mixtures were extrapolated to 100% of X to find out $(T_1/\rho)^{0-X}$, i.e. the proton spin-lattice relaxation time due to ortho-H_2 and X collisions alone, by a linear variation of T_1/ρ versus composition as well as by using an empirical relation

$T_1/\rho = A_o + A_1 X_x + A_2 X_x^2$, X_x is the concentration of X, A_o etc. are constants (6.1)

to take any non-linearity in T_1/ρ versus composition into account. These $(T_1/\rho)^{O-X}$ data along with those in H_2-Ar and H_2-N_2 mixtures available in literature at low temperatures were analysed using Bloom-Oppenheim theory to obtain information about the intermolecular potentials. The isotropic parts of the intermolecular potentials for H_2-X pairs were assumed to be 12--6 Lennard-Jones potential. The anisotropic parts were assumed to have repulsive as well as attractive terms. For H_2-N_2 and H_2-N_2O, the radial and angular dependence of the attractive terms were taken to be the same as given by the electrostatic multipole interaction between them whereas for H_2-Ar the radial and angle dependences of the attractive term were taken appropriate for the electrostatic interaction between a quadrupolar linear molecule and a spherically symmetric atom. The repulsive terms, for all the three pairs, viz. H_2-Ar, H_2-N_2 and H_2-N_2O were assumed to vary as $\bar{r}^{12}$ and to have the same angle dependence as that of the respective attractive terms. The strengths of the repulsive and attractive terms of the anisotropic intermolecular potential were obtained by fitting the experimental data. Various forms of the anisotropic intermolecular potential were tried to get a best representation of the experimental data. It was found that the model potentials, written below, for H_2-Ar, H_2-N_2 and

H_2-N_2O respectively represent the NMR data best (see eqs. (3.81), (3.84) and (3.85).

$$[V]_{H_2\text{-}Ar} = 4(\varepsilon)_{H_2\text{-}Ar}\left[\left(\frac{a}{r}\right)^{12}-\left(\frac{a}{r}\right)^{6}\right] + 5.59\times10^{-15}\ \text{erg.}$$

$$\times\left[1.45\left(\frac{a}{r}\right)^{12}-\left(\frac{1}{r}\right)^{6}\right]P_2(\cos\theta_1') \qquad (6.2)$$

$$\text{with } (\varepsilon)_{H_2\text{-}Ar} = 10.36\times10^{-15}\ \text{erg},\ a = 3.17\ \text{Å}$$

$$[V]_{H_2\text{-}N_2} = 4(\varepsilon)_{H_2\text{-}N_2}\left[\left(\frac{a}{r}\right)^{12}-\left(\frac{a}{r}\right)^{6}\right] + 4.25\times10^{-15}\ \text{erg}$$

$$\times\left[1.64\left(\frac{a}{r}\right)^{12}-\left(\frac{a}{r}\right)^{6}\right]\left[P_2(\cos\theta_1') + P_2(\cos\theta_2')\right]$$

$$-27.73\times10^{-15}\ \text{erg}\left(\frac{a}{r}\right)^{5}\sum_{q=-2}^{2} a_q Y_{2q}(\Omega_1')\,Y_{2q}^{*}(\Omega_2') \qquad (6.3)$$

$$\text{with } (\varepsilon)_{H_2\text{-}N_2} = 8.20\times10^{-15}\ \text{erg},\ a = 3.314\ \text{Å}.$$

$$[V]_{H_2\text{-}N_2O} = 4(\varepsilon)_{H_2\text{-}N_2O}\left[\left(\frac{a}{r}\right)^{12}-\left(\frac{a}{r}\right)^{6}\right] + 49.3\times10^{-15}\ \text{erg}$$

$$\times\left[2.10\left(\frac{a}{r}\right)^{12}-\left(\frac{a}{r}\right)^{5}\right]\sum_{q=-2}^{2} a_q Y_{2q}(\Omega_1')\,Y_{2q}^{*}(\Omega_2') \qquad (6.4)$$

$$\text{with } (\varepsilon)_{H_2\text{-}N_2O} = 11.54\times10^{-15}\ \text{erg},\ a = 3.759\ \text{Å},$$

where r is the intermolecular separation, ε and a are the Lennard-Jones energy and distance parameters for the corresponding pair, θ_1' and θ_2' are the angles that the symmetry axes of molecules 1 and 2 (colliding pair) respectively make

with $\vec{r}$ and Ω_1' and Ω_2' are the orientations of the symmetry axes with respect to $\vec{r}$.

For H_2-Ar and H_2-N_2 pairs the relative anisotropies, $a_2/4\varepsilon$, in the anisotropic attractive r^{-6} term where a_2 is its strength, were obtained as 0.137 and 0.131 respectively. These are in good agreement with the value (≃0.128) obtained from polarizability data. This justifies the use of the proposed model potentials to explain the NMR data in these systems.

For H_2-N_2O taking the value of the quadrupole moment of H_2 as 0.63×10^{-26} esu cm^2, the value of quadrupole moment of N_2O was obtained from the strength of the attractive anisotropic potential as 4.67×10^{-26} esu cm^2 while the recommended value is 3.0×10^{-26} esu cm^2. Hence the proposed model potential needs to be improved.

(2) Proton spin-lattice relaxation times T_1 in CH_3Cl gas were measured at room temperature using the same spectrometer as described in previous paragraphs (a [$\pi/2$ burst]-$\pi/2$-π pulse sequence was used to produce the echo to save the experimentation time) and in the density region of 0.2-6.5 amagats. The value of T_1 minimum was obtained. By analysing the T_1/ρ data the value of the effective spin-rotation coupling constant was obtained as 0.32 KHz assuming that the spin-rotation interaction is the dominent mechanism for proton

spin-lattice relaxation in CH_3Cl gas. The effective cross-section for molecular reorientation was obtained as 4.01 $\mathring{A}^2$. Comparing this cross-section with the kinetic cross-section it was found that it takes about 14 collisions to randomize the rotational angular momentum, thus the collisions are neither very weak nor very strong.

(3) The existing T_1/ρ data in HCl, F_2, NH_3 and BF_3 were interpreted using Bloom-Oppenheim theory and a model first proposed and used by Rajan et al. which gives an estimate for the correlation time of the dominant intramolecular interaction. According to this model the correlation time of the spin-rotation interaction, which is the dominant mechanism of relaxation in the molecules quoted above, can be taken equal to the life time of the molecule in a J state.

The intermolecular potentials for HCl-HCl, F_2-F_2, NH_3-NH_3 and BF_3-BF_3 pairs of molecules were assumed to consist of isotropic and anisotropic parts. The isotropic parts were assumed to be a 12-6 Lennard-Jones potential. The anisotropic parts were assumed to contain attractive as well as repulsive terms. The radial and angular dependences of the attractive terms were taken as the electrostatic multipole interaction between the molecules whereas the repulsive terms were assumed to have a $\bar{r}^{12}$ radial dependence

and the same angle dependence as that of the attractive parts. The strengths of the attractive and repulsive parts of the anisotropic potentials were calculated from the T_1/ρ data and the scaler values of the multipole moments of the molecules were obtained, in turn, from the strength of the corresponding attractive terms. The dipole moment μ of HCl and the quadrupole moment Q of F_2 were obtained as 1.25×10^{-18} esu cm and 0.99×10^{-26} esu cm^2 respectively which are in good agreement with the respective values 1.18×10^{-18} esu cm and 0.886×10^{-26} esu cm^2 obtained by other methods. The values of μ for NH_3 and Q for BF_3 were obtained as 0.29×10^{-18} esu cm and 1.32×10^{-26} esu cm^2 respectively which are far off from the reported values that are respectively 1.47×10^{-18} esu cm and 7.99×10^{-26} esu cm^2. Thus it may be concluded that the model proposed by Rajan et al to find out the correlation time of the intramolecular interaction works well in some cases especially for spherical top molecules such as CH_4, CF_4 and SiF_4 as discussed by them and also in linear molecules as was found in the present work. Perhaps the model does not work in symmetric top molecules.

It may be pointed out that Armstrong et al.[45] obtained the value of C^2_{eff} from the T_1 minimum studies in many symmetric top molecules. They found that the values obtained for C^2_{eff} from N.M.R. data are in good agreement with those obtained from other methods only for BF_3 and CHF_3 whereas

there is a wide discrepancy in the values for CH_3F, PH_3 and NH_3. They concluded that the theory for spin-relaxation in symmetric top molecules should be reassessed. The present analysis also shows a discrepancy only for symmetric top molecules. This may be due to the inadequacy of the model proposed by Rajan et al. or due to the inadequacy of the spin-relaxation theory for symmetric top molecules itself as pointed out by Armstrong et al.

REFERENCES

1. A. Abragam, 'The Principles of Nuclear Magnetism' (Oxford University Press, 1961).

2. Charles P. Slichter, 'Principles of Magnetic Resonance', (Harper and Row, New York, 1963).

3. N. Bloembergen, E. M. Purcell and R. V. Pound, Phys. Rev., 73, 679 (1948).

4. G. T. Needler and W. Opechowski, Can. J. Phys., 39, 870 (1961).

5. C. S. Johnson and J. S. Waugh, J. Chem. Phys., 36, 2266 (1962).

6. I. Oppenheim and M. Bloom, Can. J. Phys., 39, 845 (1961).

7. M. Bloom and I. Oppenheim, Can. J. Phys., 41, 1580 (1963).

8. I. Oppenheim, M. Bloom and H. C. Torrey, Can. J. Phys., 42, 70 (1964).

9. M. Bloom, I. Oppenheim, M. Lipsicas, C. G. Wade and C. F. Yarnell, J. Chem. Phys., 43, 1036 (1965).

10. M. Bloom and I. Oppenheim in 'Advances in Chemical Physics', Vol. 12, ed. J. O. Hirschfelder (Interscience Publishers, New York, 1967).

11. J. L. Kinsey, J. W. Riehl and J. S. Waugh, J. Chem. Phys., 49, 5269 (1968).

12. K. R. Foster and J. H. Rugheimer, J. Chem. Phys., 56, 2632 (1972).

13. R. Shafer and R. G. Gordon, J. Chem. Phys., 58, 5422 (1973).

14. R. G. Gordon, J. Chem. Phys., 44, 228 (1966).

15. R. G. Gordon, J. Chem. Phys., 45, 1635 (1966).

16. R. G. Gordon, J. Chem. Phys., 45, 1649 (1966).

17. S. Rajan, K. Lalita and S. V. Babu, J. Mag. Res., 16, 115 (1974).

18. M. Lipsicas and M. Bloom, Can. J. Phys., 39, 881 (1961).

19. M. Lipsicas and A. Hartland, Phys. Rev., 131, 1187 (1963).

20. K. Lalita, M. Bloom and J. D. Noble, Can. J. Phys., 47, 1355 (1969).

21. K. Lalita and M. Bloom, Can. J. Phys., 49, 1018 (1971).

22. J. W. Riehl, C. J. Fisher, J. D. Baloga and J. L. Kinsey, J. Chem. Phys., 58, 4571 (1973).

23. J. W. Riehl, J. L. Kinsey, J. S. Waugh and J. H. Rugheimer, J. Chem. Phys., 49, 5276 (1968).

24. D. L. Williams, Can. J. Phys., 40, 1027 (1962).

25. R. L. Armstrong and T. A. J. Hanrahan, J. Chem. Phys., 49, 4777 (1968).

26. J. A. Courtney and R. L. Armstrong, J. Chem. Phys., 52, 2158 (1970).

27. E. Tward and R. L. Armstrong, J. Chem. Phys., 47, 4067 (1967).

28. E. L. Hahn, Phys. Rev., 80, 980 (1950).

29. T. C. Farrar and E. D. Becker, 'Pulse and Fourier Transform Spectroscopy' (Academic Press, New York and London, 1971).

30. F. Bloch, Phys. Rev., 70, 460 (1946).

31. W. N. Hardy, Ph.D. Thesis, University of British Columbia (1964).

32. J. D. Noble, Ph.D. Thesis, University of British Columbia (1964).

33. W. G. Clark, Rev. Sci. Instr., 35, 316 (1964).

34. S. Rajan, Ph.D. Thesis, Indian Institute of Technology Kanpur, India (1975).

35. H. Y. Carr and E. M. Purcell, Phys. Rev., 94, 630 (1954).

36. J. M. Deutch and I. Oppenheim, 'Advances in Magnetic Resonance', Vol. 2, J. S. Waugh, Ed., (Academic Press, New York, 1967).

37. W. N. Hardy, Can. J. Phys., 44, 265 (1966).

38. M. E. Rose, 'Elementary Theory of Angular Momentum' (John Wiley and Sons. Inc., 1957).

39. G. Herzberg, 'Molecular Spectra and Molecular Structure, Vol. II. Infrared and Raman Spectra of Polyatomic Molecules' (Van Nostrand Reinhold Company, New York), p. 437.

40. P. S. Hubbard, Phys. Rev., 131, 1155 (1963).

41. P. S. Hubbard, J. Chem. Phys., 42, 3546 (1965).

42. J. S. Blicharski, Acta Phys. Polon., 24, 817 (1963).

43. M. Bloom, F. Bridges and W. N. Hardy, Can. J. Phys., 45, 3533 (1967).

44. R. Y. Dong and M. Bloom, Can. J. Phys., 48, 793 (1970).

45. R. L. Armstrong and J. A. Courtney, Can. J. Phys., 50, 1262 (1972).

46. F. R. McCourt and S. Hess, Z. Naturforsch., 25a, 1169 (1970).

47. N. J. Bridge and A. D. Buckingham, Proc. Roy. Soc. (Lond). 295A, 334 (1966).

48. J. O. Hirschfelder, C. E. Curtiss and R. B. Bird, 'Molecular Theory of Gases and Liquids' (John Wiley and Sons, Inc., New York, 1964).

49. W. Kalechstein and R. L. Armstrong, Can. J. Phys., 55, 1083 (1977).

50. C. G. Gray, Can. J. Phys., 46, 135 (1968).

51. D. W. Breck, 'Zeolite Molecular Sieves' (John Wiley and Sons., New York, 1974).

52. G. Herzberg, 'Molecular Spectra and Molecular Structure, Vol. I. Spectra of Diatomic Molecules' (Van Nostrand Reinhold Company, New York), p. 81.

J. A. Leavitt, M. R. Baker, H. M. Nelson and N. F. Ramsey, Phys. Rev., 124, 1482 (1961).

D. B. Stogryn and A. P. Stogryn, Mol. Phys., 11, 371 (1966).

APPENDIX

CIRCUIT DIAGRAMS

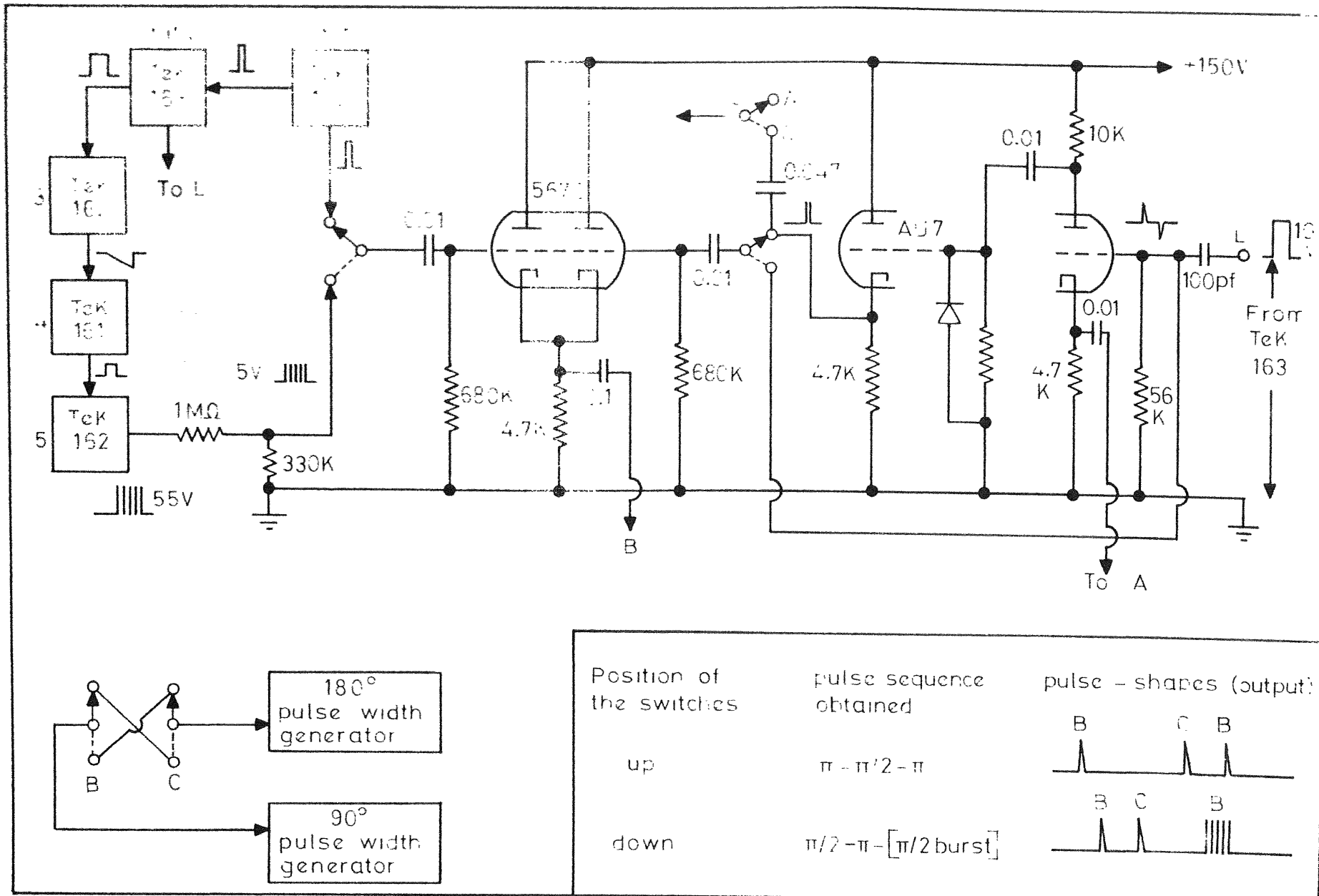

Fig. A1 Pulse sequencer

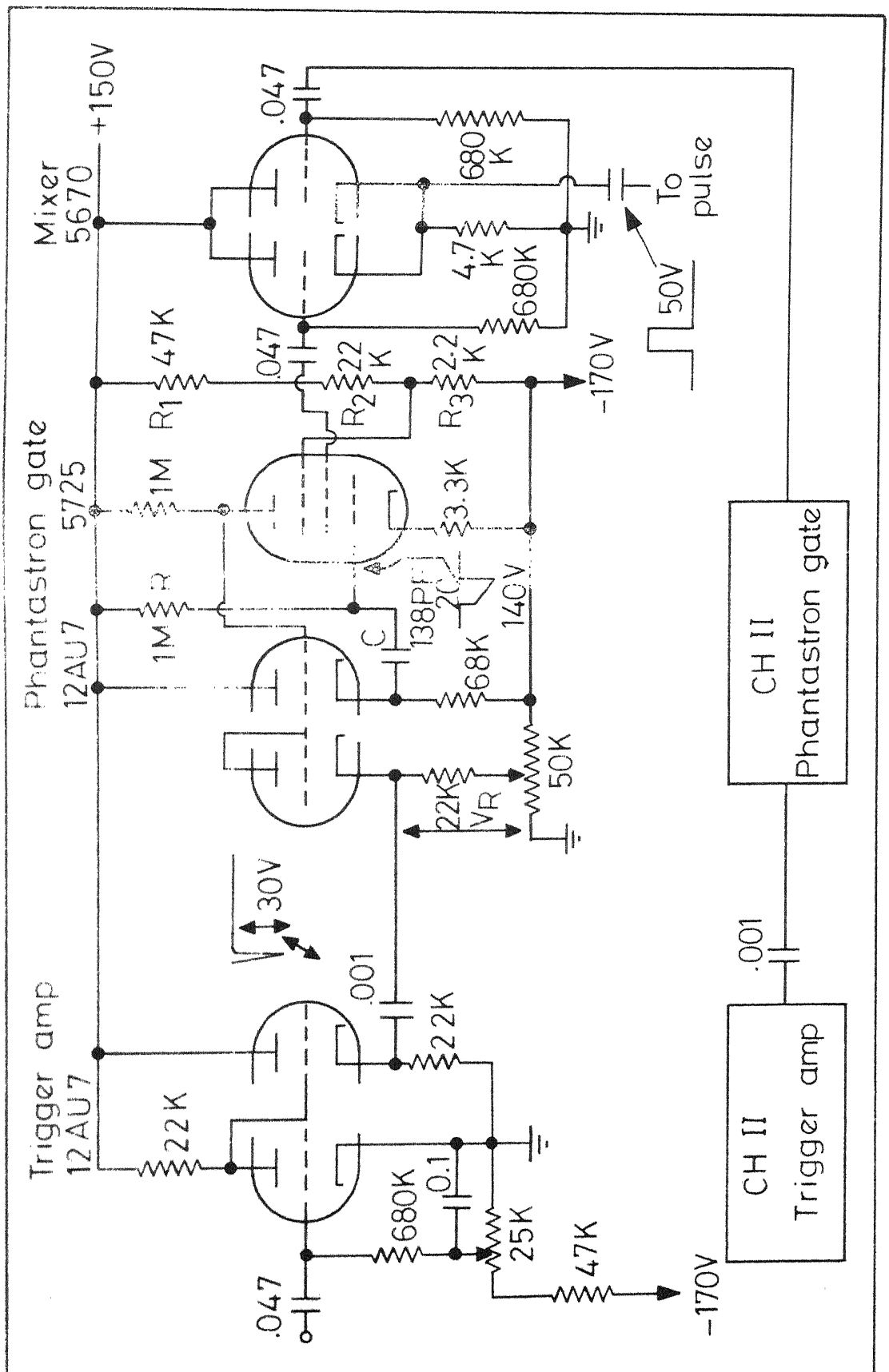

Fig. A 2 Pulse width generator.

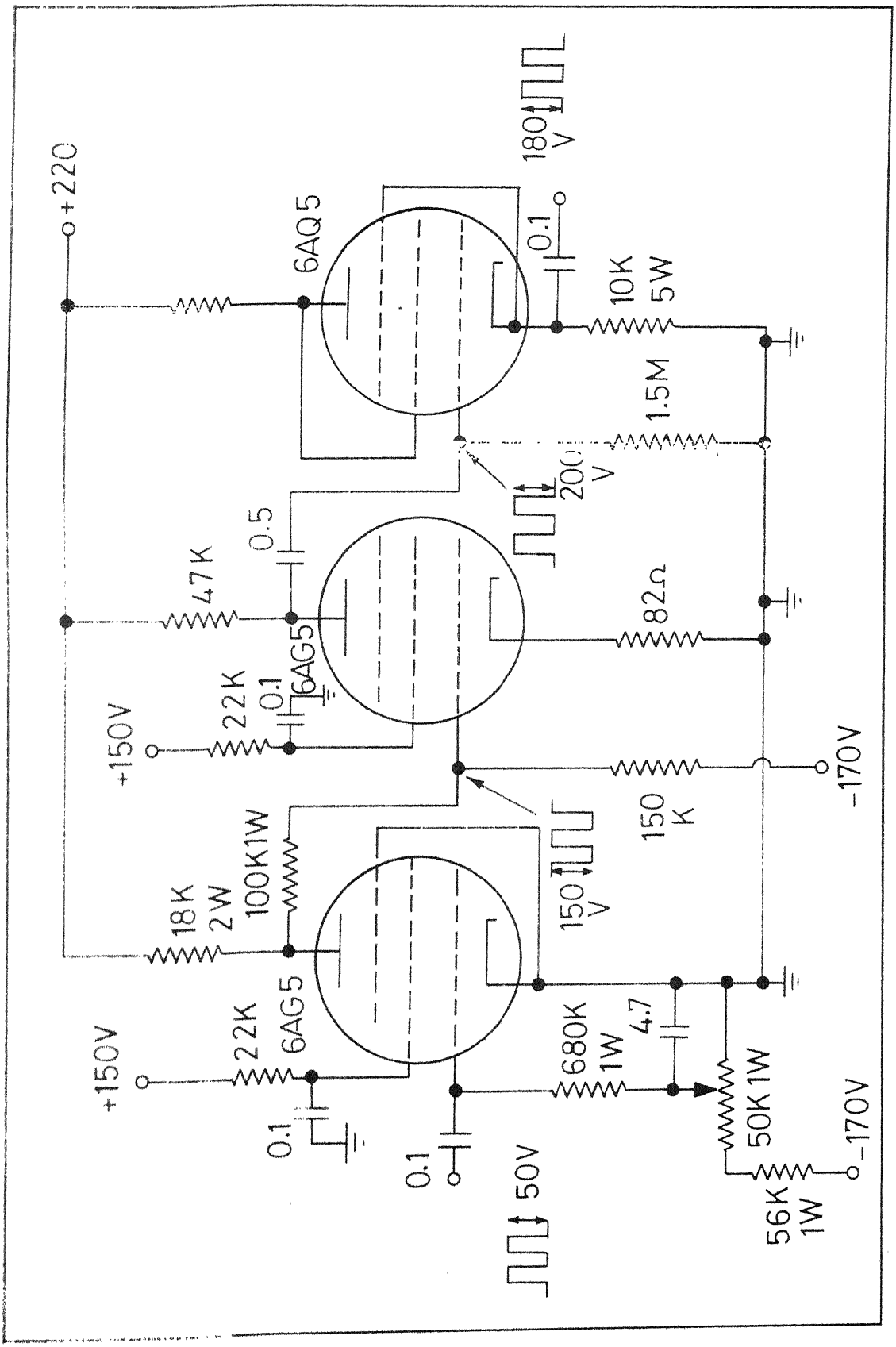

Fig. A3 Pulse shaper and amplifier

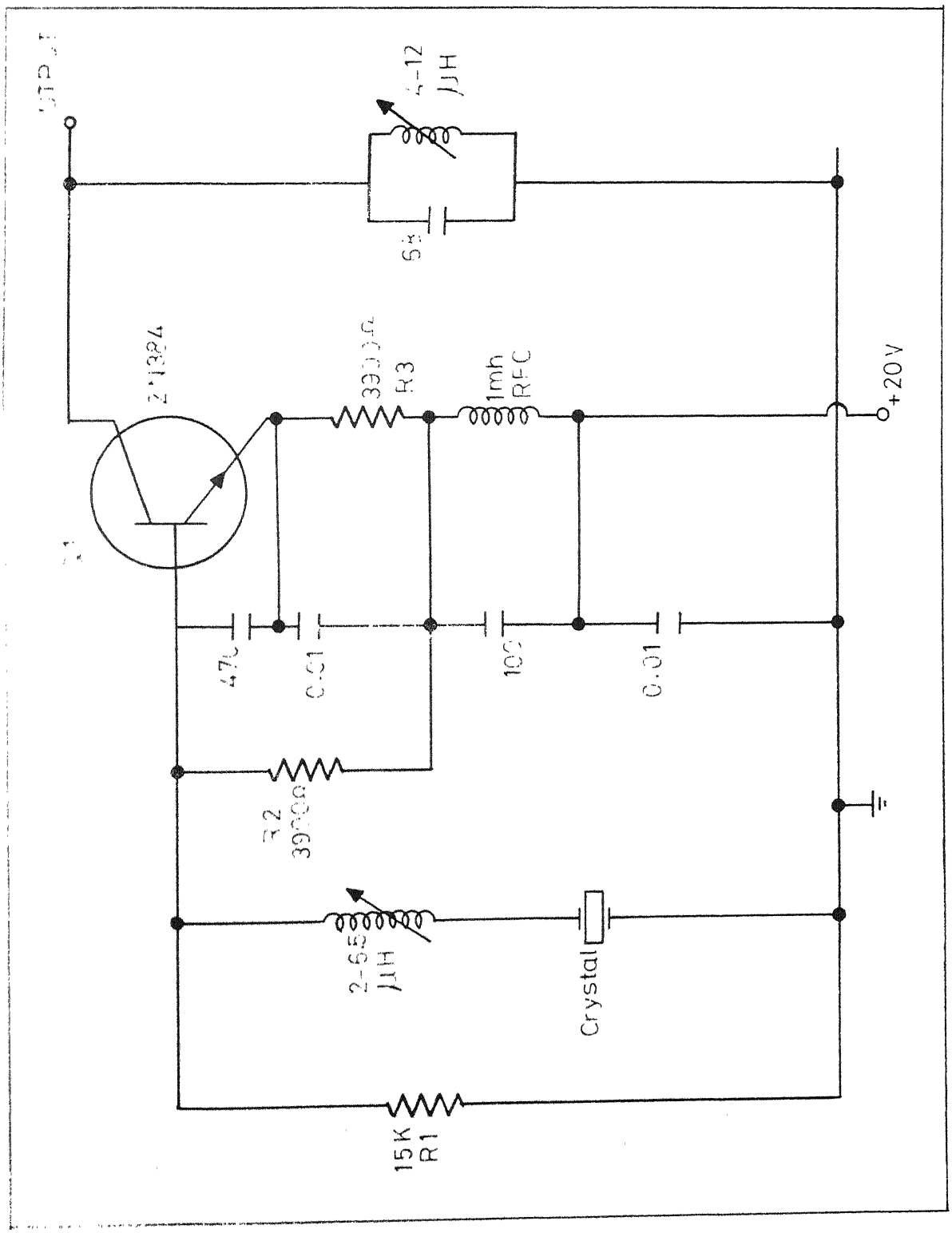

Fig. A4 10 MHz crystal controlled oscillator.

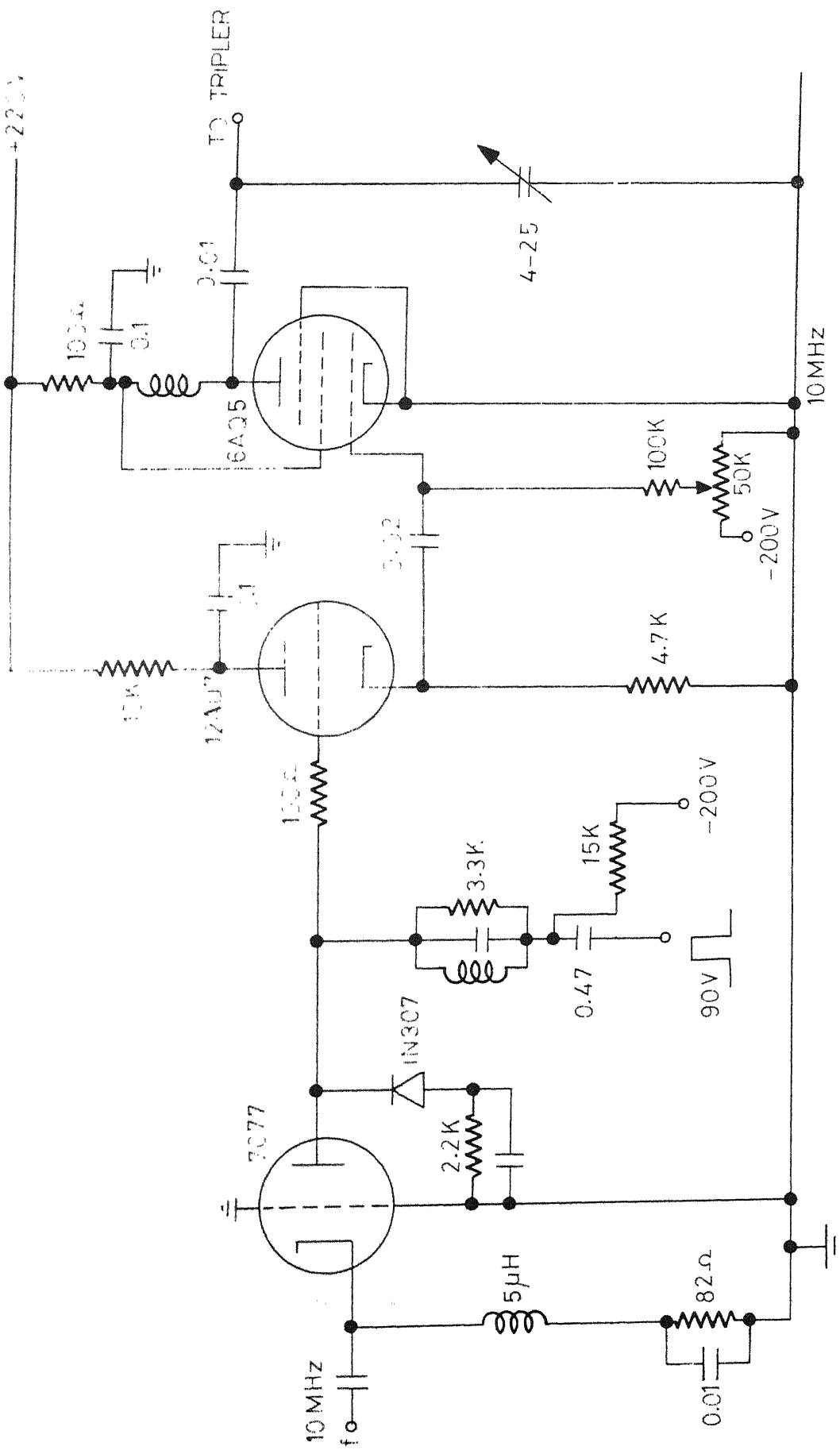

Fig. A5 Coherence gated and 10MHz amplifier.

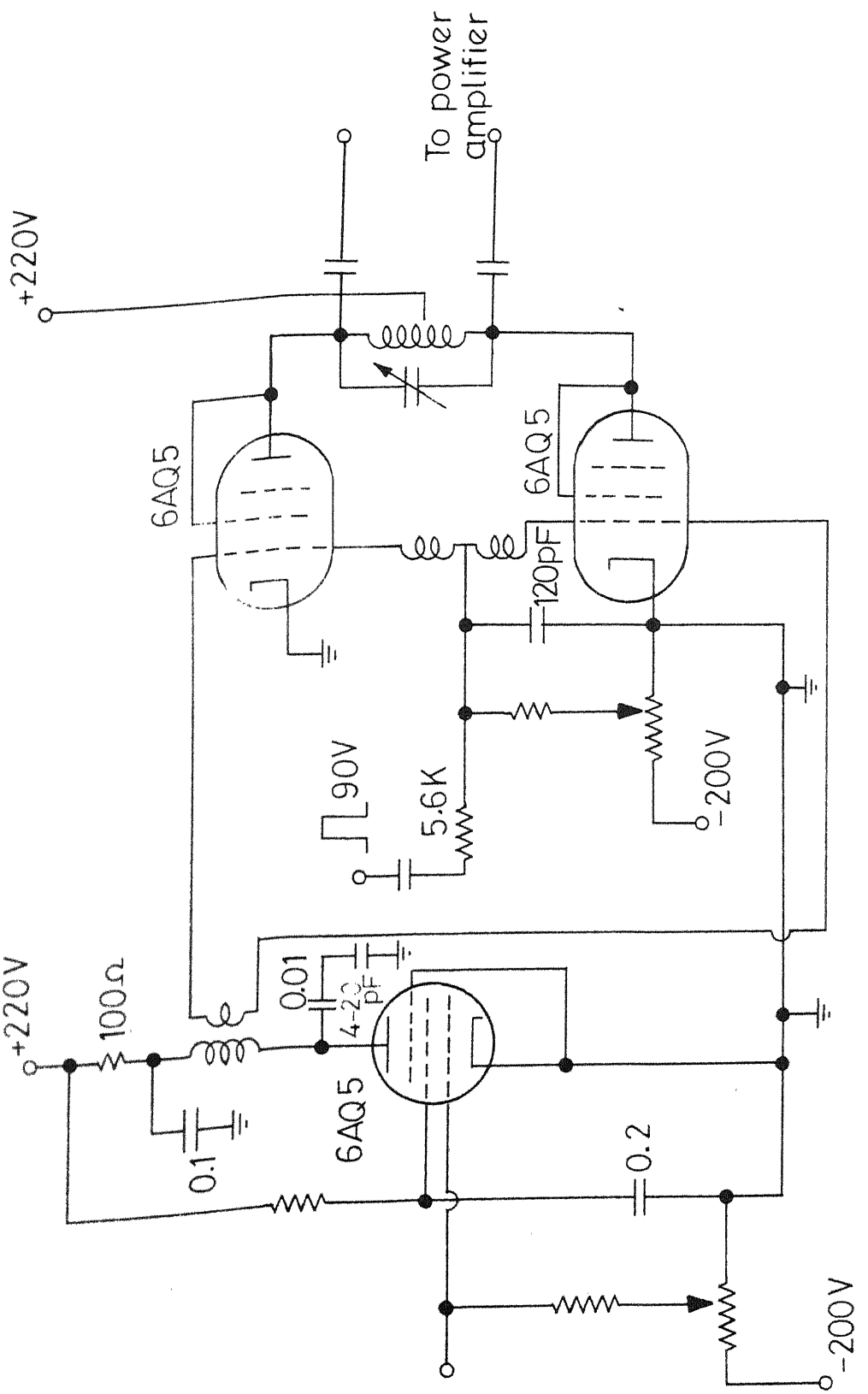

Fig. A6 30 MHz tripler

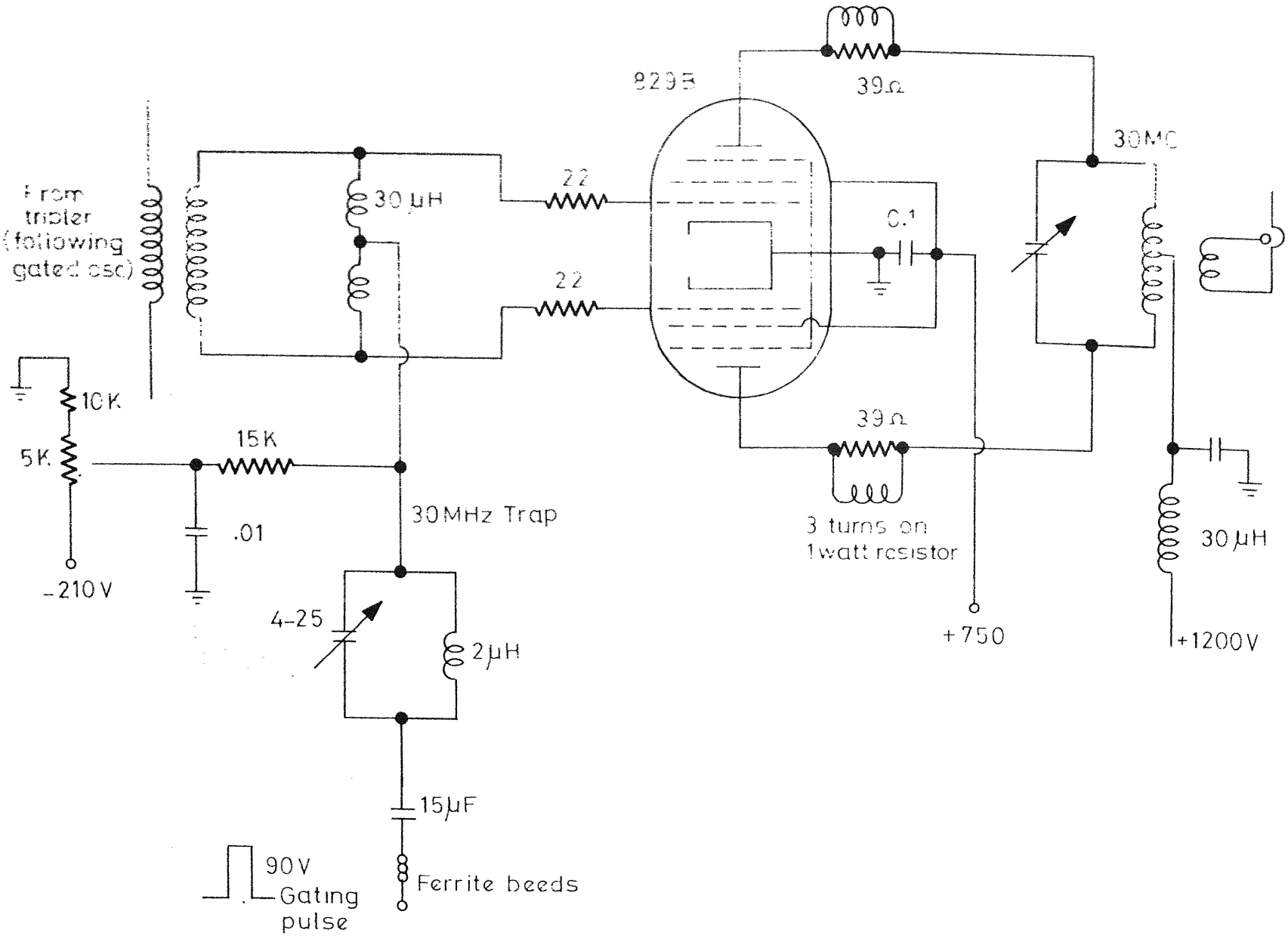

Fig. A7 Power amplifier

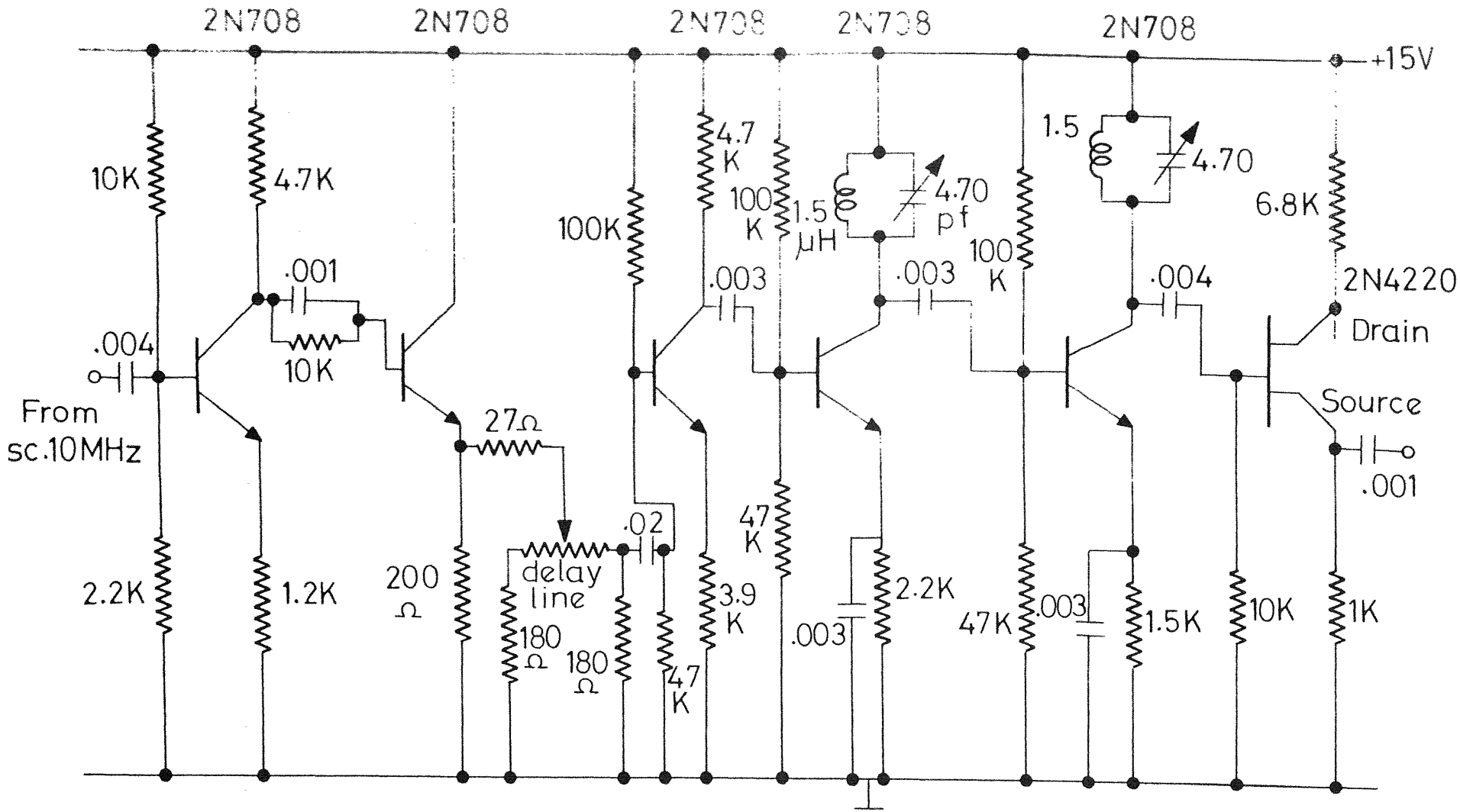

Fig. A8 Tripler

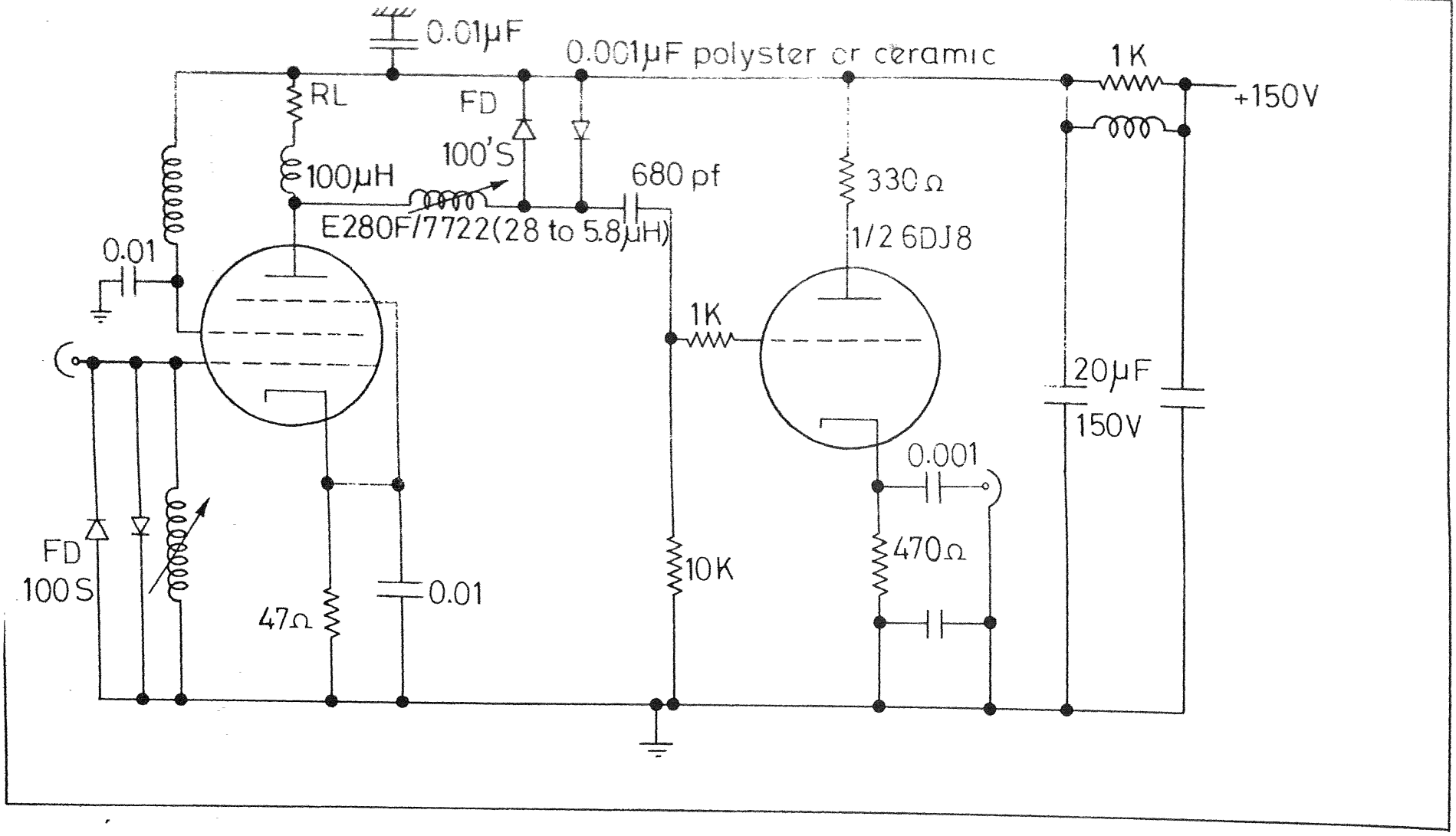

Fig. A 9 Pre – amplifier

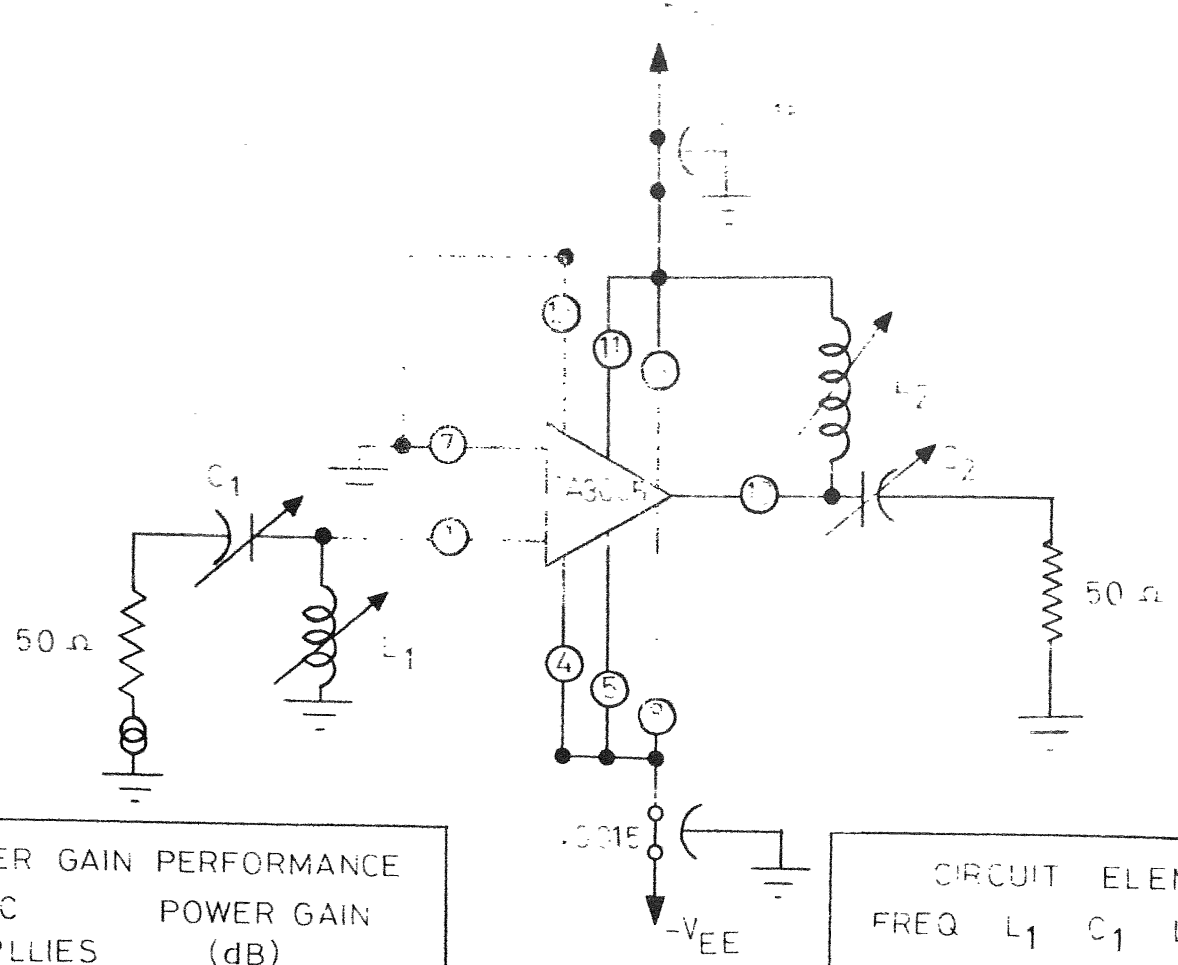

POWER GAIN PERFORMANCE	
DC SUPPLLIES	POWER GAIN (dB)
±6VOLTS	29

CIRCUIT ELEMENTS

FREQ (MHz)	L_1 (μH)	C_1 (PF)	L_2 (μH)	C_2 (PF)
30	1.2-2	5.40	1.2-2	1.5-20

Fig.A10 CA 3005 integrated circuit RF amplifier.